Interaction of 1,4 – Dicarboxylic Acids with a Cu(110) Surface

Dissertation

zur

Erlangung der naturwissenschaftlichen Doktorwürde

(Dr. sc. nat.)

vorgelegt der

Mathematisch – naturwissenschaftlichen Fakultät

der

Universität Zürich

von

Chrysanthi Karageorgaki

aus

Griechenland

Promotionskomitee

Prof. Dr. Karl-Heinz Ernst (Vorsitz)

Prof. Dr. Kim Baldridge

Prof. Dr. Jay S. Siegel

Zürich, 2015

Acknowledgements

First of all, I would like to thank Prof. Karl-Heinz Ernst for giving me the opportunity to do my doctoral work in his group. The subject was both interesting and demanding, helping me learn new things and acquire valuable skills.

In times of doubt or frustration Manfred Parschau was always willing to help with his calming demeanor, both scientifically and experimentally. Günther Hobi and Sasa Vranjkovic were always available to lend tools, advice and help, with a smile on their faces, which made working with UHV systems a breeze.

Margrith Meier performed the experiments and analysis for one of the molecules in this thesis during her Master's work. Supervising her work occasionally forced me to find answers to very good questions that had not previously crossed my mind or look at the results from another perspective and for that I am grateful.

Dr. Daniele Passerone performed the DFT calculations for one of the molecules in this work, helping us move a little bit closer to understanding the interaction with the surface and for that I would like to thank him.

All past and present members of the department of Nanoscale Materials Science played an important role these past four years. Everybody was approachable and willing to help if a problem came up, or even just to socialize. In particular I would like to thank my fellow group members, Quirin and Johannes for being very nice office mates for three years and Jingyi and Alexandra, who joined the office during the last few months of this work. Exchanging ideas, lots of laughs and even the occasional "horror" story from our respective labs was a very constructive outlet for any and all pressure.

Last but not least, I would like to thank my husband Christian, who has very patiently let me bounce ideas off of him for the past four years and pointed out any faults in my train of thought, as well as the rest of my family for their help and continuing support. It is deeply appreciated.

Table of contents

Summary

The adsorption and influence of several 1,4-dicarboxylic acids with a Cu(110) surface was investigated under ultra-high vacuum (UHV) conditions with X-ray photoelectron spectroscopy (XPS), low energy electron diffraction (LEED), reflection absorption infrared spectroscopy (RAIRS), scanning tunneling microscopy (STM) and temperature programmed desorption (TPD). Three of the molecules used, fumaric, maleic and acetylenedicarboxylic acid, had no substituents in carbons 2 and 3, but introduced a steric hindrance in their backbone in the form of a double and triple carbon bond. For the first two molecules this resulted in the formation of both achiral and enantiomorphous structures, all of which had already been reported for two previously investigated 1,4-dicarboxylic acids, succinic and malic acid. Acetylenedicarboxylic acid formed no ordered structures upon adsorption and remained disordered. High resolution STM investigation of the fumaric and maleic acid structures revealed a chiral (1,1) reconstruction of the underlying, formerly achiral, copper surface and the existence of two distinct unit cells defining the arrangement of the molecules and the copper adatoms on the crystal, respectively. The remaining three molecules that were investigated in this work, 2,3-dimethyl succinic acid, *trans*-1,2-cyclohexane dicarboxylic acid and phthalic acid, had substituents attached to carbons 2 and 3. This created a kind of steric hindrance, due to the inability to freely rotate the bond between carbons 2 and 3. STM revealed a reconstruction of the copper substrate, in this case following a (1,2) periodicity, when 2,3-dimethyl succinic acid was used as an adsorbate. Adsorption of *trans*-1,2-cyclohexane dicarboxylic acid led to the superposition of several LEED patterns also observed for other molecules investigated in this work. Phthalic acid revealed a variety of ordered structures, both with LEED and STM, leading to similar results as those previously reported for malic and tartaric acid. RAIRS measurements for all investigated molecules showed that when the molecules remain disordered, they prefer a mono- configuration, i.e. they are bound to the substrate through chemical bonds formed between the oxygen atoms of one of the carboxylic acid groups, while the other one remains unaffected. The molecular configuration varies however, when the molecules are arranged in ordered structures. TPD revealed that all molecules exhibit characteristics of explosive decomposition, with the rate of desorption at maximum shifting to higher temperatures with increasing coverage.

This work established that the chirality transfer in self-assembled monolayers derives from the substrate, instead of inter- or intramolecular bonding. Additionally, it showed that the molecules as well have an influence on the substrate, forcing it to reconstruct. After partial decomposition of molecules, areas of a truly chiral metal surface were identified.

Zusammenfassung

Die Adsorption und deren Wirkung auf eine Cu(110) Oberfläche wurde für verschiedene 1,4-Butandisäuren mittels Röntgenphotoelektronenspektroskopie (XPS), Beugung langsamer Elektronen (LEED), Reflexion-Infrarotspektroskopie (RAIRS), Rastertunnelmikroskopie (STM) und Temperatur-programmierter Desorption (TPD) im Ultrahochvakuum (UHV) bestimmt.

Drei der verwendeten Moleküle, Fumarsäure, Maleinsäure und Acetylendicarbonsäure, haben zwar am zweiten und dritten Kohlenstoffatom keine Substituenten, jedoch verleihen ihnen Doppel- bzw. Dreifachbindungen zwischen C2 und C3 eine gewisse Steifigkeit. Als Resultat wurden für die beiden ersten Moleküle sowohl achirale als auch enantiomorphe Strukturen gefunden. Diese Gitterstrukturen waren vorher schon für zwei andere Butandisäuren – Bernsteinsäure und Äpfelsäure – gefunden worden. Für Acetylendicarbonsäure konnten nach der Adsorption keine geordneten Strukturen gefunden werden.

Hochaufgelöste STM Untersuchungen der für Fumarsäure und Maleinsäure gefundenen Strukturen zeigten eine chirale (1, 1) Rekonstruktion der darunterliegenden, ansonsten achiralen, Kupferoberfläche, sowie die Existenz zweier verschiedener Einheitszellen, welche die Anordnung der Moleküle und Adatome beschreiben. Die drei weiteren in dieser Dissertation untersuchten Moleküle – Dimethylbernsteinsäure, Cyclohexan-1,2-dicarbonsäure und Phtalsäure – haben voluminöse Substituenten am zweiten und dritten Kohlenstoffatom. Wie mittels Rastertunnelmikroskopie gezeigt werden konnte, gibt es bei der Adsorption von Dimethylbernsteinsäure ebenfalls eine Rekonstruktion der Kupferoberfläche, diesmal aber mit (1, 2) Periodizität. Für Cyclohexan-1,2-dicarbonsäure konnten mittels LEED koexistierende Strukturen nachgewiesen werden. Diese Periodizitäten waren zuvor schon für andere Moleküle (Äpfelsäure und Weinsäure) gefunden worden. Für Phtalsäure konnten mittels LEED und STM ebenfalls verschiedene geordnete Strukturen nachgewiesen werden. Mittels RAIRS konnte gezeigt werden, dass alle ungeordneten Moleküle eine Mono-Konfiguration bevorzugen, d.h. die chemische Bindung zum Substrat erfolgt mittels der Sauerstoffatome von nur einer Carboxylatgruppe. Dagegen ändert sich die molekulare Konfiguration in den geordneten Strukturen. TPD zeigte für alle Moleküle eine charakteristische, explosionsartige Zersetzung. Je grösser die Bedeckung, je höher war dabei die Desorptionstemperatur.

Diese Dissertation zeigt vor allem, dass der laterale Chiralitätstransfer in selbstangeordneten Monolagen übers Substrat erfolgt, und nicht von zwischen- oder intramolekularen Wechselwirkungen. Zudem konnte gezeigt werden, dass die Moleküle selbst einen starken Einfluss auf die Struktur der Oberfläche haben. Ausgehend von dem achiralen Substrat erfolgt dabei eine chiral Rekonstruktion der Metalloberfläche, die selbst ohne Moleküle erhalten bleibt.

1: Introduction and previous studies

1.1 Chirality

The term chirality was first introduced by Lord Kelvin and published in his 1904 Baltimore lectures where he stated "I call any geometrical figure or group of points chiral, and say it has chirality if its image in a plane mirror, ideally realized, cannot be brought into coincidence with itself" [1]. The term to describe this property derives from the Greek word for hand (χειρ), with the human hands being the most universally recognized example of a chiral object.

Although not always realized, chirality exists in almost every aspect of the everyday world, with examples including, among others, the left and right sides of the human body, the coiled shells of snails and several types of sea shells (Figure 1.1), or even the braided cables of traditional Celtic and Irish clothing designs. It doesn't only exist in the macroscopic world, but plays a very important role at the micro and nano scale as well. Basically all physiological amino acids other than glycine are chiral, consequently, proteins are chiral as well. DNA, which contains chiral carbohydrates, forms a chiral double helix [2-5].

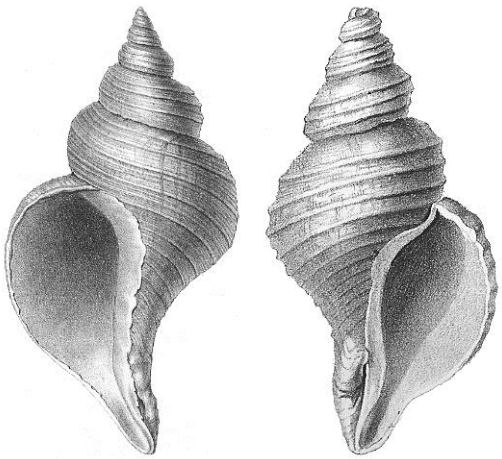

Figure 1.1: Left- and right-handed shells of a sea snail.

Molecular chirality was first discussed by Louis Pasteur in 1848 when, after manually separating the left and right handed crystals of ammonium sodium tartrate, he discovered that

their aqueous solutions rotated the plane of linearly polarized light counterclockwise and clockwise respectively, whereas the racemic mixture of both canceled each other's effect and no longer rotated the plane of linearly polarized light [6]. In 1874, J. H. van't Hoff [7] and J. A. Le Bel [8] made a major advancement in stereochemistry by suggesting that the four atoms around a carbon atom are organized in a tetrahedral arrangement. When these atoms are different from each other, then the carbon is a chiral center and the molecule itself is chiral. The two resulting molecules, which are mirror images of one another, are called enantiomers and are named *R* (for rectus), in the case of a right-handed configuration and *S* (for sinister), in the case of a left handed one. They both rotate the plane of linearly polarized light into opposite directions, as reported originally for enantiomers of quartz crystals, but are otherwise similar, i.e. they have the same physical properties. However, in several cases, they exhibit completely different biomedical behavior. Such difference can sometimes be mild, as in the case of iso-butyl-propanoic-phenolic acid (the active substance in Ibuprofen), where the *R*-enantiomer is relatively inactive in the body, whereas, the *S*-enantiomer is 160 times more active as a pain killer [9]. It can also be, however, that the different biomedical action of enantiomers has dramatic consequences, as in the case of thalidomide, which was released in 1956 as a mild sedative used to treat nausea in pregnant women [10]. The *R*-enantiomer has indeed the intended result, but the *S*-enantiomer has a teratogenic effect. Although thalidomide racemizes in the human body and separation is therefore obsolete, it is generally of paramount importance for the pharmaceutical industry that enantiomers of chiral drugs can be separated and tested.

1.2 Heterogeneous enantioselective catalysis

The demand for chemical products has increased exponentially in the past few decades, be it in the form of active substances in pharmaceutical products, pesticides or aroma compounds for the fragrance industry. As it has become clear that enantiomerically pure compounds are needed in order to avoid negative effects, several efforts have been made for strategies to produce enantiopure compounds. Beyond separation of enantiomers, one strategy is enantioselective synthesis, awarded with Nobel Prizes in chemistry to Knowles, Noyori and Sharpless for "their work on chirally catalyzed reactions" in 2001 [11].

The idea behind combining enantioselectivity and heterogeneous catalysis [12] is fairly straightforward, the application itself, however, is quite complex. The process is called

heterogeneous, because the catalyst and the product are in different physical phases, i.e. the catalyst is a solid, whereas the reactants are in solution or gas phase. The reactant adsorbs on the surface of the catalyst by forming either weak bonds, as in the case of physisorption, or by forming strong chemical bonds, as in the case of chemisorption. There are different mechanisms describing the reactions that take place on the surface of the catalyst [13-16], but the result is always similar. After the reaction has been completed, the final product desorbs from the surface of the catalyst, leaving the active site free to accommodate another reactant so that the process can be repeated. An example of such a heterogeneous catalytic reaction is shown in Figure 1.2.

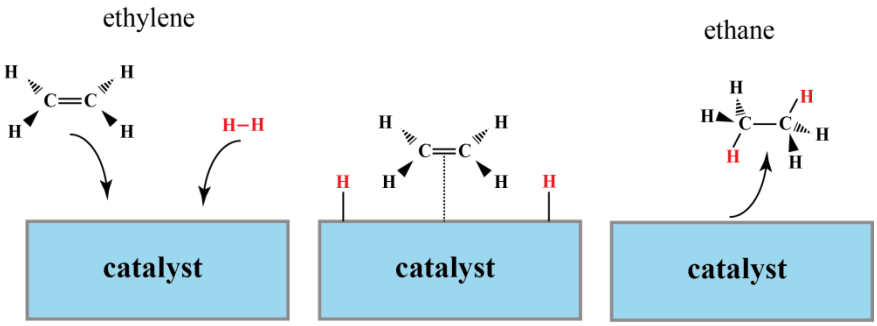

Figure 1.2: Schematic representation of the mechanism of heterogeneous catalysis, depicting here the hydrogenation of ethylene. The molecular hydrogen adsorbs to the catalyst surface, therefore forming adsorbed hydrogen atoms (left). Ethylene adsorbs to the catalyst surface (middle) and finally reacts with the adsorbed hydrogen atoms to produce ethane, which then desorbs from the catalyst surface (right).

During any synthesis reaction of a chiral molecule, without any external manipulation, a racemic mixture of equal amounts of left and right handed enantiomers would be produced, but since in most cases only one enantiomer is desired, catalysts are being used to produce enantiopure products. Ideally, in the case of heterogeneous catalysis metals are chirally modified with the help of so-called modifier molecules and then used as catalysts. Depending on the handedness of the modifier the resulting end product should also have the same chirality. However, the mechanism of such a process is still poorly understood. Therefore, homogeneous catalysts are mainly used for the production of enantiopure compounds for the pharmaceutical industries [17].

At present there are basically two established examples of heterogeneous enantioselective catalysis, that of the hydrogenation of α- and β-ketoesters by cinchona modified platinum

catalysts and tartaric modified nickel catalysts, respectively [18, 19]. There are several models trying to explain the mechanism of the catalytic process [20-23], the most prominent are the template and the active chiral site models.

According to the template model the modifier molecule creates a chiral grid on the surface of the catalyst with locations where the reactant adsorbs. This way the reactant is forced to assume only one handedness, dependent on that of the chiral modifier molecule, therefore creating a chiral product. The active chiral site model is similar to the template model, but suggests that a chiral grid is not necessary. Instead, there is direct interaction between the chiral modifier molecule and the reactant, leading to the same effect (Figure 1.3).

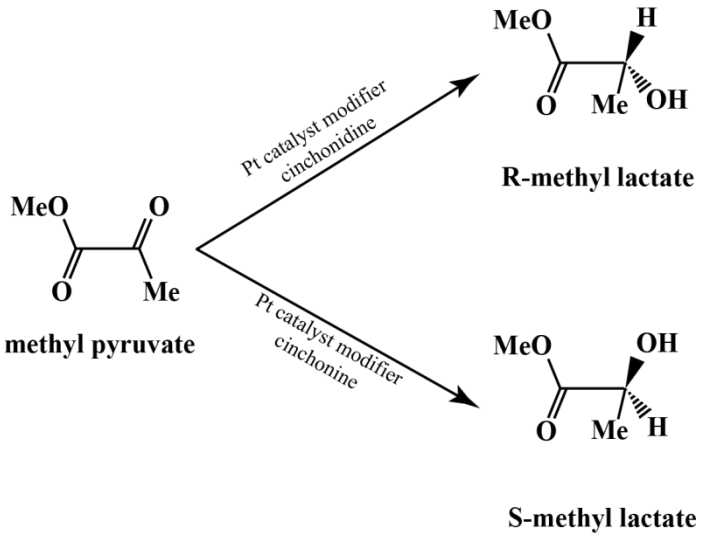

Figure 1.3: Schematic diagram of the Orito reaction showing the structures of methyl pyruvate and the enantiomeric products R- and S-methyl lactate, produced with use of cinchonidine and cinchonine as modifiers, respectively.

Although the models are promising, the mechanism of this catalytic process is not yet understood. In order to obtain more insight on the interactions between potential modifier molecules and catalytic surfaces, scientists have been investigating model systems of both chiral and achiral molecules on single crystals. These experiments are typically performed under ultrahigh vacuum (UHV) conditions (base pressure $\leq 5 \times 10^{-10}$ mbar), and in this way several potential problems, such as contaminations, are eliminated, making it easier to study these systems.

1.3 Previous achievements in chiral surface science

The field of molecular surface science, investigating molecules on different crystals and the overlayer structures that these produce upon adsorption, is an ever-growing one. Several types of molecules have been investigated, ranging from bowl-like fragments of the fullerene [24-26], helical molecules made of benzene rings [27-29], but also smaller carboxylic [30] and amino acids [31-37]. Several review articles exist with detailed information on such systems [38-45]. This thesis focuses on chiral and achiral dicarboxylic acids and therefore this chapter will provide a small literature review of such molecules.

1.3.1 Notation of overlayer structures

It should be noted that several ways exist to define an overlayer structure. Commonly the Wood [46] or the matrix notation [47] are used.

The Wood notation is the simplest method for describing surface structures, but works only when the substrate and the overlayer structure have a common periodicity. It specifies the lengths of the overlayer vectors, b_1 and b_2 in relation to the substrate vectors, a_1 and a_2. It is then written in the following format:

$$(|b_1|/|a_1| \times |b_2|/|a_2|)$$

In the matrix notation the structure and overlayer vectors are related to each other by a matrix M as shown below:

$$\begin{pmatrix} b_1 \\ b_2 \end{pmatrix} = \begin{pmatrix} m_{11}\, m_{12} \\ m_{21}\, m_{22} \end{pmatrix} \begin{pmatrix} a_1 \\ a_2 \end{pmatrix}$$

Which is defined as:

$$b_1 = m_{11} \cdot a_1 + m_{12} \cdot a_2$$

$$b_2 = m_{21} \cdot a_1 + m_{22} \cdot a_2$$

For practical reasons, the matrix is presented here in the form $(m_{11}\, m_{12},\ m_{21}\, m_{22})$. Recently, new universal rules were introduced for the notation of overlayer structures [48]. However, for the sake of clarity, we retain in this chapter the original notations that were used by the authors.

1.3.2 Tartaric acid

One of the most prominent molecules investigated in chiral surface science, both experimentally and theoretically, is tartaric acid (TA).

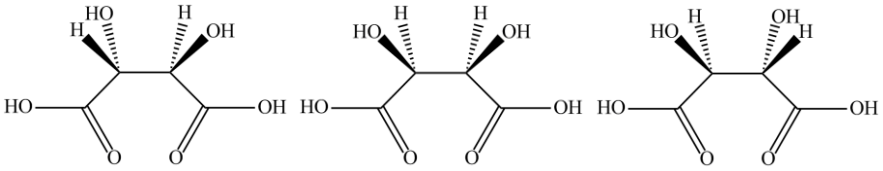

Figure 1.4: Diastereomers of tartaric acid. From left to right: (*R*,*R*)-TA, meso-TA, (*S*,*S*)-TA.

Tartaric acid is a member of the butanedioic acid family, with carboxylic acid groups at each end of the molecule and hydroxyl groups attached to carbons 2 and 3. It may appear in three stereoisomers, as shown in Figure 1.4, the achiral meso compound and two left and right handed isomers. Tartaric acid's involvement in the catalytic hydrogenation of β-ketoesters was the original motivation to study this molecule at surfaces. It has been investigated on a number of different surfaces and provided a wide array of ordered overlayer structures.

1.3.3 TA/Ni(110)

Humblot and coworkers have investigated (*R*,*R*)-TA on a Ni(110) surface using RAIRS, STM, TPD and DFT calculations [49, 50]. According to their RAIRS results, at low coverage and room temperature the chiral molecule was bound to the surface in a bi-tartrate form, i.e. via both oxygen atoms of both carboxylate groups. Alternatively, the molecule can be bound in a so-called mono-configuration, i.e. with the oxygen atoms of only one of the carboxylic acid groups. A schematic representation of the two different adsorption modes is shown in Figure 1.5.

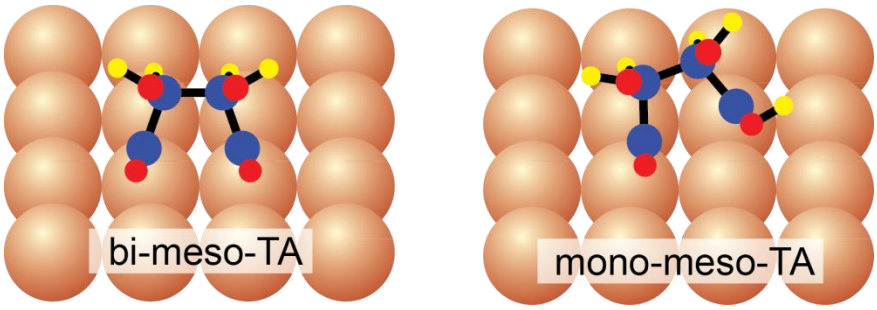

Figure 1.5: Schematic representation of mono- and bi-tartrate adsorption motifs, shown here for the achiral meso compound.

DFT calculations were used in order to determine the nature of the adsorbed species, specifically the position of the molecule on the surface [51]. Different orientations of the molecule on the surface were considered, but the energetically most stable one showed that the molecules were bound with the oxygen atoms within each carboxylate group attached to adjacent Ni atoms along the [110] direction of the crystal. Moreover, the interaction of the chiral OH groups of the molecule with the Ni atoms of the surface led to an acute distortion of the molecular backbone, which was translated as strain into the surface. In an attempt to relieve this stress, the surface became reconstructed, something that was in accordance with the severe distortions observed in STM close to the adsorbed molecules. Two different reconstruction models were suggested, the paired-row structure and the missing-row structure, as seen in Figure 1.6, although no experimental data was available to help discriminate between the two models.

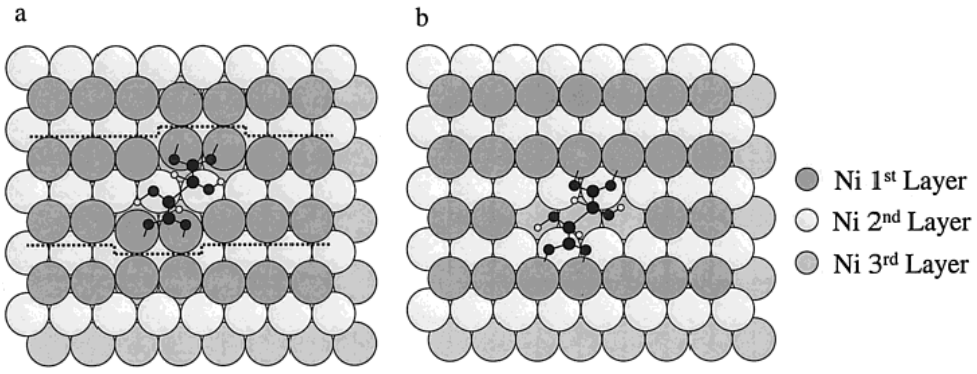

Figure 1.6: Schematic models of the (a) paired-row and (b) missing-row reconstructions of the Ni(110) surface upon adsorption of TA. Adapted from [49].

Highly interesting is the fact that this restructuring of the surface did not require a minimum amount of molecules adsorbed on the surface to take place, but could already be observed at very low coverage, suggesting that the molecule-metal bond was very strong. This was supported not only by the DFT calculations, which revealed a very high binding energy of the molecules on the surface, but also by the TPD results, which showed explosive decomposition of the molecules in the form of fragments, leading to the conclusion that the intramolecular bonds break at a lower temperature than the molecule-metal bond.

1.3.4 TA/Ni(111)

Baddeley et al investigated TA on the Ni(111) surface, using LEED, RAIRS, STM and TPD experiments, in order to determine any potential significance of the produced overlayer structures in heterogeneous catalysis [52]. They performed experiments for various dosing times and sample temperatures. Interestingly, in all cases they were unable to obtain any usable data from the LEED experiments, as the electron beam made the molecules decompose, producing a LEED pattern that has been reported for C/Ni(111) [53]. The STM results showed, however, growth of ordered structures, the stability of which grew with increasing coverage. The RAIRS results helped to identify that the adsorbed molecules assumed a bi-tartrate configuration at low coverages, in which case the carboxylate groups could be bound via a monodentate or bidentate geometry. As the amount of molecules on the crystal increased, their configuration changed to monotartate, with one of the carboxylate groups being re-protonated by hydrogen atoms lying on the crystal surface. Unfortunately, no correlations could be made between the results of that work and its significance in heterogeneous catalysis.

1.3.5 TA/Cu(110)

Although interesting advancements have been made by investigating systems like the ones described above, nickel is a very reactive substrate, making it difficult to investigate polar molecules. Therefore, tartaric acid has been widely investigated on copper surfaces, from several groups within the surface science community.

Raval and coworkers studied (*R,R*)-TA on Cu(110) and introduced a plethora of different structures depending on coverage and sample temperature [54-56]. Their experiments showed

that at low coverage and with the sample at room temperature, TA was bound to the surface in a monotartrate configuration, with the LEED showing a (4 0, 2 3) structure. Interestingly, with increased exposure to the electron beam of the LEED, this structure changed to a (4 0, 2 1). Upon increasing the temperature of the sample, but maintaining the coverage, this structure turned into a (9 0, 1 2) with the molecules now bound in a bi-tartrate configuration. This structure turned into the initial (4 0, 2 3) mono-tartrate configuration simply by increasing the number of the adsorbed molecules. When starting again from the initial (4 0, 2 3) structure and with increasing the coverage, the structure could change to a (4 1, 2 3) and, upon annealing the sample to a temperature higher than 400 K, the structure changed to a (4 1, 2 5), all the while maintaining the mono-tartrate configuration. In the case of the (4 1, 2 3) structure, the RAIRS results gave rise to the conclusion that adjacent molecules interacted with each other via the OH units in the carboxylic acid groups, therefore forming cyclic bonded dimers. In the case of the (9 0, 1 2) bi-tartrate structure the experiments showed rows of 3 molecules running along the $[1\bar{1}4]$ direction of the crystal. The STM showed an empty two-atom wide space between the rows of molecules which was later referred to as an "empty trough" by theoreticians [57, 58].

The theoretical calculations of Sautet et al came to the conclusion that the adsorption of the TA molecules in the (9 0, 1 2) structure induces stress on the surface, expressed as an increase in the distance between two adjacent copper atoms in the [110] direction of the crystal [57, 58]. In its relaxed form, the Cu(110) surface has an interatomic distance of 2.58 Å in the [110] direction, but upon adsorption of the bitartrate molecules, this distance increased to 2.62 Å. Sometimes the surface stress is released by a restructuring of the (110) surface, like in the case of the added/missing row reconstruction observed for Cu(110) upon adsorption of oxygen [59]. In the case of the (9 0, 1 2) structure of TA however, the calculations were performed on the non-reconstructed surface and the formation of the trough was interpreted as the release of the surface stress induced from the molecular adsorption. It was suggested that the existence of intramolecular hydrogen bonds between the α-hydroxy groups is what stabilizes the structure. However, it is unlikely that the chiral domains of TA are formed due to these bonds, but the formation is rather governed by the substrate [57, 60]. In addition, it was suggested that the molecule undergoes a zig zag distortion of its backbone, something that was later confirmed experimentally by Fasel et al [61].

Fasel et al performed angle resolved X-ray photoelectron diffraction measurements (XPD) on chiral TA on Cu(110) and by measuring the hemispherical intensity distribution of the

photoelectron C1s emission line they could identify the absolute conformation of the molecule on the crystal. The measurements revealed that the molecular backbone was twisted in a zigzag fashion, as shown in Figure 1.7.

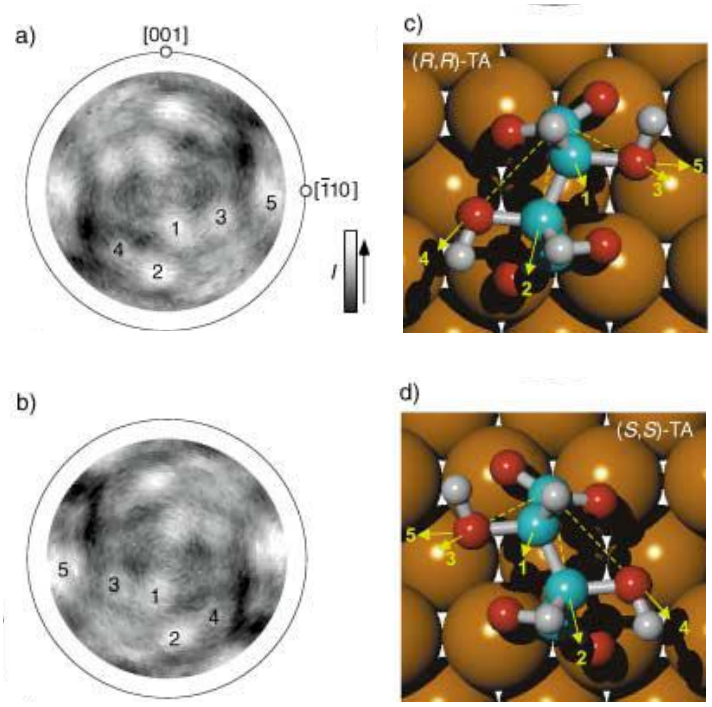

Figure 1.7: a) and b) experimental C1s XPD patterns of (*R,R*)- and (*S,S*)-bitartrate species on Cu(110). c) and d) molecular conformations deriving from the evaluation of a) and b). Adapted from [61].

The achiral component of this compound, meso –TA, has also been investigated by Parschau et al on Cu(110), and based on their LEED and XPS results they suggested the possible configurations of the molecules on the crystal [62, 63]. For a coverage of 0.094 ML the LEED showed an achiral (13 0, 0 5) diffraction pattern. By increasing the coverage to 0.156 the structure changed to a (6 ±1, –1±2) and finally for a coverage of 0.25 ML, the diffraction pattern showed a c(8×2) periodicity. The interesting aspect was that the (6 ±1, –1±2) structure showed similarities with the (9 0, ±1 1) structure observed for (*R,R*)-TA and led to the conclusion that the molecules were, also in this case, bound to the surface in a bitartrate configuration. Models that were developed by DFT calculations showed intramolecular hydrogen bonds between the carboxylate oxygens and those of the hydroxyl groups in C_2 and C_3, whereas an empty trough was again observed between the rows of molecules [62, 63].

Although the different structures obtained by TA when adsorbed on the Cu(110) surface have been widely explored, the effect that its chemisorption has on the substrate itself was only recently investigated by Lawton et al [64]. They showed that at the densely packed configurations of mono-TA on the Cu(110) crystal, the molecule drives the substrate into an atomic reconstruction. This is achieved by removing copper atoms from the top-most atomic rows and forcing them into a chiral configuration on top of the surface, which brakes the symmetry directions of the achiral crystal. Reconstructions of the underlying metal surface have been reported, among others, for formic [65] and benzoic acid [66].

1.3.6 Malic acid

A dicarboxylate – induced reconstruction of the underlying substrate had already been reported by Roth et al for malic acid on Cu(110) [67, 68]. Malic acid is a chiral molecule and another member of the butanedioic acid family, with a hydroxyl group located at carbon 2 (Figure 1.8).

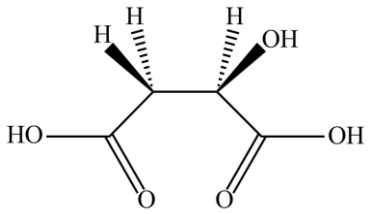

Figure 1.8: Structural model of malic acid (MA).

Both enantiomers and the racemic mixture of the molecule were investigated using an array of different experimental methods. The molecule is special in the sense that not only can it exist in the single and double deprotonated configurations, as described for TA above, but both monomalate and bimalate configurations have additional features of their own. In the monomalate case, the substituted hydroxyl group can either be attached to the second or the third carbon away from the surface, whereas in the bimalate case, rotation of the molecule by 180^{o} leads to a different alignment with respect to its neighbors. For the two enantiomers eleven different structures were identified by LEED and STM, although not all could be observed by both techniques. With the exception of the c(2×4) structure recorded at saturation

coverage, all other structures identified were chiral in nature, many of which were mirror images of each other between the two enantiomers. Interestingly, one of the chiral assemblies exhibited by malic acid is identical to the (9 0, 1 2) structure observed for (*R,R*)-TA. However, in the case of MA the structure was not as well ordered and therefore less stable than that of TA and only observed in small islands on the crystal by STM.

Faint lines were observed by STM, which were running between the molecules along non-symmetry directions of the crystal. They were ascertained as an indication for a reconstruction of the underlying substrate, something that had already been assumed for TA on Cu(110) and Ni(110), but until that time not observed experimentally in STM.

More evidence for the reconstruction of the underlying copper substrate was found with the investigation of racemic malic acid on Cu(110), which showed four different structures, three of which had not been previously observed for the enantiopure compound. Therefore, all of these structures were assumed to be heterochiral, i.e. containing both enantiomers of the molecule. STM clearly revealed rows of adatoms that ran between the molecular lines and along the <1,1> direction of the crystal. Regarding the observed adatoms, it was suggested that they were in fact Cu atoms. Interestingly, a (1 1, –5 2) structure was observed, identical to the (7 0, 1 1) reported earlier for succinic acid [69], another 1,4-dicarboxylic acid. It should be noted again that the difference in notation here is based on new unambiguous rules for naming these structures. The SU structures were discovered before the new rules were set, whereas the malic acid structures were discovered later. The STM experiments showed not only the existence of restructured copper adatoms within the molecular rows, but also areas on the surface where the molecules had apparently desorbed due to the annealing of the sample, leaving behind exposed areas of the reconstructed surface.

1.3.7 Succinic acid

Along with TA and MA, another dicarboxylic acid molecule, succinic acid (SU), has been widely investigated and its results are often compared to those for TA. Succinic acid is an achiral molecule and the most basic member of the butanedioic acid family, with only hydrogen atoms attached to carbons 2 and 3 (Figure 1.9).

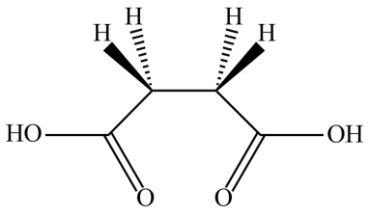

Figure 1.9: Structural model for succinic acid (SU).

This makes it an achiral molecule, but still able to form chemical bonds with a surface, since the metal-bonding oxygen atoms of the carboxylic acid groups are present. Humblot et al investigated SU on a Cu(110) surface and compared the results with those for TA/Cu(110) [60]. According to their experiments, upon adsorption on the surface SU was bound in a doubly deprotonated bisuccinate form. The LEED showed a globally achiral structure that was a superposition of two chiral ones, with the matrix notations (9 0, –1 1) and (1 1, –9 0) describing the two enantiomorphous domains. Upon increasing of the coverage, the situation changed and then two different types of molecules could be detected on the surface, one with a bisuccinate and one with a monosuccinate configuration. In this case the LEED results showed the superposition of the two structures mentioned above and an achiral c(2×4), which was associated with the monosuccinate arrangement of the molecules. The schematic representations for both adsorption geometries are very similar to those reported for TA (Figure 1.5) and can be seen in Figure 1.10. Theoretical calculations performed by Barbosa et al, showed that in the bisuccinate configuration the molecule sustained symmetry breaking in the form of a zig-zag distortion of the molecular backbone [57].

The STM experiments performed for these structures showed islands of the c(2×4) structure coexisting with islands of two chiral structures that were in this case identified as (9 0, –2 2) and (2 2, –9 0). This discrepancy between the <1,1> periodicity of the unit cell observed in the LEED and the <2,2> periodicity of the one in the STM was addressed by 3 models. For the same coverage, Parschau et al later reported another structure for SU, with the notation (7 0, ±1 1) that could be obtained by annealing the sample to 580 K [69].

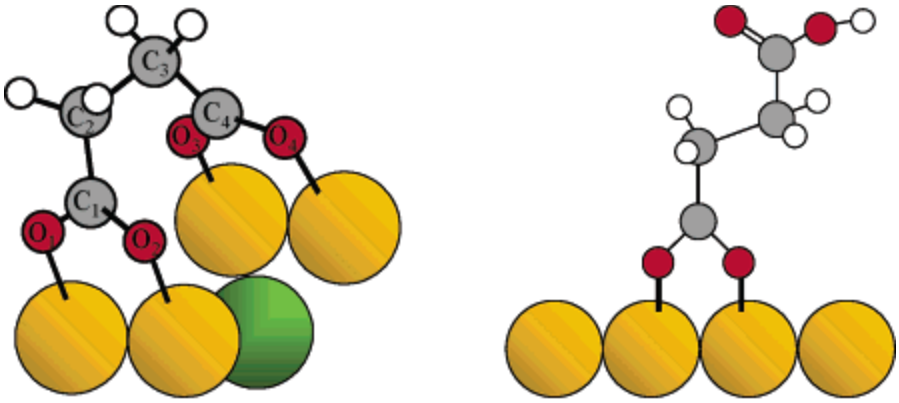

Figure 1.10: Schematic representation of SU adsorbed in its mono- (right) and bisuccinate (left) forms on Cu(110). Adapted from [60].

Upon increasing the amount of molecules to a local coverage of 0.25 ML (1 molecule per 4 Cu atoms) the only structure observed in the LEED was a c(2×4) with a monosuccinate configuration according to the RAIRS. The STM results showed in this case a well ordered achiral c(8×2) structure. As mentioned before, DFT calculations showed that the molecule exhibited enantiomorphism because of a zig-zag distortion of its molecular backbone (Figure 1.11) [70].

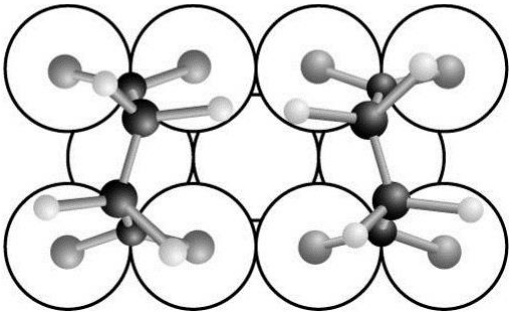

Figure 1.11: Structural models depicting the zig-zag distortion of the SU molecular backbone. Adapted from [70].

Liu et al later reported that for an even higher coverage and consequent annealing of the sample to 473 K, a p(2×4) structure could be observed in the LEED, with the RAIRS now indicating a bisuccinate configuration [71]. Interestingly, this structure showed missing spots in its diffraction pattern, which was explained by the existence of glide planes along the $[1\bar{1}0]$ and [001] directions of the crystal. STM imaging showed the presence of two different

molecular orientations on the crystal, with the molecules exhibiting an offset of ± 65^{o} with respect to the [001] direction of the crystal. Based on this observation it was reported that the produced structure was in fact racemic and built up from homochiral chains. DFT calculations supported these two adsorption geometries and additionally showed that the molecules have to undergo a severe backbone distortion to accommodate this configuration. This model was, surprisingly, energetically more stable than the one with a smaller distortion induced on the molecules.

1.3.8 Desorption of dicarboxylic acids

All of the molecules mentioned above assemble in different structures on the various crystals and can exist in several configurations. Regardless of such differences, they all show similar desorption pathways, as observed by TPD. Upon flash heating of the sample, each molecule desorbs, not as a whole, but instead in fragments that are products of the molecule's decomposition. The usually obtained fragments are CO_2, CO and H_2, with CO_2 having normally the highest intensity. The fact that the molecule decomposes means that the intramolecular bonds break before the metal-molecule bonds.

Raval et al studied the decomposition of SU and TA on a Cu(110) surface and their experiments showed that the (9 0, 1 2) structure of TA decomposes at a temperature of 440 K, whereas the (9 0, 1 1) structure of SU is stable until 600 K, with both molecules showing very sharp decomposition peaks [60]. This led them to the conclusion that the presence of the hydroxyl groups in TA significantly destabilizes the intramolecular bonds, making the molecule more sensitive to the increase of the temperature. Ernst et al described the concept of a "surface explosion" decomposition reaction, which was originally introduced for autocatalytic reactions [72]. In order to start a surface explosion decomposition reaction a carboxylate group must be brought into contact with the substrate. In close packed structures the initial available sites for this to happen are limited and therefore as soon as one molecule decomposes from the surface it leaves an empty space where the carboxylate group of another molecule can be attached and consequently decompose, causing an autocatalytic mechanism. The desorption peaks of such reactions normally exhibit very small full width at half maximum (FWHM) values and shift to higher temperatures with the increase of the coverage [73]. In order to determine if this explosion decomposition is initiated by the existence of defects on the substrate, Gellman et al studied the desorption kinetics of the explosive

decomposition of TA on an achiral Cu(110) surface and a chiral Cu(651) surface [74]. Their results showed that potential defects in the monolayer are not what drives the surface explosion. They also found that, during the process, the surface atoms were forced to reconstruct and TA was then arranged in a (± 6 7, ±2 1) structure that had not been previously discovered. The decomposition reaction of MA has been investigated by Roth et al and in comparison to SU and TA, MA exhibited two decomposition peaks in its TPD spectrum, one characteristic of a surface explosion at 512 K and another broader one and with a smaller intensity at 570 K, which seemed to saturate already at low coverages [75]. The second decomposition peak was attributed to a stable intermediate configuration of the molecule that survives until a higher temperature. Additionally, no differences were observed between the decomposition temperatures of the racemate and the pure enantiomers, as opposed to the situation reported for TA [72, 76].

1.4 Aim of the thesis

As documented in this chapter extensive research has already been performed on the topic of chirally modified crystal surfaces and has produced very interesting results. However, several questions still remain unanswered and others have emerged from the discovered results. To this end, several dicarboxylic acid molecules have been investigated in this thesis, in an attempt to answer as many of these questions as possible. The study of tartaric acid showed that intramolecular hydrogen bonds stabilize the produced structures, whereas succinic acid revealed that chirality transfer derives from the substrate itself and malic acid uncovered a reconstruction of the crystal surface induced by the molecules. To further test the theory regarding the hydrogen bonding, only molecules that lack OH groups as substituents were used here. In order to address the issue of the zigzag binding footprint proposed for SU and to investigate if this really is the reason for the self-assembly of the adsorbed species, molecules with a steric hindrance in their backbone, in the form of double and triple carbon bonds, were investigated. Finally, the potential role of the type and size of the molecular substituents was reviewed, by studying molecules with bulkier substituents.

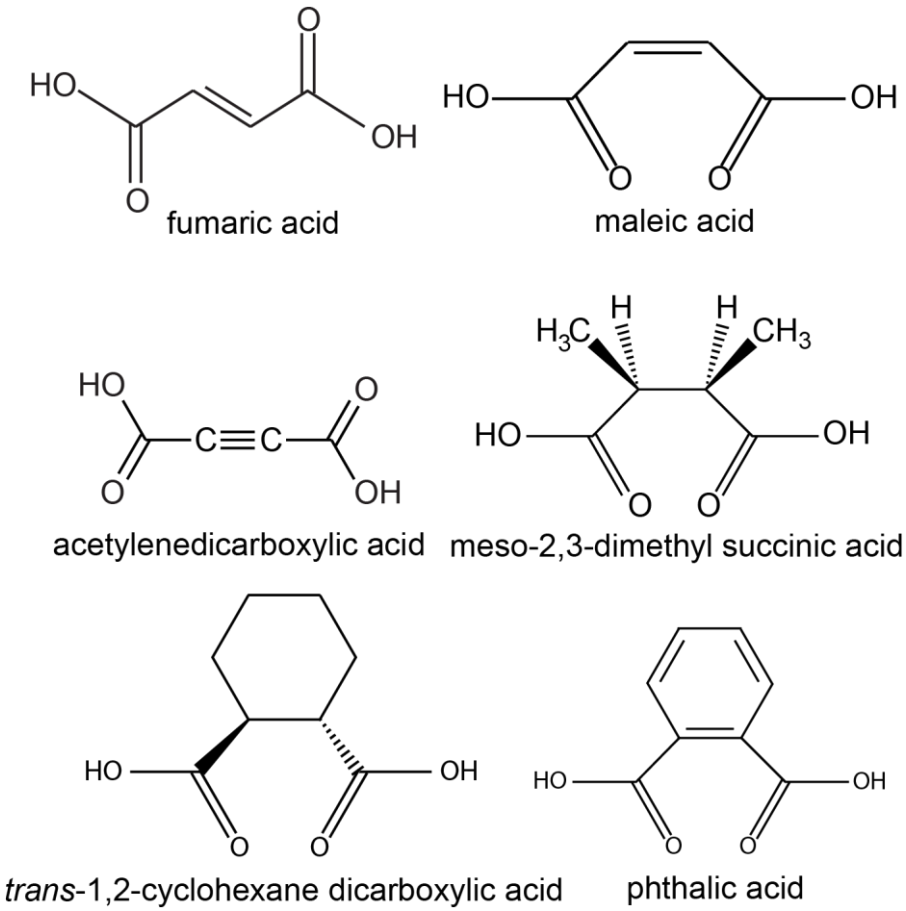

Figure 1.12: 1,4-dicarboxylic acids investigated in this work.

A small introduction on the experimental methods used in this thesis and the preparation routine of the samples can be found in Chapter 2. Chapter 3 addresses the investigation of fumaric acid, examining the existence of a double carbon bond in the molecular backbone, whereas the study of its cis- isomer, maleic acid, can be found in Chapter 4. In Chapter 5 a summary of acetylene dicarboxylic acid is documented, dealing with a triple carbon bond in the molecular backbone. In Chapter 6 the results of the stereoisomers of 2,3-dimethyl succinic acid are reported. Chapter 7 deals with the investigation of *trans*-1,2-cyclohexane dicarboxylic acid and Chapter 8 reports the results for phthalic acid. A small introduction for every molecule can be found in the beginning of each corresponding chapter. The thermal decomposition of the above molecules is documented in Chapter 9 and a comparison and discussion of all systems is given in the conclusions section.

2: Experimental methods

All experiments were performed under UHV conditions (base pressure $\leq 5 \cdot 10^{-10}$ mbar) in two separate chambers. The first chamber (System A) was equipped with facilities for sample cleaning, X-ray photoelectron spectroscopy (XPS), low energy electron diffraction (LEED) and temperature programmed desorption (TPD), whereas the second chamber (System B) had, in addition to the above, facilities for reflection absorption infrared spectroscopy (RAIRS) and scanning tunneling microscopy (STM) measurements.

2.1 Sample preparation

Two different Cu(110) single crystals were used, both purchased from MaTeck. The crystals were cleaned on a daily basis prior to the deposition of the molecules by cycles of Ar^+ sputtering and consequent annealing. The pressure during sputtering was $1 \cdot 10^{-5}$ mbar and a sputtering voltage of 1 kV was used. This amounted to approximately 4 μA of current crystal to ground. After the sputtering process, the crystal was annealed for 2 min at 600^{o}C, in order to obtain atomically flat terraces. The cleanliness of the crystal and its crystallographic quality was then tested by XPS and LEED, respectively. The deposition of the molecules was subsequently performed by evaporation from effusion cells, which were isolated from the main chamber by gate valves and were pumped differentially by a turbomolecular pump, in order to avoid degassing of the molecules and subsequent contamination of the sample. Prior to evaporation the molecules were degassed for 20-30 minutes. After the evaporation the coverage on the crystal was monitored with XPS, by comparing the ratio of the C1s and Cu3s signals of the adsorbed molecules and the crystal, respectively. A more detailed description of the coverage calibration is given in Chapter 3.

2.2 XPS

X-ray photoelectron spectroscopy (XPS), also known as electron spectroscopy for chemical analysis (ESCA), is a surface sensitive spectroscopic technique developed in the 1960s by Kai M. Siegbahn in Uppsala, Sweden, which led to the awarding of the Nobel Prize in Physics in 1981 “for his contribution to the development of high-resolution electron spectroscopy” [77].

XPS works by irradiating a sample with soft X-rays of a specific energy, causing photoelectrons to be ejected from the sample. Depending on the kinetic energy of the ejected electrons, the elemental composition of the sample can be identified and according to the intensity of the ejected photoelectrons the relative concentrations of the detected elements can be determined [78-82]. The principle of XPS is based on the photoelectric effect [83] which is depicted in Figure 2.1.

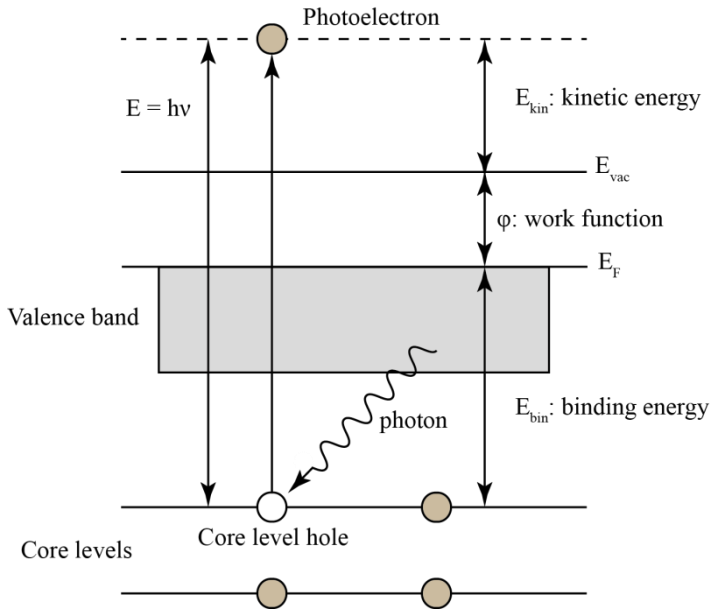

Figure 2.1: The principle of the photoelectric effect.

A core level electron is excited by a photon with energy $E = h \cdot \nu$, resulting in the creation of a core level hole and the emission of a photoelectron with kinetic energy E_{kin}. The binding energy of the electron in its initial state can then be calculated from $E_{bin} = h \cdot \nu - E_{kin} - \varphi$. Since each chemical element has a unique set of core levels, the measured kinetic energy – and subsequently the calculated binding energy – can be used for qualitative analysis of the chemical composition of a sample, whereas the intensity of the observed peaks gives quantitative information. Moreover, any variation of the detected binding energies from reference spectra is an indication of the chemical state of the sampled atoms.

The experimental setup of an X-ray photoelectron spectrometer consists of the X-ray source, the sample, the electron energy analyzer and the electron-counting detector. A schematic representation of such a system can be seen in Figure 2.2.

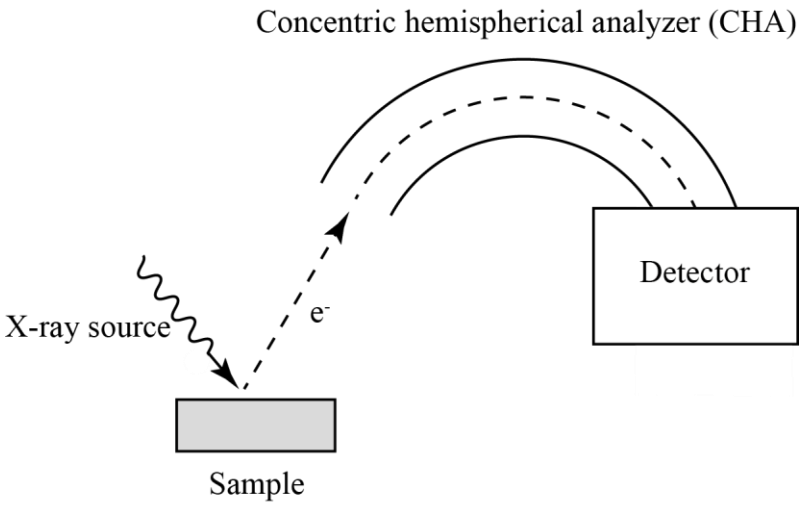

Figure 2.2: Schematic representation of the experimental setup of an XPS.

The X-ray radiation is produced by accelerating electrons from a hot cathode towards a cold metal anode through the application of an electric field. Typical anode materials are aluminum and magnesium, producing radiation with characteristic energies of 1486.6 eV and 1253.6 eV, respectively. The most common electron energy analyzer used is the concentric hemispherical analyzer, where the electrons travel in a circular orbit through the hemispheres. A charge $-V_1$ is applied to the inner plate, whereas a $-V_2$ charge is applied to the outer plate, with $V_2 > V_1$. This difference in potential between the two plates only allows photoelectrons of a certain voltage to pass through to the detector. If they have a too low kinetic energy they crash into the inner plate and if they have a too high kinetic energy they crash into the outer hemisphere. In this way only electrons of a specific voltage will make it to the detector and produce a signal. The large distance that the emitted electrons have to travel, between the sample and the detector, necessitates the use of very low pressures and therefore X-ray spectrometers are typically operated under UHV conditions.

2.3 LEED

Low energy electron diffraction (LEED) is one of the most widely used methods for the determination of surface structures. The first experiment was performed in 1927 by Davisson and Germer [84, 85], who confirmed de Broglie's conjecture of the wave-like nature of particles. LEED can be used both qualitatively and quantitatively. In the former case the

analysis of the diffraction spot positions gives information on the size, symmetry and rotational alignment of the adsorbate unit cell with respect to the substrate, whereas in the latter case the intensities of the diffracted spots are recorded as a function of the intensity of the electron beam, creating in this way so-called I-V curves, which can give information about the atomic positions [86-89].

LEED uses monoenergetic electrons with typical energies of 20-500 eV which are diffracted from a single crystal surface. Diffracted electrons (elastically scattered) and secondary electrons (inelastically scattered) are then back-scattered towards the LEED optics, as seen in Figure 2.3.

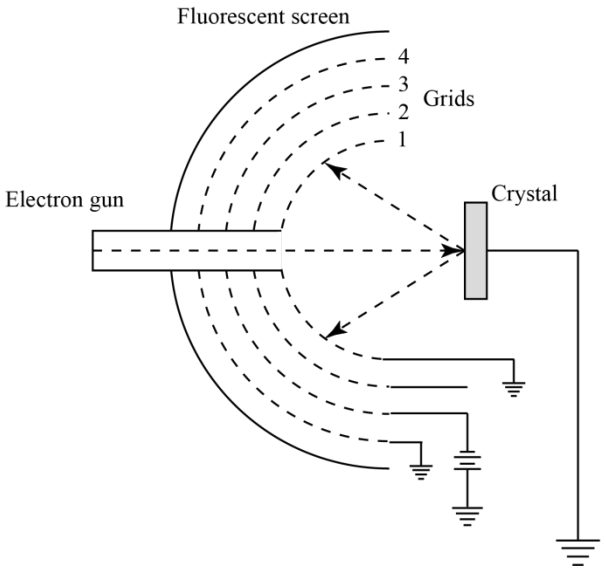

Figure 2.3: Schematic representation of the LEED instrumentation.

Of the four hemispherical concentric grids of the detector, the second and third are kept at a negative potential in order to repel the secondary electrons, therefore filtering the elastically scattered from the inelastically scattered ones. The first and fourth grid are kept at ground potential and after passing them, the elastically scattered electrons are accelerated towards the screen, where they excite the phosphorous film creating the diffraction pattern, which is then captured with a camera.

The resulting diffraction lattice shows in fact the arrangement of the surface unit cell in reciprocal space, Figure 2.4.

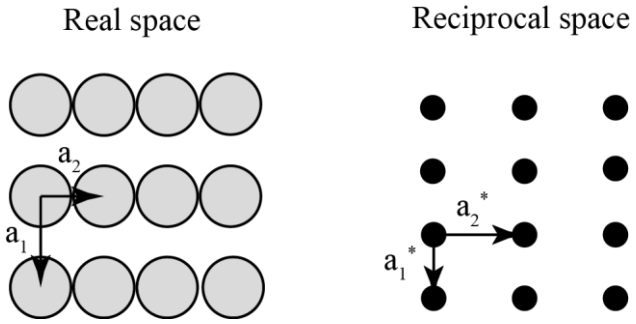

Figure 2.4: Schematic representation of the relation between reciprocal and real space for an fcc(110) surface.

In order to define the real space lattice the relation between the real space and the reciprocal space vectors has to be considered. In particular, if a_1 and a_2 are the real space lattice vectors and a_1^* and a_2^* are the reciprocal lattice vectors, then they are related to each other by:

$$a_1 \cdot a_2^* = a_2 \cdot a_1^* = 0$$

Which means that $a_1 \perp a_2^*$ and $a_2 \perp a_1^*$. There is therefore an inverse relation between a_1 and a_1^*, meaning that:

$$a_1 \cdot a_1^* = |a_1| \cdot |a_1^*| \cdot \cos\theta = 1$$

$$a_2 \cdot a_2^* = |a_2| \cdot |a_2^*| \cdot \cos\theta = 1$$

When the reciprocal and real space vectors are parallel to each other, then $\cos\theta = 1$ and the situation is as follows:

$$|a_1| = \frac{1}{|a_1^*|} \quad \text{and} \quad |a_2| = \frac{1}{|a_2^*|}$$

2.4 RAIRS

Reflection absorption infrared spectroscopy (RAIRS) is an analytical technique that excites vibrations of adsorbed molecules by shining infrared light onto the surface. Its principle of operation is that molecules with a dipole moment can absorb infrared light at specific frequencies associated with the excited vibrations of the molecule. These vibrations are very characteristic for functional groups and can be used in order to determine the binding motif of

a molecule to the surface. Furthermore, surface selection rules help to identify the orientation of molecules adsorbed on the surface. Apart from the qualitative analysis described, RAIRS can also be used for quantitative analysis, by comparing the intensities of different spectra. As the amount of adsorbed molecules increases, so does the intensity of the recorded vibrational bands [90-93].

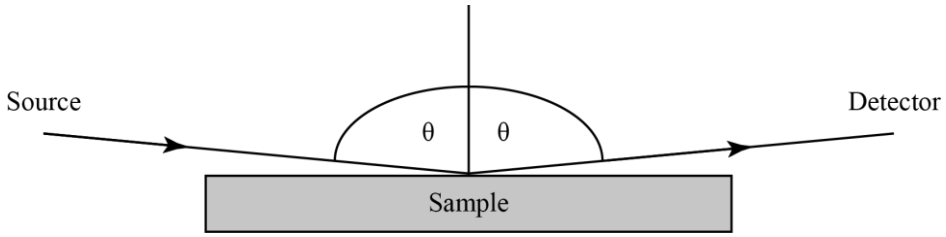

Figure 2.5: Schematic representation of the RAIRS principle of operation

The result is calculated by the application of Lambert-Beer's law, as seen below, and can be expressed by the transmission, T, or the absorption, A, of the IR light:

$$T: = \frac{I_{ads}}{I_{metal}}$$

$$A: = -log(T)$$

With I_{ads} expressing the intensity of the absorbed IR light when molecules are adsorbed on the surface, and I_{metal} expressing the intensity of the absorbed IR light of the clean metal surface.

Typically, several oscillation modes exist. For a linear molecule, for example, with n atoms, the molecule will have 3n – 5 vibrational modes, whereas a non-linear molecule will have 3n – 6 vibrational modes. Not all of these modes are, however, IR active. The vibrational modes that can excited by IR and therefore detected by RAIRS are governed by the "surface selection rules" [91, 93].

The most descriptive explanation of the "surface selection rule" is given by considering the dipole on the metal surface, induced by that of the adsorbed molecules. The molecular dipole will create an image dipole in the electron gas of the metal substrate. If the dipole of the molecule is parallel to the surface, the one of the electron gas will also be parallel, but with an

inverted orientation. This has the effect that the dipole moment changes due to vibrations are cancelled and are therefore invisible to the RAIRS. On the other hand, if the molecular dipole is perpendicular to the surface, then the substrate dipole is also perpendicular and with the same orientation, making the vibration detectable by the RAIRS, i.e. “IR-active” (Figure 2.6).

It has been shown that the best sensitivity for IR measurements on metal surfaces can be obtained by using a grazing-incidence reflection of the IR beam [90]. In this case the S–component of the polarized light parallel to the surface is minimal, whereas the P–component perpendicular to the surface is large. Therefore, the adsorbed molecules are exposed to an oscillating electric field perpendicular to the surface, leading to the excitation of only those vibrational modes with a dynamic dipole moment perpendicular to the surface, offering the best possible sensitivity.

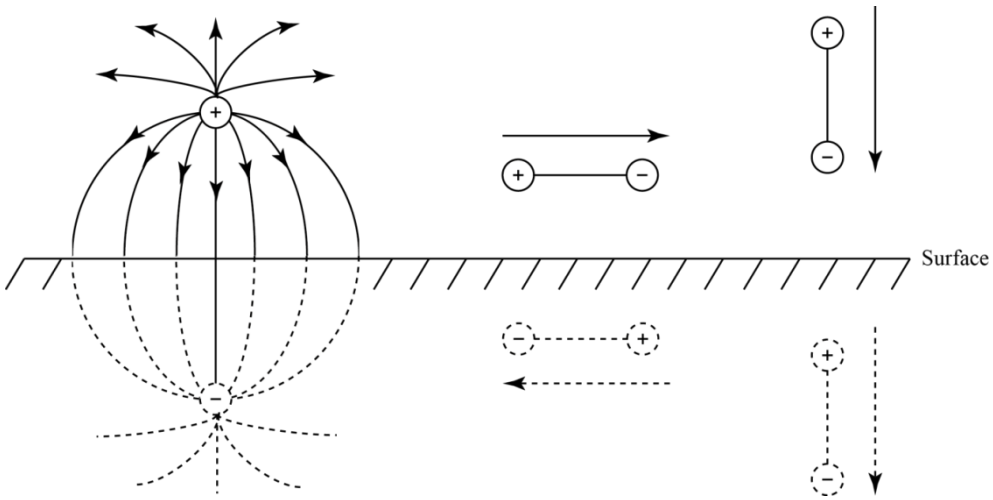

Figure 2.6: Schematic representation of the surface dipole selection rule. From left to right: electric field lines and their image resulting from a positive charge over the surface, dipole moment and its image parallel to the surface, dipole moment and its image perpendicular to the surface.

The use of the surface selection rule can help determine the orientation of a molecule on the surface by the appearance or absence of certain vibrations of the molecule.

2.5 STM

Scanning tunneling microscopy (STM) is an analytical technique for imaging surfaces at the atomic level. It was developed at IBM Zürich and because of its invention Gerd Binnig and Heinrich Rohrer were awarded the Nobel Prize in Physics in 1986 [94-97].

STM is based on the quantum mechanical effect of tunneling. Due to the wave-particle duality electrons have wavelike properties and therefore when they reach a barrier that they classically would not be able to overcome as particles, their wavelike properties come into effect. In the barrier the wave function ψ describing the electron starts to decay, but if the barrier is thin enough, then the probability function, which is proportional to $|\psi \cdot \psi^*|$, could extent to the other side, making some of the electrons capable to tunnel through the barrier. However, if the barrier is broad, then the wave will not be able to tunnel through [95-100]. This is described schematically in Figure 2.7.

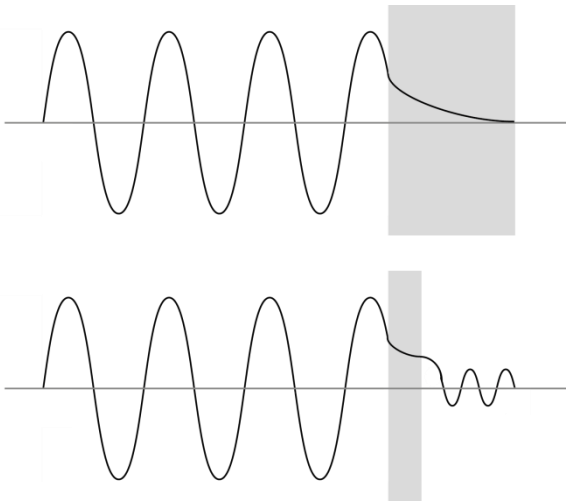

Figure 2.7: Schematic representation of a diminishing wave function through a barrier. If the barrier is too wide then the wave function cannot tunnel through, but if the barrier is thin then tunneling takes place.

In the case of a rectangular potential well it can be shown that the wave function of an electron inside it can be written as [100]:

$$\psi = e^{\pm kd}$$

With $k = \sqrt{2m(V_B - E)/\hbar^2}$

Where E is the energy of the electron, V_B is the potential of the barrier and $\hbar$ the Plank constant. The tunneling current is proportional to $|\psi \cdot \psi^*|$ and therefore decays exponentially with the width of the potential well:

$$I \propto e^{-2kd}$$

Applying this theory to the actual STM measurement, the starting point of the electrons is the Fermi level of the tip or the sample and the barrier that the electrons have to tunnel through is the vacuum gap between the two. By monitoring the current through this barrier a good control of the tip-sample distance can be achieved. A prerequisite for the tunneling to be able to take place is that the Fermi level of the tip has to match a certain level in the molecule. This can be achieved by applying a bias voltage between tip and sample, thus allowing the tunneling of electrons from the tip Fermi level into an unoccupied molecular orbital, or from an occupied molecular orbital into the Fermi level.

There are two principle scanning modes in STM, the constant current mode (CCM) and the constant height mode (CHM), schematic representations of which can be seen in Figure 2.8. In the constant current mode the tunneling current is held constant via a feedback loop while the tip scans the surface, providing in this way information on the topography of the sample. In constant height mode the tip is held at a constant voltage (height) while it scans over the surface. The resulting image presents the changes of the tunneling current over the surface, giving information about the charge density. The measurement is faster than in the CCM case, but it is only suitable for very flat surfaces, due to danger of the tip crashing on the sample.

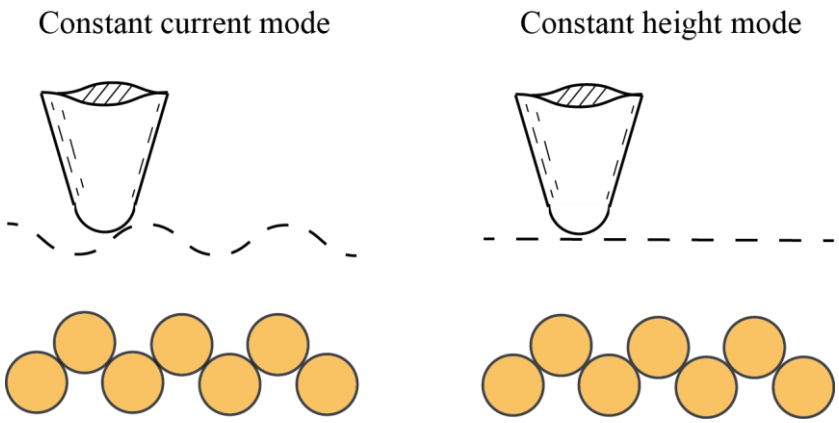

Figure 2.8: Schematic representations of the constant current and constant height STM modes of operation.

Historically, during the STM measurement the tip position was controlled by three piezoelectric actuators, each of them controlling one direction where the tip can travel. These were ceramic positioning devices, to each of which a certain voltage could be applied, making them expand or contract, moving in this way the tip in the desired direction. Contemporary STM systems, including the one used in this thesis, are equipped with piezoelectric tube actuators, which exhibit superior insensitivity to vibrations. In this case only one piezoelectric tube exists, made of two concentric electrodes, the outer of which is divided into four equal quarters. The x–y position of the tip is adjusted by the bending of the tube when voltage is applied to two adjacent quarters of the outer electrode, whereas application of a voltage to the inner electrode adjusts the z position. The tunneling current and the piezoelectric voltage are monitored and depending on the desired mode of operation (CCM or CHM) the respective voltage is adjusted (Figure 2.9).

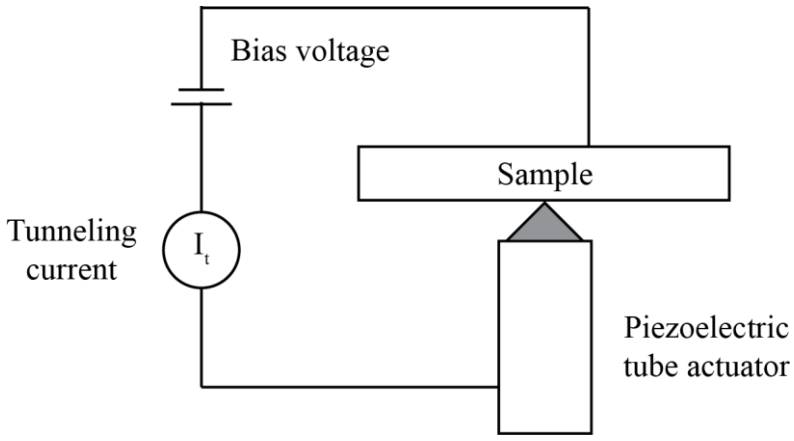

Figure 2.9: Schematic representation of the experimental STM setup.

2.6 TPD

Temperature programmed desorption (TPD) is a method for observing the desorption process of molecules from a metal surface. The crystal sample with the adsorbed molecules is heated, with a steady heating rate, and the partial pressures of the desorbing atoms or molecules are measured by a mass spectrometer. It is a very quick and simple method that can give information about the activation energy of desorption and the order of the kinetic reaction [101-105]. It is however destructive, which means that the adsorbed species cannot be retrieved as whole. In cases where the molecule-metal bonds are stronger than the intermolecular bonds the latter break first and only decomposition products leave the surface

and reach the mass spectrometer. In the case of reversible non-activated adsorptions, i.e. when the adsorbate desorbs upon heating without the existence of an activation barrier, the heat of adsorption can be calculated from the TPD experiment, since it is equal to the heat of desorption [101].

In the case of autocatalytic decomposition kinetics described in chapter 1.3.8, the decomposition peak shifts strongly to higher temperatures with increasing coverage and at saturation the desorption peak becomes very narrow [73].

TPD experiments are performed under UHV conditions and the principle experimental setup is shown in Figure 2.10.

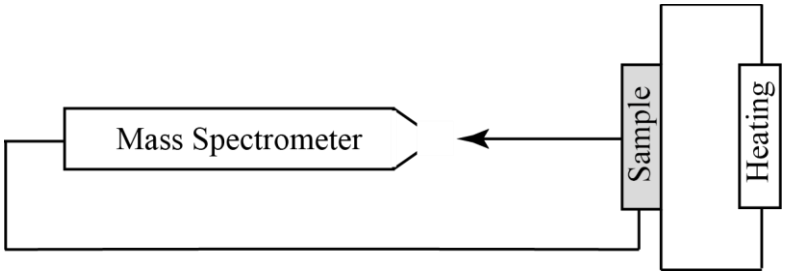

Figure 2.10: Schematic representation of the setup of a TPD experiment.

During the TPD experiments the single crystal surface is usually oriented in front of the quadrupole mass spectrometer in a short distance. The crystal is heated with a steady heating rate, causing the molecules adsorbed on the crystal to desorb and fly into the mass spectrometer where their masses are recorded. A connection between the mass spectrometer and the thermocouple of the crystal allows direct recording of the crystal temperature during the experiment. The resulting spectrum shows the relation of the partial pressure of the detected fragments against the corresponding temperature.

3. Fumaric acid

Fumaric acid (FUA) or trans-butenedioic acid is a chemical compound with the structural formula shown in Figure 3.1. It was first isolated from the herb *Fumaria officinalis* by the German chemist F. L. Winckler in 1832, who gave it the name Fumarsäure, or fumaric acid. It was re-discovered two years later by the French chemist Théophile Jules Pelouze, who distilled malic acid and ended up with two different compounds that had the same structures but different properties [106]. With the development of modern stereochemistry it became clear that those two compounds were the cis and trans isomers of the same compound, named maleic and fumaric acid.

Fumaric acid has a double bond between carbons two and three, with the four carbon atoms being sp^2-hybridized. They therefore lie within a single plane, creating a steric hindrance which should eliminate any chiral zigzag distortion in the molecular backbone, as the one suggested for succinic acid [70]. The molecule can bind on the surface with similar configurations as those described for SU, TA and MA, i.e. in a *monofumarate* arrangement with one of the carboxylic acid groups deprotonated, or in a *bifumarate* arrangement with both carboxylic acid groups deprotonated (see Figures 1.5 and 1.10 for these two adsorbate modes in the case of TA and SU).

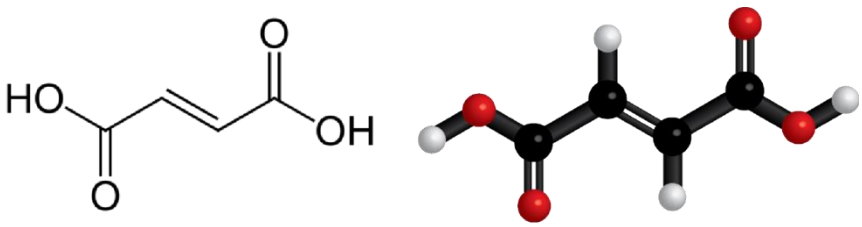

Figure 3.1: Structural formula and ball-and-stick model for fumaric acid.

3.1 XPS

The saturation point at RT of the amount of adsorbed molecules is observed experimentally with XPS by monitoring the intensity of the C1s peak as compared to one of the copper peaks. That is, a calibration of the coverage is performed by dividing the area of the C1s peak of the

adsorbates with that of the Cu3s peak of the substrate, after performing Shirley background subtraction on both XPS spectra. Figure 3.2 shows the C1s/Cu3s ratio with increasing exposure time of the Cu surface to the molecular effusive beam. The inset shows a series of C1s spectra with increasing coverage. The C1s/Cu3s value increases with increasing exposure until it becomes stable after approximately 15 min of evaporation. Such saturation is explained by the limited number of adsorption sites on the crystal surface, allowing only a certain amount of molecules to be accommodated in the first layer. For fumaric acid the C1s/Cu3s ratio is 0.43 at saturation coverage (Figure 3.2). However, when the crystal sample is cooled below room temperature (RT) more molecules can be physisorbed in additional layers on the surface. These layers, however, desorb upon heating below RT. Consequently, evaporation of the molecules onto the crystal surface at RT leads to saturation after some time.

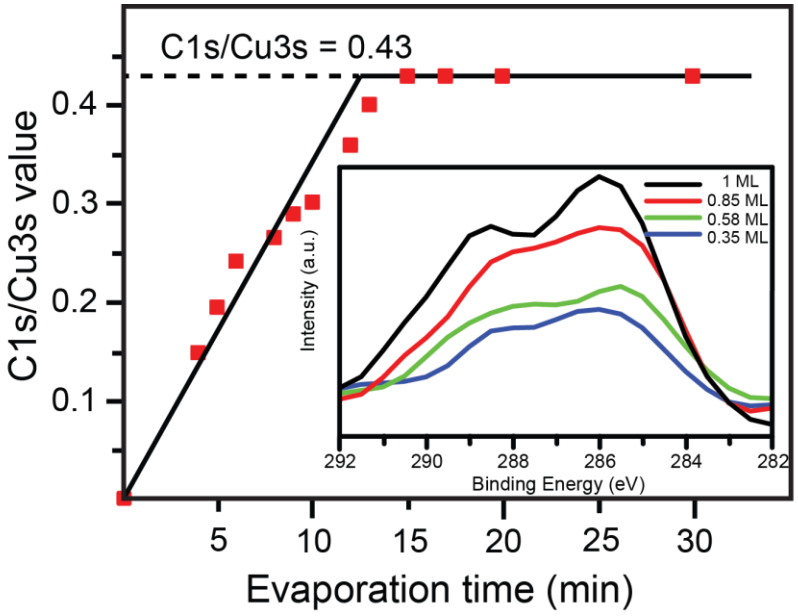

Figure 3.2: Coverage versus evaporation time. The C1s/Cu3s ratio was calculated after Shirley background subtraction for binding energies between 282-291 eV. The inset shows the C1s spectra for different coverages.

It should be noted that this is the situation when the molecular cell has a temperature of 343 K. When the temperature of the evaporation cell is increased or decreased, the amount of time taken to reach the saturation point changes accordingly. However, once the saturation coverage is reached the value of the C1s/Cu3s ratio remains the same.

In order to analyze the binding mechanism of FUA (monofumarate/bifumarate) on the crystal, peak fitting of C1s XPS spectra for two ordered structures (named (1 1, –5 2) and (1 1, –6 3), see chapter 3.2) was performed (Figure 3.3). In the case of a single deprotonated configuration (monofumarate), the XPS spectrum would consist of three different peaks with a ratio of 1:2:1, corresponding to the signal obtained by the -COO^-, -CH and -COOH parts of the molecule, respectively. In the case of a doubly deprotonated configuration (bifumarate), the XPS spectrum would consist of two peaks with a ratio of 1:1, this time corresponding to the signals obtained by the -COO^- and -CH parts of the molecule.

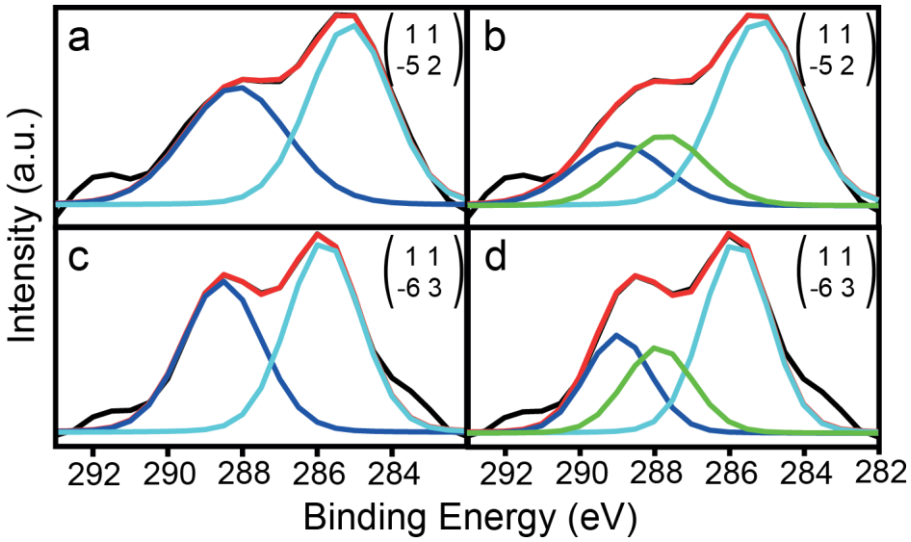

Figure 3.3: Fitted C1s XPS spectra. The black line depicts the spectrum as measured, whereas the red line represents the sum of the fitted peaks. a) (1 1, –5 2) structure fitted with 2 peaks; b) (1 1, –5 2) structure fitted with 3 peaks; c) (1 1, –6 3) structure fitted with 2 peaks; d) (1 1, –6 3) structure fitted with 3 peaks.

The specific positions of the fitted peaks depicted in Figure 3.3 are listed in Table 3.1, along with values for (*R*,*R*)-TA and MA from the literature.

Table 3.1: The C1s binding energies in eV obtained from the peak fitting of the curves presented in Figure 3.3. Values from the literature are also listed for TA [63].

	Monofumarate		**Bifumarate**		**Mono-**	**Bi-**
	(1 1, –5 2)	**(1 1, –6 3)**	**(1 1, –5 2)**	**(1 1, –6 3)**	**(*R*,*R*)-TA**	**(*R*,*R*)-TA**
COO-	287.7	287.8	288.2	288.5	287.8	287.9
COOH	289	289	-	-	288.4	-
=C(H)-	285.2	285.8	285.1	285.8	-	-

Unfortunately, it is possible to perform a satisfactory fitting of the spectra for both adsorbate modes, meaning that XPS fitting cannot conclusively reveal if the molecules are in a mono- or bifumarate arrangement. RAIRS was used instead to help with this identification.

3.2 LEED

Unless stated otherwise, the experimental procedure for obtaining LEED patterns is the same for all molecules investigated in this work. Different amounts of the compounds are adsorbed on the crystal at RT, followed by investigation with LEED. When no ordered structures are observed, the crystal is annealed for a certain time (ranging from 15 to 90 min) at various temperatures (typically 323 – 523 K). The heating is interrupted at intervals of 15 min, the crystal is allowed to cool down to RT and is subsequently investigated with LEED. When a structure is observed, its stability to prolonged heating is tested, as well as its resistance to heating at higher temperatures.

Upon adsorption of FUA on the crystal at RT only a low quality c(2×4) structure is observed at monolayer saturation. However, subsequent annealing of the crystal leads to several well-ordered structures. A phase diagram describing all these structures is presented in Figure 3.4 and the resulting LEED patterns are shown in Figure 3.5.

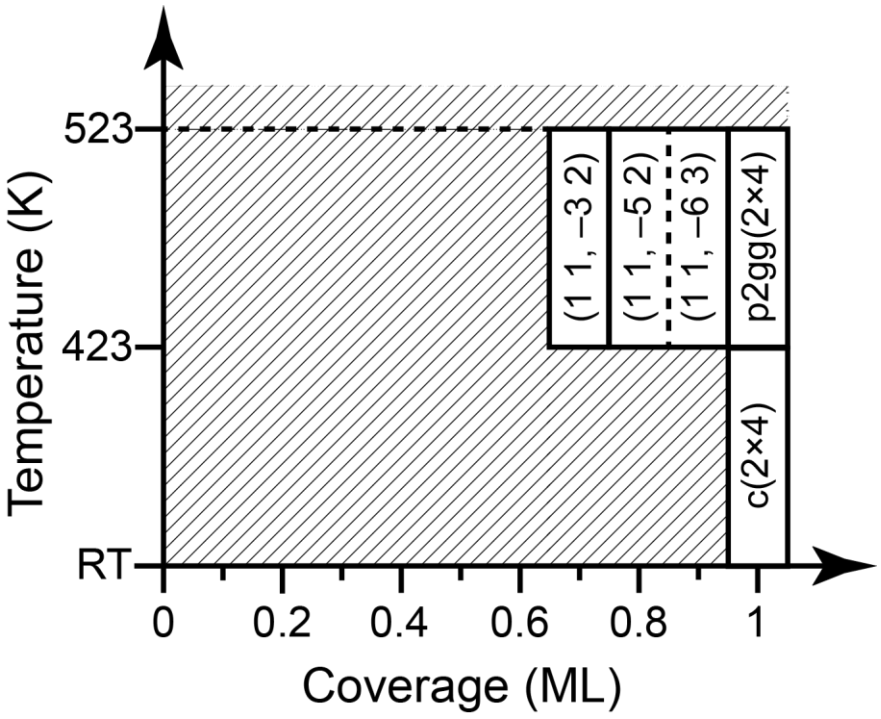

Figure 3.4: Phase diagram for FUA on Cu(110), i.e. observed structures in LEED depending on coverage and annealing temperatures. No structures were observed at conditions represented by the shaded areas.

After annealing the saturated crystal at 373 K for 15 min the low quality c(2×4) becomes much more defined, showing now sharp diffraction spots and low background intensity (Figure 3.5a). A model of this structure is shown in Figure 3.5g. Further annealing of the same structure at 423 K for 15 min causes a transition into a well-ordered p(2×4) structure with missing (0,n) spots, n = 1/2 , 3/2, etc and missing (n,0) spots, n = 1/4, 3/4, etc. This suggests the existence of glide planes parallel to the [001] and $[1\bar{1}0]$ directions of the crystal. The same LEED structure, also with the indication of glide plane symmetry being present, was previously reported for SU [71]. This structure belongs to the p2gg plane group and is therefore called p2gg(2×4) in the following. A model describing this structure is shown in Figure 3.5h. The model accounts for the presence of the glide planes in the [001] and $[1\bar{1}0]$ directions of the crystal. As indicated in Figure 3.4, for coverages below 0.7 ML no ordered structures were observed under all experimental conditions. For coverages between 0.7 and 0.85 ML and after annealing the crystal at 423 K for 15 min, three different enantiomorphous structures are observed (Figure 3.5c-e). All three of them are actually composed of the superposition of mirror domains. This observation is explained by a coexistence of enantiomorphous domains with lateral sizes smaller than the probing electron beam diameter. With increasing coverage these are a (1 1, –3 2) at 0.7 ML, a (1 1, –5 2) at 0.78 ML and

finally at a coverage of 0.81 ML the diffraction spots of a (1 1, –6 3) and a c(2×4) structure appear together. At coverages between 0.81 and 0.93 ML the (1 1, –5 2) and (1 1, –6 3) phases coexist, but prolonged annealing at 423 K leaves only the (1 1, –5 2) structure on the surface and XPS shows a small decrease in coverage. All FUA-induced LEED patterns are observed up to 473 K, whereas at higher temperatures they disappear and XPS measurements show a decrease in coverage.

The LEED pattern of the (1 1, –5 2) structure (Figure 3.5d) shows weak stripes running parallel to the <1,1> and <1,–1> directions of the crystal, but at ½ of that periodicity, suggesting an additional (2, ±2) periodicity in real space. This is an indication of two different sublattices, possibly molecular and substrate lattice, with one of them being either a weaker scatterer or poorly ordered.

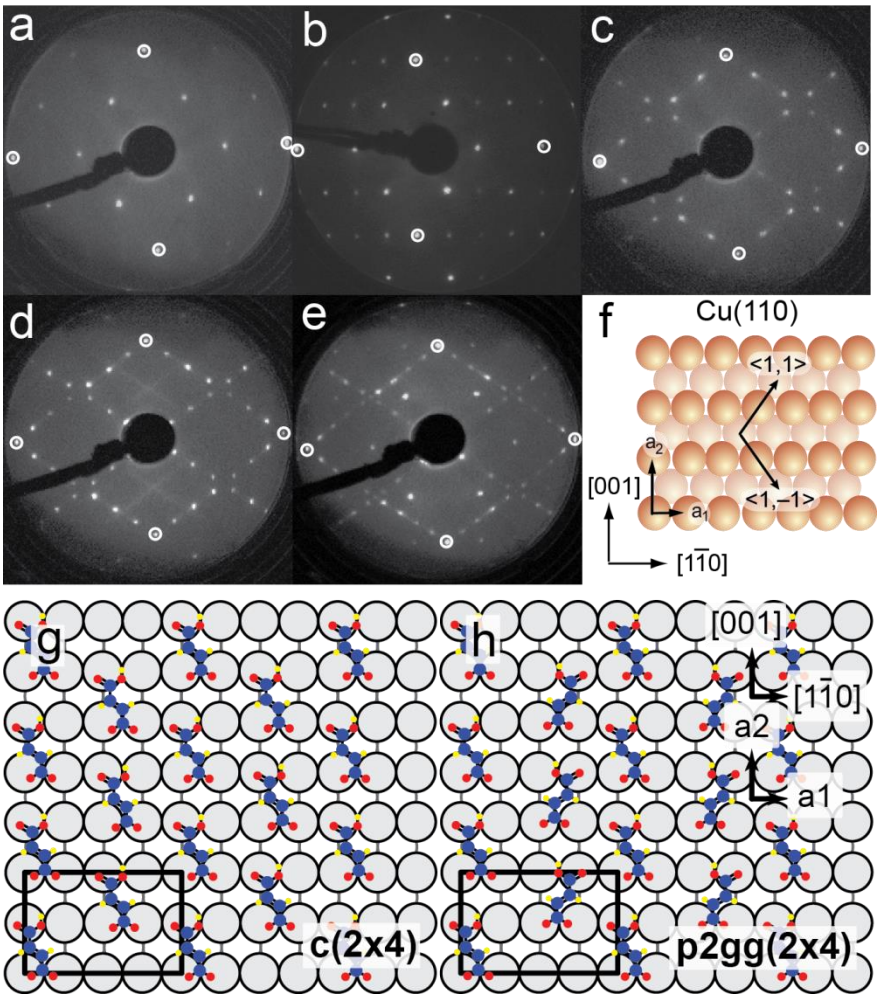

Figure 3.5: LEED patterns of FUA on Cu(110). The 1×1 diffraction spots of the clean copper surface are marked with circles. a) c(2×4) structure, E_p = 48 eV; b) p2gg(2×4) structure, E_p = 53 eV; c) (1 1, –3 2) structure, E_p = 56 eV; d) (1 1, –5 2), E_p = 53 eV, the faint lines in the background suggest an additional (2,2) periodicity; e) (1 1, –6 3) structure coexisting with a c(2×4) structure, E_p = 52 eV; f) real space lattice of the Cu(110) surface aligned to the same orientation as the LEED patterns; g, h) tentative models of the c(2×4) and p2gg(2×4) structures.

3.3 RAIRS

All assignments of the IR vibrations described in this thesis are based on literature [49, 50, 54, 60, 67, 68, 107-110]. Figure 3.6 shows a series of IR spectra for different coverages on the crystal. For all coverages an intense band can be detected around 1420 cm^{-1}, which is assigned to the symmetric OCO stretching vibration. This indicates that at least one of the carboxyl groups is deprotonated and bound to the Cu. The asymmetric OCO stretching vibration is observed at around 1530 cm^{-1}, albeit with much lower intensity. Since the strong C=O stretching vibration can be detected around 1700 cm^{-1}, it is clear that the other carboxyl group is not bound to the substrate. This is confirmed by the presence of the broad band at 3159 cm^{-1}

which is associated with the stretching vibration of the OH entity in the carboxylate. It should be noted here that part of this vibration can also be attributed to the water condensing in the detector of the RAIRS. The three vibrations at high wavenumbers, at 3088 cm^{-1}, 3050 cm^{-1} and 2930 cm^{-1} give information about the state of the double bond between carbons 2 and 3. Since the two former ones are both characteristic of olefinic CH stretching modes, it seems that the two hydrogen atoms are in different chemical environments. The reason for observing different CH stretch vibrations could be due to the fact that only one carboxyl group is interacting with the surface, therefore making the CH groups chemically dissimilar. Alternatively, an interaction of the double bond with the surface could also have an influence on the chemical states of both CH groups.

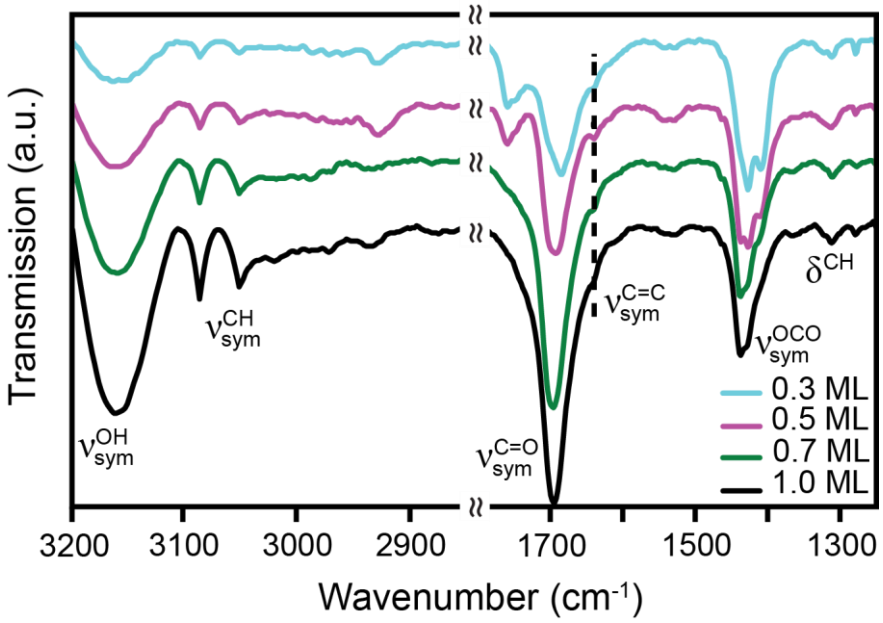

Figure 3.6: RAIRS spectra showing the transmission of a coverage series of FUA adsorbed at RT, with no additional heating treatment. All spectra show a strong C=O vibration band around 1700 cm^{-1}, which suggests a monofumarate configuration.

A weak band at 2930 cm^{-1}, representing alkane CH vibrations, is observed as well, indicating partial hydrogenation of the double bond. However, the stretching vibration of the carbon double bond can be detected in the form of a shoulder at 1640 cm^{-1}. This observation suggests that the adsorbate layer is not homogeneous in its entirety. Moreover, the low intensity of the stretching vibration for the double bond could be an indication of the orientation of the molecules on the surface. If the surface selection rule is considered, the low intensity of this

vibration could simply mean that the molecules are oriented with the double bond almost parallel to the surface. Finally, the fact that at low coverages a splitting of both the $\nu_{sym}^{C=O}$ and the ν_{sym}^{OCO} is observed, further supports the scenario of different adsorbate modes in the molecular layer. It should be noted here, that the shape of the bands around 2930 cm^{-1}, which are characteristic of alkane vibrations and which are attributed to the potential hydrogenation of the C=C could be due to a contamination of the FTIR spectrometer. It seems that those bands grow with time, i.e. when the optical parts get warm and outgassing occurs. All bands with their respective assignments are listed in Table 3.2.

Table 3.2: Frequencies and assignment of vibrational modes identified for a non-tempered sample, the two achiral and one enantiomorphous structure (sh: shoulder, w: weak, b: broad, s: strong, m: medium).

Mode	0.5 ML	c(2×4)	p2gg(2×4)	(1 1, –5 2)
ν_{sym}^{OH}	3159 b,m	3159 b,m	3159 b,m	3159 b,m
ν_{sym}^{CH}	3085 s,m	3085 s,m	3085 s,m	3085 s,m
	3050 b,w	3050 b,w	3050 b,w	3050 b,w
ν_{sym}^{CH}	2928 w	2929 w	2928 w	2931 w
$\nu_{sym}^{C=O}$	1759 w	1709	1680	1709
	1693 s	1683		1688 sh
$\nu_{sym}^{C=C}$	1640 sh		1645 sh	
ν_{asym}^{OCO}	1535 w	1592 sh	1519	1599 sh
ν_{sym}^{OCO}	1437 b	1428	1429	1428
	1425 b	1415 sh	1416 sh	1418
	1408 b			1400
δ^{CH}	1313 w		1311 w	1317 w

RAIRS measurements were also performed on three ordered structures. The spectra of the well-ordered c(2×4), the p2gg(2×4) and the enantiomorphous (1 1, –5 2) are shown in Figure 3.7. The vibrations with their assignments are also listed in Table 3.2. The same major vibrations observed for the non-tempered samples are identified for the three ordered structures. However, the symmetric ν^{OCO} is more pronounced in the case of the (2×4) structures, and shows a triple splitting for the (1 1, –5 2) structure. The higher intensity of this

vibration indicates that more molecules are now bound to the surface with both carboxylate groups, in a bifumarate configuration. Consequently a significant decrease in the intensity of the $\nu^{C=O}$ vibration is detected.

The splitting of the ν_{sym}^{OCO} band in the case of the (1 1, –5 2) structure stands for different carboxylate groups, either in a single bifumarate or in two different adsorbate species. Strain within the –COO groups of a bifumarate may explain a shift in wavenumber with respect to the value observed for monofumarate.

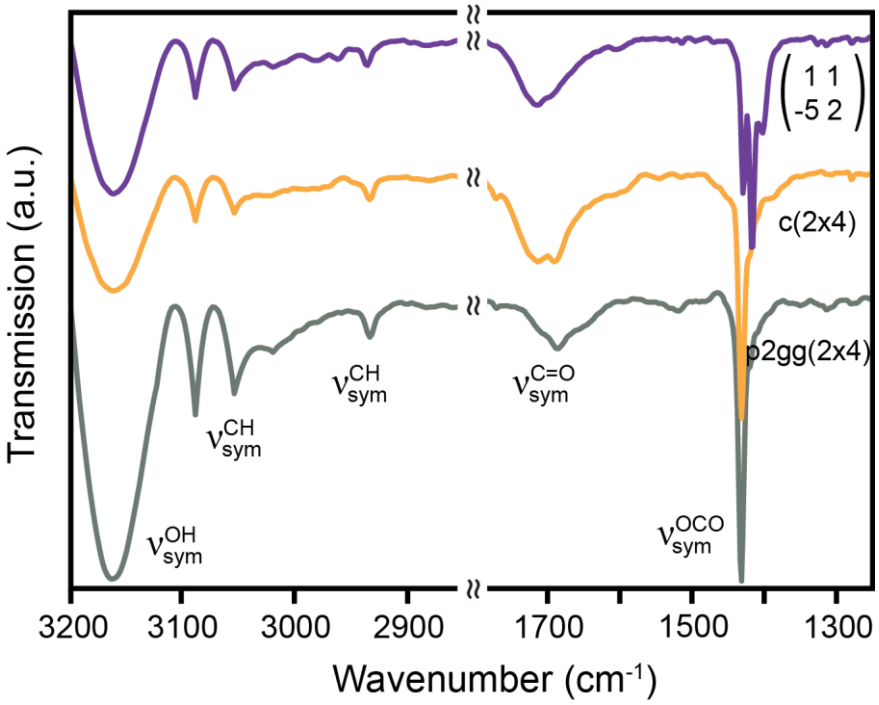

Figure 3.7: RAIRS spectra showing the transmission of one enantiomorphous and the two achiral structures of FUA. Compared to the non-tempered samples, here a much smaller intensity of the C=O stretching mode can be observed, as well as a splitting of the OCO vibrational band in the (1 1, –5 2) structure.

3.4 STM

STM experiments were performed for the (1 1, –5 2) and (1 1, –6 3) structures. In Figure 3.8 the results for the (1 1, –5 2) structure are shown. The brighter, slightly stretched-out features represent the molecules, but additional fainter lines running between the molecular rows are observed as well in the STM images (Figure 3.8a). High resolution imaging (Figure 3.8d and f) reveals that the faint lines actually consist of smaller round features. In areas on the crystal

with no adsorbed molecules these round features are easier to identify. Similar results were reported for malic acid (MA) [68]. It was then concluded that the small features were Cu adatoms on the underlying copper surface. The faint lines in the STM images, running along the <1,–1> direction of the surface, are therefore assumed to be Cu adatoms here as well. The slight annealing needed to obtain the (1 1, –5 2) structure is presumed to cause the desorption of a small amount of molecules, which eventually leads to the creation of the empty patches shown in Figure 3.8d.

An investigation of the distances between two adjacent molecules and two adjacent atoms along the <1,±1> direction of the crystal revealed that the periodicity of the molecules is doubled with respect to that of the atoms (Figure 3.8b). This leads to the existence of two distinct unit cells, describing the arrangement of the molecules and copper adatoms, respectively. The Cu-atomic unit cell is the same as the one identified from the sharp diffraction spots in LEED, whereas the molecular unit cell exhibits a (2, ±2) periodicity, observed as faint lines in LEED. Models for the molecular and atomic unit cells are shown in Figures 3.8c and e, respectively.

Figure 3.9 shows the (1 –1, 6 3) structure, which coexists with the c(2×4). This is the enantiomorph of the (1 1, –6 3) structure which can alternatively be named $(1\ 1, -6\ 3)^{M}$ [48]. As shown in Figure 3.9a, this structure is not as well ordered as the (1 1, –5 2). Instead, in some cases two molecules are next to each other, whereas in other areas there is only a single molecule in the row. Switching the polarity of the tunneling current and voltage allows the identification of faint features aligned between the molecular rows, suggesting also here a reconstruction of the underlying copper substrate (Figure 3.9b). Interestingly, as in the case of the (1 1, –5 2) structure, line scans along the <1,–1> direction revealed that the molecules follow a (2,–2) periodicity, instead of the (1,–1) identified in the LEED. The molecules are therefore arranged in a (2 2, –6 3) unit cell. The (1 1, –6 3) unit cell identified in the LEED is most likely due to the reconstruction of the underlying copper surface.

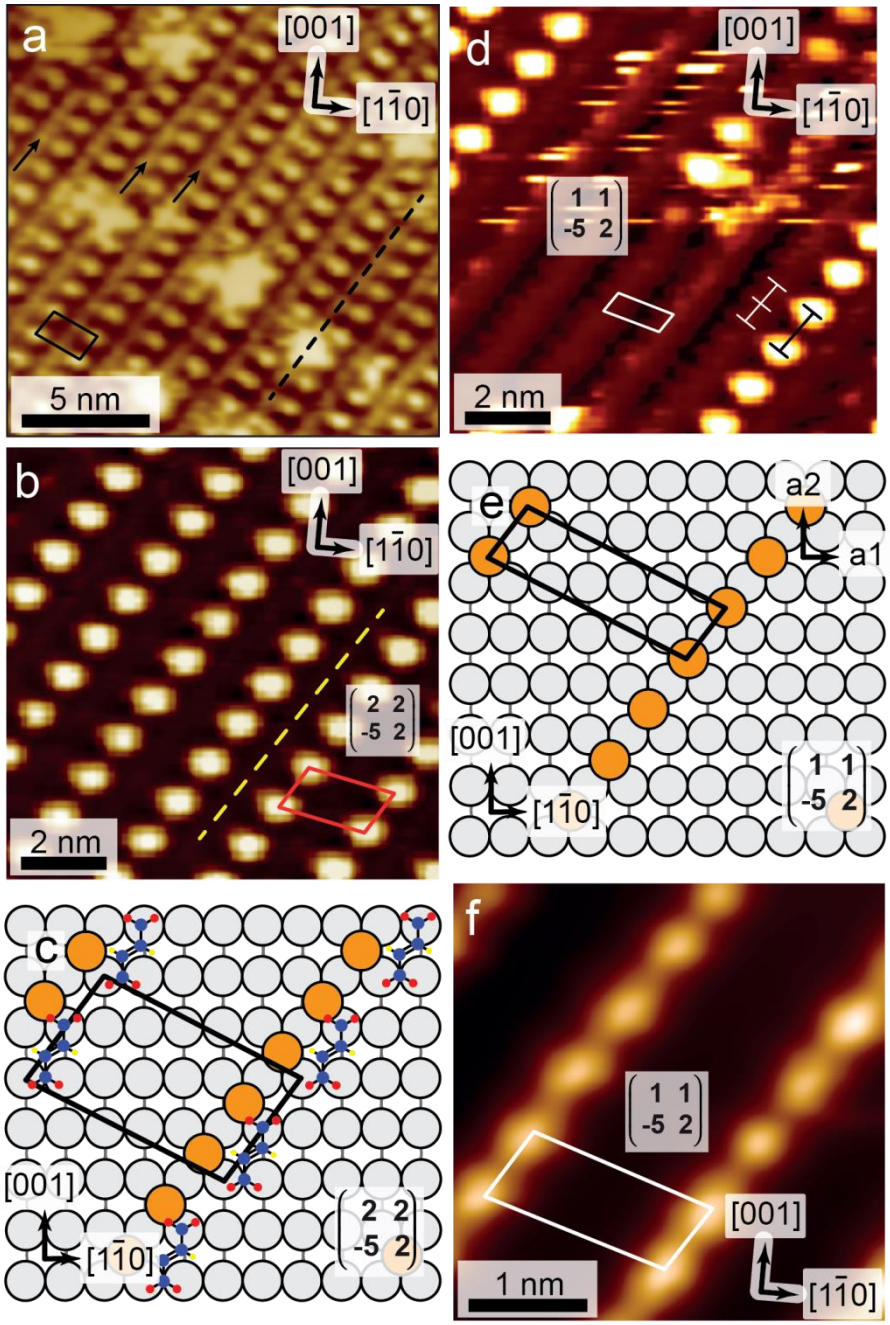

Figure 3.8: STM images of chirally reconstructed (1 1, –5 2) domains. a) STM image (16.9 nm × 16.9 nm, I = –630 pA, U = –423 mV) of the (1 1, –5 2) structure. The bright, elongated features represent the molecules, with the weaker features in-between (indicated by arrows) portraying the reconstructed copper atoms; b) close-up STM image (10.1 nm × 10.1 nm, I = –600 pA, U = –478 mV) of the same domain. The molecular cell indicated has double the periodicity observed in LEED in the <1,–1> direction. The dashed lines in a and b indicate translational domain boundaries; c) model of the reconstructed surface with the molecular unit cell. The model is rotated in such a way to match the orientation of the crystal. The substrate vectors are indicated in e; d) STM image (10.1 nm × 10.1 nm, I = –600 pA, U = –478 mV) of an area on the crystal devoid of molecules. The difference between the molecular and atomic periodicities can easily be observed here; e) model depicting the unit cell of the copper adatoms in the areas where no molecules are present; f) high resolution STM image (3.6 nm × 3.6 nm, I = –360 pA, U = –423 mV) revealing Cu adatom rows along the <1,–1> direction. Image averaged 5×.

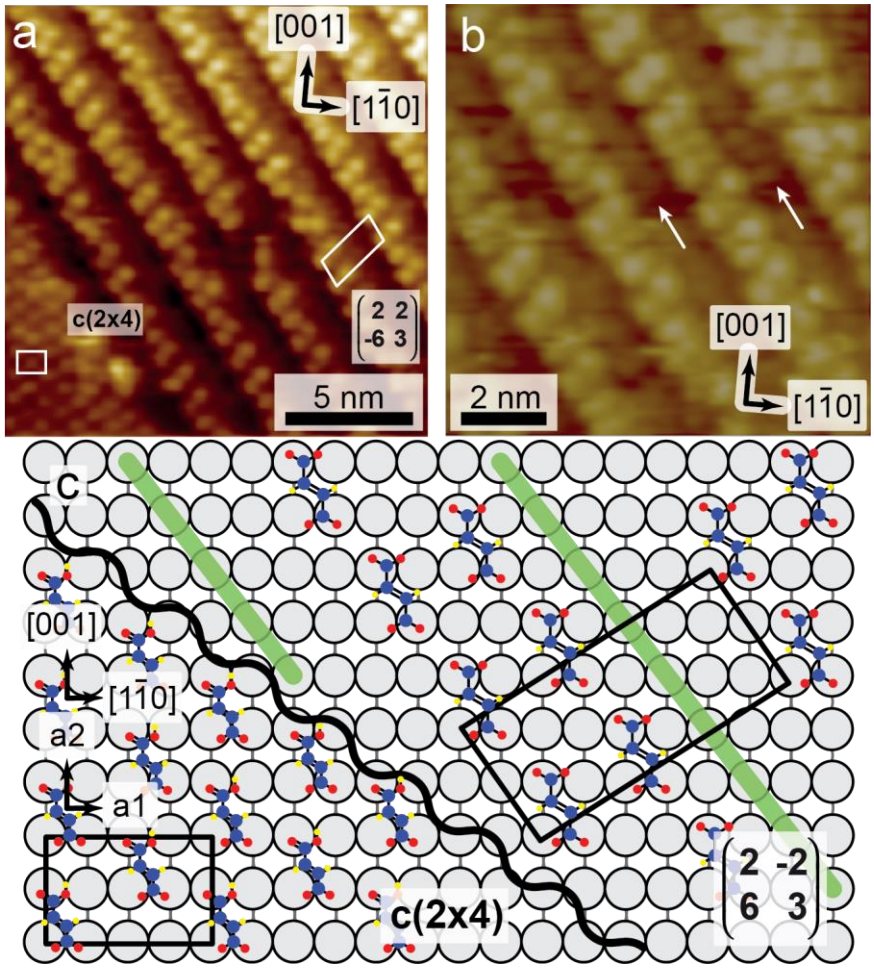

Figure 3.9: STM images of the (1 1, –6 3)^{M} structure of FUA. The molecular unit cell observed in the STM exhibits a (2, –2) periodicity. a) STM image (16.9 nm × 16.9 nm, I = 410 pA, U = 478 mV) of the (1 –1, 6 3) domain, which is the enantiomorph of the (1 1, –6 3). Rows of molecular pairs can be observed, albeit not perfectly ordered and with several vacancies. On the bottom left side of the image the coexisting c(2×4) phase is also detected; b) STM image (10.1 nm × 10.1 nm, I = 440 pA, U = 478 mV) of the same structure. The arrows indicate faint lines between the molecules. These lines suggest a reconstruction of the underlying surface; c) models for the (1 1, –6 3)^{M} and c(2×4) structures of FUA. The molecular unit cell depicted in the (1 1, –6 3)^{M} structure exhibits doubled periodicity that the one identified in the LEED, similar to the result described for the (1 1, –5 2) structure. The green lines in the model indicate reconstructed copper atoms.

The model in Figure 3.9c shows the coexistence of the c(2×4) and (1 –1, 6 3) domains. According to the RAIRS results described in Chapter 3.3, the molecules adopt a monofumarate configuration in the c(2×4) structure, whereas in the (1 –1, 6 3) domain they adopt a bifumarate configuration. As mentioned above, the (1 –1, 6 3) structure is not perfectly ordered, depicting in some areas two molecules next to each other and in others only

one. This was not taken into consideration in the model and only rows with pairs of molecules are shown. The green lines running along the <1,1> direction of the substrate in the model represent reconstructed copper atoms and only the molecular unit cell is shown.

3.5 DFT Calculations

In order to determine the energetically most favorable configurations of FUA on the surface, DFT calculations were performed by collaborators. Details about the software and parameters used will not be described here, as the calculations were not performed by the author, but have been described previously in [111]. Calculations have been performed for the single molecules in the mono- and bifumarate configurations, as well as for the molecules in the (1 1, –5 2) structure, taking the experimentally observed reconstructed copper surface into consideration. Figure 3.10 shows evaluated configurations for monofumarate on the unreconstructed surface.

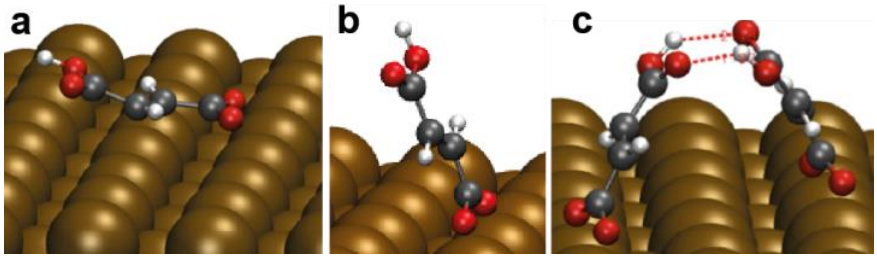

Figure 3.10: DFT modeling of the single deprotonated configuration of FUA. a) Mono-FUA lying with the molecular backbone almost parallel to the surface, interacting with the surface via the double bond as well. This arrangement is the one with the lowest energy; b) Standing configuration of mono-FUA, less stable than the lying down configuration by 0.33 eV; c) Two standing mono-FUAs forming a cyclic dimer. This configuration is less stable than two single mono-FUAs lying on the surface.

Of the three possible configurations depicted in Figure 3.10 the lowest energy is found for the monofumarate configuration with the molecule lying with its backbone parallel to the surface. In this configuration the double bond is also interacting with the first atomic layer of the substrate, without subsequent hydrogenation (Figure 3.10a). A similar bonding configuration has been described previously for propene on Cu(211) [112]. This configuration is 0.33 eV lower in energy than the upstanding arrangement shown in Figure 3.10b. The cyclic dimer formation shown in Figure 3.10c is less stable by 0.39 eV when compared to two

monofumarates lying on the surface. The bifumarate configuration on the unreconstructed copper surface is by 1.5 eV less stable than the monofumarate.

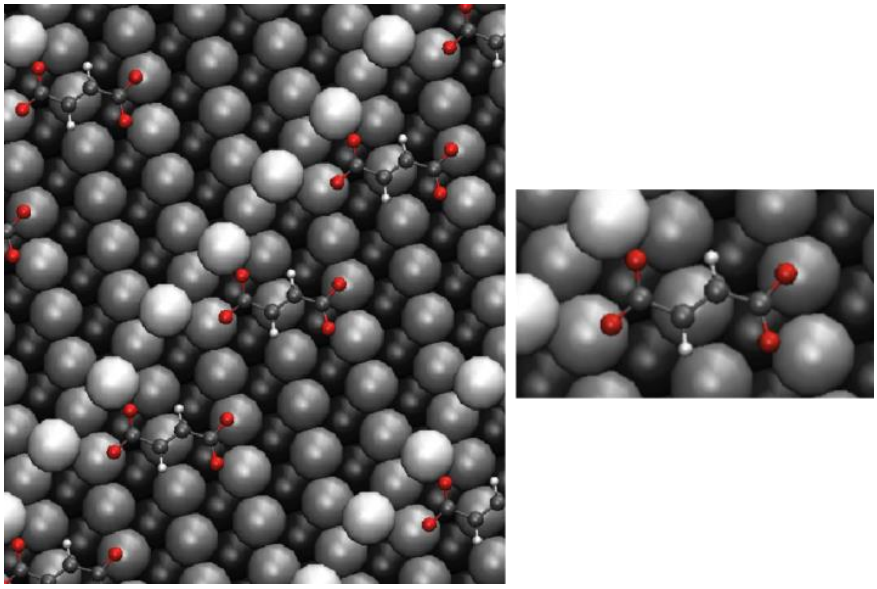

Figure 3.11: DFT modelling of the (1 1, –5 2) structure including a reconstruction of the underlying substrate. The molecules are adsorbed in a bi-FUA configuration with three oxygen atoms attached to the first layer of the copper substrate and one oxygen bound to every second reconstructed copper atom in the <1,–1> direction.

However, when the reconstructed surface is taken into consideration, the situation changes drastically. Figure 3.11 shows the arrangement of fumaric acid on the surface within the (1 1, –5 2) unit cell. The most stable configuration consists of doubly deprotonated molecules lying with their backbone almost parallel to the surface. Three of their oxygen atoms are attached to a surface copper atom and the fourth is bound to every second reconstructed copper atom. The copper adatoms were placed into the fourfold hollow sites along the <1,±1> direction of the surface. Unfortunately, the DFT calculations are not conclusive, as the most stable configuration calculated does not match the experimental STM results [107].

3.6 Conclusions

The saturation point of the molecules on the surface was determined by means of XPS.

To answer the question of the binding mode of the molecules on the surface RAIRS was used, showing that the monofumarate configuration is favored over the bifumarate. However, due to inhomogeneity in the molecular layer, the possibility of an additional doubly deprotonated arrangement could not be excluded. The lack of homogeneity in the non-tempered samples was further supported by the existence of several vibrational bands associated both with alkanes and alkenes.

Investigation with LEED after slight annealing led to the discovery of five different structures. Two were the achiral c(2×4) and p2gg(2×4), which showed sharp diffraction spots and low background intensity. The remaining three were the enantiomorphous (1 1, –3 2), (1 1, –5 2) and (1 1, –6 3). The enantiomorphous structures exhibited also weak stripes in the background, suggesting the existence of an additional (2,±2) periodicity. Both the (1 1, –5 2) and (1 1, –6 3) structures have already been reported for SU [60, 69], whereas the (1 1, –5 2) structure was also observed for racemic MA [68]. In the case of SU it was assumed that the formation of a chiral structure from an achiral molecule was due to a zigzag distortion of the molecular backbone. The double bond between carbons 2 and 3 in FUA allows, however, only a small distortion without the opening of the bond, due to the sp^2-hybridization of the carbon atoms. Consequently, an alternative adsorbate structure, than the one suggested for SU, had to be proposed, as shown in Figures 3.8 and 3.9.

STM investigation of the (1 1, –5 2) and (1 1, –6 3) structures revealed a reconstruction of the underlying copper substrate and the existence of two distinct unit cells, describing the arrangement of the molecules and reconstructed copper atoms, respectively. The molecular unit cell exhibited a doubled periodicity with respect to the atomic one. The presence of the two unit cells also explained the weak stripes in the background of the LEED patterns. The reconstructed copper atoms act as the main electron scatterers, whereas the molecules are not as well ordered, manifesting their superstructure arrangement only as weak stripes in the LEED. Due to the slight annealing needed to obtain the ordered structures and the subsequent desorption of some molecules, areas on the surface were formed, which were void of molecules. These areas allowed direct investigation of the reconstructed copper surface and the observation of a now truly chiral metal surface. This discrepancy between the (1,±1) periodicity determined in the LEED and the (2,±2) periodicity found in the STM was also

reported for SU on Cu(110) [60]. Several possible models were discussed, but the lack of high resolution STM images made a direct experimental observation difficult.

DFT calculations in the case of the absence of an ordered structure showed that the monofumarate configuration is energetically more stable, in particular because of the interaction of the double bond with the substrate. Simulations for the (1 1, –5 2) structure, however, favored a bifumarate configuration with one of the oxygen atoms bound to a reconstructed copper atom. Unfortunately, in the case of the (1 1, –5 2) structure, the DFT calculations were inconclusive, making it difficult to derive a final model for the entire surface.

4. Maleic acid

Maleic acid (MAL) or cis-butenedioic acid is the cis- isomer of fumaric acid, as described in Chapter 3. The structural formula of maleic acid is shown in Figure 4.1.

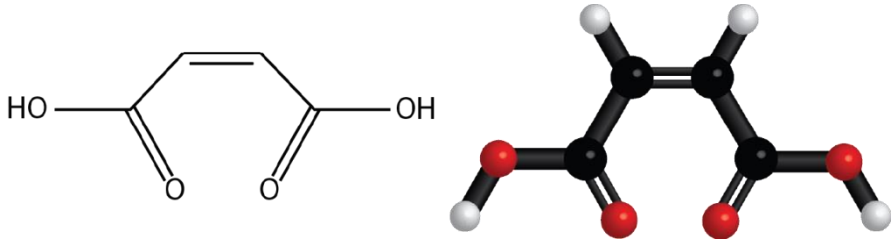

Figure 4.1: Structural formula and ball-and-stick model for maleic acid.

As in the case of its stereoisomer, all four carbon atoms of the molecule are sp^2-hybridized. The molecule can bind on the substrate in the two configurations described in previous chapters, i.e. as a *bimaleate*, with all four oxygens atoms of both carboxylic acid groups bound to the copper, or as a *monomaleate*, with only one carboxylic acid group deprotonated.

The XPS investigation of this molecule, as well as its coverage calibration can be found in the Appendix.

4.1 LEED

Upon adsorption of MAL on the surface no ordered structures can be observed at low coverages, under all experimental conditions. However, annealing of the crystal leads to several well-ordered structures. A phase diagram describing them is shown in Figure 4.2 and their LEED patters are presented in Figure 4.3. Increasing the coverage to 0.65 ML and subsequent annealing at 423 K for 15 min leads to the formation of a (1 1, –5 2) structure (Figure 4.3a). The LEED exhibits sharp diffraction spots indicating a well ordered structure, but also weak stripes running parallel to the <1,1> and <1,–1> directions of the crystal, that suggest the existence of an additional (2,±2) periodicity, as observed for FUA in Chapter 3.

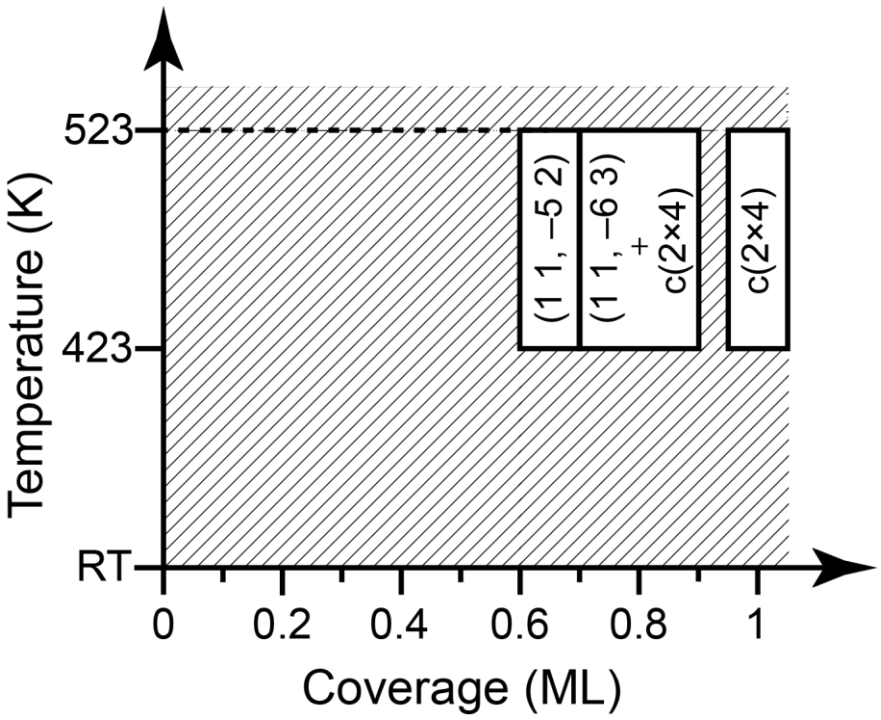

Figure 4.2: Phase diagram for MAL on Cu(110). No ordered structures were observed at conditions represented by the shaded areas.

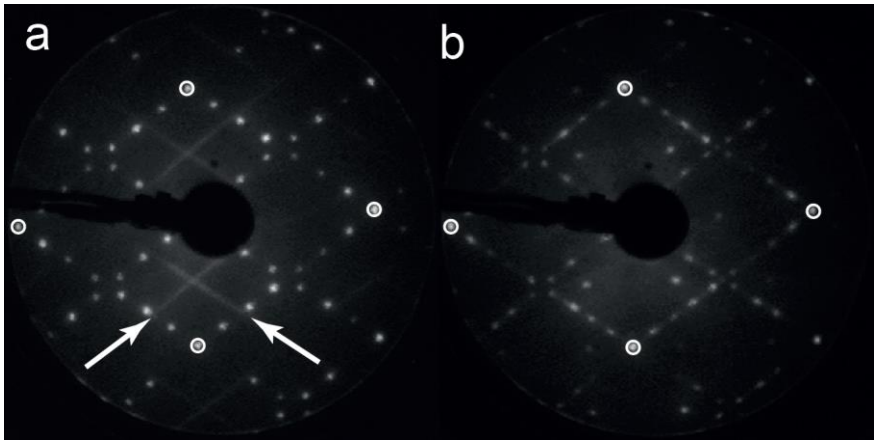

Figure 4.3: LEED patterns of MAL on Cu(110). The 1×1 diffraction spots of the clean copper surface are marked with circles. a) (1 1, –5 2) structure, E_p = 55 eV, the faint lines in the background (marked by the arrows) suggest an additional (2,2) periodicity; b) (1 1, –6 3) structure coexisting with a c(2×4) structure, E_p = 54 eV.

Increasing the coverage to 0.74 ML and annealing for 15 minutes at 423 K produces a (1 1, –6 3) structure, co-existing with a c(2×4) structure, as shown in Figure 4.3b. At saturation

coverage a low quality c(2×4) can be observed on the entire crystal. Both (1 1, –5 2) and (1 1, –6 3) structures reported here for MAL have also been observed for FUA (chapter 3), SU [60, 69] and racemic MA [68]. The fact that the molecules have different structural formulas but exhibit the same diffraction patterns begs the question of whether maleic acid also induces a reconstruction of the underlying copper substrate, similar to the one observed for FUA and MA.

4.2 RAIRS

RAIRS was used to study a series of non-tempered samples of different amounts of molecules on the surface (Figure 4.4) as well as the (1 1, –5 2) structure (Figure 4.5).

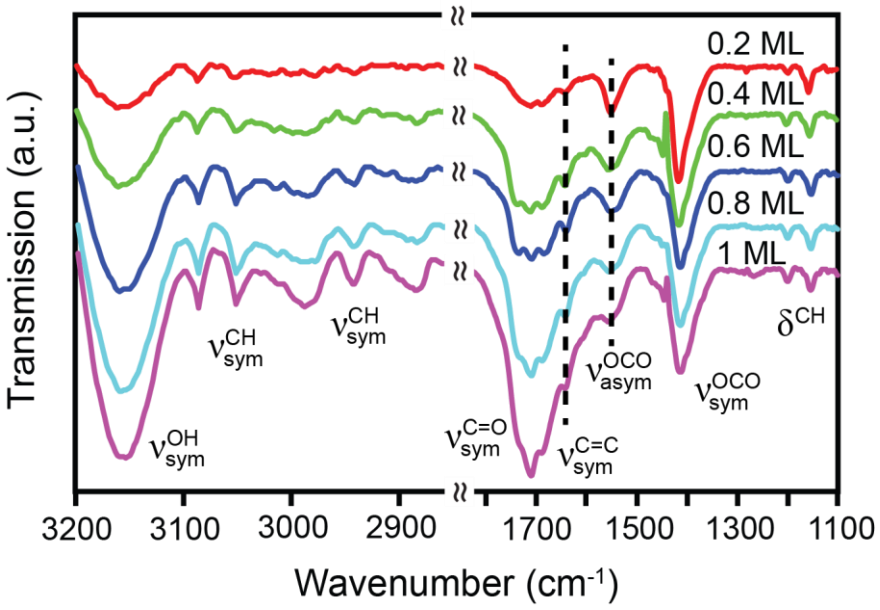

Figure 4.4: RAIRS spectra showing the transmission of a coverage series of MAL adsorbed at RT. All spectra show a strong C=O vibration band around 1700 cm^{-1}, which is indicative of monomaleate configuration.

For all coverages in Figure 4.4 a strong band can be detected at 1414 cm^{-1} which denotes the symmetric OCO stretching vibration. This is therefore an indication that at least one carboxyl group is bound to the substrate. The asymmetric OCO stretching vibration can be observed at 1548 cm^{-1}, with decreasing intensity as the coverage increases. Since the strong C=O stretching vibration can be detected around 1700 cm^{-1}, it is evident that the other carboxylic

acid group is not bound to the surface. At low coverages the intensity of the ν_{sym}^{OCO} is higher than that of the $\nu_{sym}^{C=O}$, but with increasing coverage the situation is reversed. This could mean that at low coverages the molecules have more space available on the crystal and therefore a percentage is more likely to bind in a bimaleate form. However, as the coverage increases, there is less unoccupied space, forcing the molecules to bind in a monomaleate configuration. The fact that the $\nu_{sym}^{C=O}$ band exhibits several shoulders for all coverages indicates that there is inhomogeneity in the molecular layer. This is further confirmed by the existence of several bands for the CH vibration at higher wavenumbers. The presence of several bands for the CH stretching vibration could also be due to the interaction of only one of the carboxylic acid groups with the surface, making the CH groups chemically different from each other. Additionally the potential breaking of the C=C bond in some of the molecules would create a different environment for the CH groups. The observed bands with their respective assignments are listed in Table 4.1.

Table 4.1: Frequencies and assignment of vibrational modes identified for a non-tempered sample and the (1 1, –5 2) structure (sh: shoulder, w: weak, b: broad, s: strong, m: medium).

Mode	**0.5 ML**	**(1 1, –5 2)**
ν_{sym}^{OH}	3153 b,m	3159 b,m
ν_{sym}^{CH}	3085 s,m	3085 s,m
	3048 b,w	3050 b,w
ν_{sym}^{CH}	2984 w	3015 b,w
	2942 b,w	
	2882 w	
$\nu_{sym}^{C=O}$	1734 w	1702 b,w
	1706 b	
	1679 sh	1660 b,w
$\nu_{sym}^{C=C}$	1638 sh	1630 b,w
ν_{asym}^{OCO}	1548 w	1524 w
ν_{sym}^{OCO}	1443 sh,w	1428 sh,w
	1414 s	1414 s
δ^{CH}	1198 w	
	1153 w	

In order to determine the configuration of the adsorbed molecules after the annealing, RAIRS experiments were performed for the enantiomorphous (1 1, –5 2) structure. Two spectra are depicted in Figure 4.5, one corresponding to the structure itself and one before the annealing, that serves as comparison.

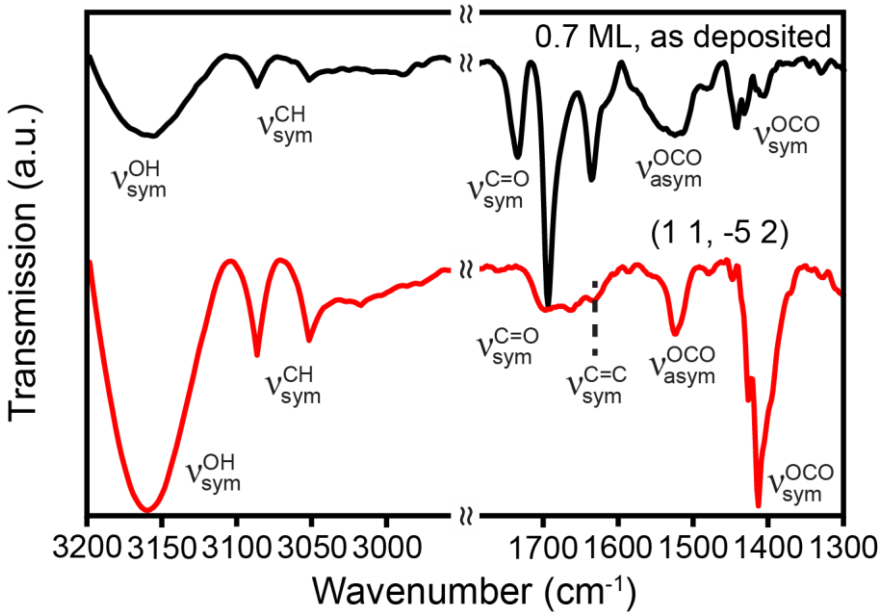

Figure 4.5: RAIRS spectra showing the transmission of the (1 1, –5 2) structure with the same coverage before the annealing serving as comparison. A much smaller intensity of the C=O stretching mode can be observed in the (1 1, –5 2) structure, suggesting a bimaleate configuration in the adsorbed layer.

The most distinct features are identified around 1400 cm^{-1} and in the 1700 cm^{-1} region. The band for the symmetric stretching vibration of the carbonyl group shows a dramatic increase in intensity, whereas at the same time the C=O stretching vibration behaves in an opposite manner. This indicates that the majority of the molecules is now bound in a bimaleate configuration with both carboxylic acid groups deprotonated. There are still however molecules on the crystal with a monomaleate configuration, something that is confirmed both by the shoulder at 1426 cm^{-1} as well as by the remaining $\nu_{sym}^{C=O}$ vibration around 1700 cm^{-1}. The specific positions of the bands and their respective assignments are listed in Table 4.1.

4.3 STM

STM experiments were performed when the (1 1, –5 2) structure was present on the surface and are shown in Figure 4.6.

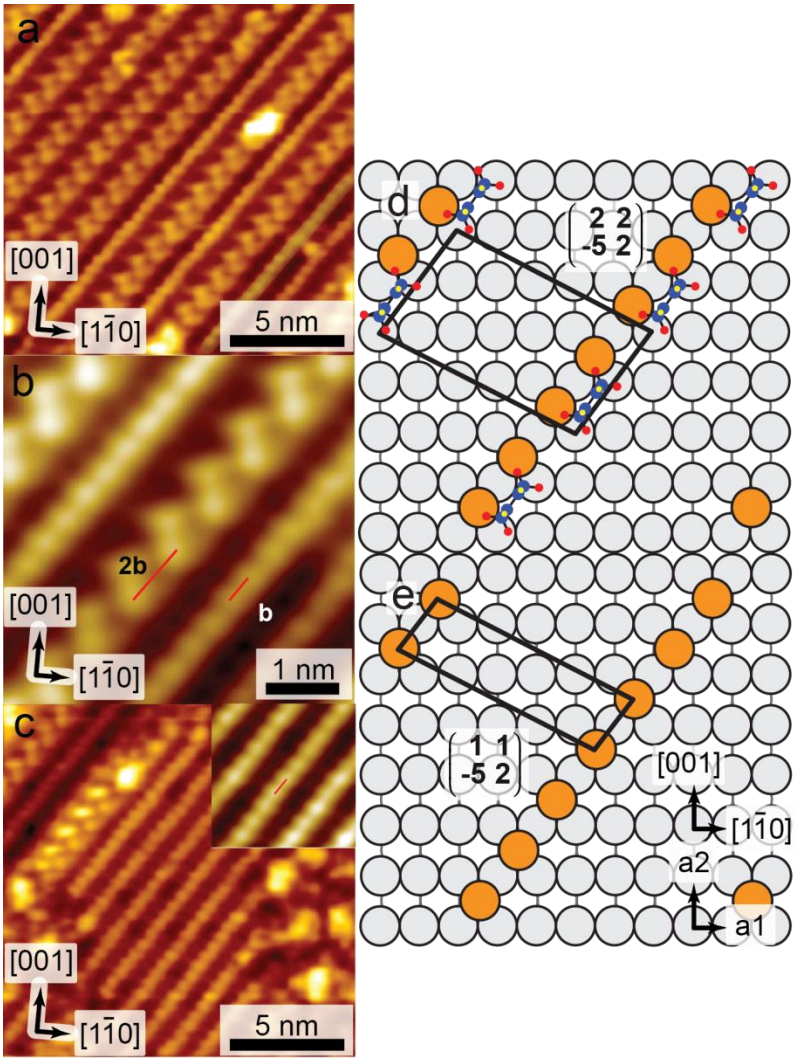

Figure 4.6: STM images of chirally reconstructed (1 1, –5 2) domains and the corresponding tentative model. a) STM image (17 nm × 17 nm, I = 680 pA, U = 464 mV) of the (1 1, –5 2) structure. The bright, zigzag rows represent a coupling of molecules with copper adatoms, with the weaker features marked with green portraying reconstructed copper atoms; b) close-up STM image (4.8 nm × 4.8 nm, I = 780 pA, U = 464 mV) of the same domain. The molecular cell has double the periodicity than that observed in LEED in the <1,–1> direction, whereas the atomic cell agrees with the LEED results; c) STM image (17 nm × 17 nm, I = 780 pA, U = 464 mV, inset 4.8 nm × 4.8 nm, averaged 5×) of an area on the crystal where no molecules can be detected; d) tentative model of the surface with the molecular and unit cell depicting the double periodicity. The copper adatoms next to the molecules are shown with orange features. The model is rotated in such a way to match the orientation of the crystal; e) model of the areas on the surface which are not decorated with molecules. Here a (1 1, –5 2) unit cell can be observed.

The molecules appear as bright lobes in the STM images and are arranged in zigzag rows along the <1,1> direction of the crystal (Figure 4.6a). Considering that the results between maleic and fumaric acid are so similar and since the coverage for this structure for both molecules is the same, it is assumed that also for maleic acid there is only one molecule present within the unit cell. The elongated features shown in Figure 4.6a depicting the molecules are therefore concluded to be a combination of a maleic acid molecule and a copper adatom, as shown in the tentative model in Figure 4.6d. In-between the molecular rows, lines of more delicate features are distinguished, which are identified as reconstructed copper atoms. Investigation of the distances between two adjacent copper atoms and two molecules, respectively, leads to the discovery of two unit cells, one atomic that follows the periodicity detected in the LEED and one molecular, which exhibits double the periodicity of the atomic one (Figure 4.6b, d and e). Areas on the crystal appear to be devoid of molecules, but the underlying copper atoms maintain their new reconstructed arrangement, creating thus true chiral copper islands on the crystal (Figure 4.6c).

4.4 Conclusions

The adsorption behavior of MAL on Cu(110) was detailed in this chapter. LEED showed the existence of two enantiomorphous structures for coverages above 0.7 ML after gentle annealing of the sample. These were a (1 1, –5 2) structure and a (1 1, –6 3) coexisting with a c(2×4) structure.

RAIRS was used to determine the configuration of the molecules in the non-tempered samples as well as for the (1 1, –5 2) structure. Without annealing, for all coverages the adsorbates were bound in a monomaleate arrangement with the molecular backbone almost parallel to the surface, since the stretching vibration for the C=C could only be detected in the form of a shoulder. When arranged in the (1 1, –5 2) structure the molecules were bound in a bimaleate configuration, with both carboxylate groups deprotonated.

STM investigation of the (1 1, –5 2) structure revealed rows of molecules running along the <1,1> direction of the crystal, with rows of reconstructed copper atoms arranged in-between. The periodicity of the atomic lines matched the periodicity detected in the LEED, whereas the periodicity of the molecular lines was twice as large, thus creating two distinct unit cells.

Noteworthy is the fact that the results presented here for MAL are very similar to those discussed for FUA in chapter 3. The molecules self-assemble in the same enantiomorphous structures, as presented in the LEED and both induce a reconstruction of the underlying copper substrate, as depicted in the STM. Both molecules assume a single deprotonated configuration in their non-tempered samples, but a doubly deprotonated arrangement in the enantiomorphous structures, as proven by RAIRS. The fact that both MAL and FUA exhibit similar results although they have different steric configurations indicates that the interaction with the surface is so strong that the molecules force the copper to reconstruct itself.

The LEED and STM results presented here have been published in [113].

5. Acetylene dicarboxylic acid

Acetylene dicarboxylic acid (ACDC) is another unsaturated dicarboxylic acid with a triple bond between carbons 2 and 3. Those carbons are sp hybridized, therefore making the molecule linear. The structural formula of the molecule is shown in Figure 5.1.

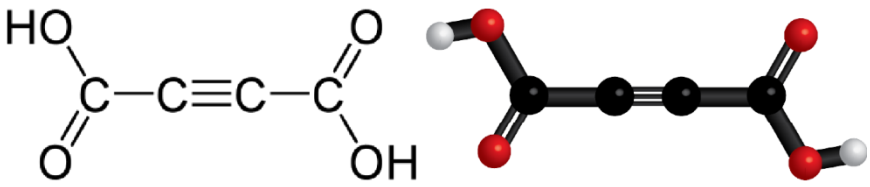

Figure 5.1: Structural formula and ball-and-stick model for acetylene dicarboxylic acid.

As with other dicarboxylic acids, the molecule can bind on the substrate in the single or double deprotonated configurations discussed in previous chapters.

ACDC was investigated on Cu(110) within the framework of a Master thesis (Margrith Meier, University of Zürich), under the guidance of the author. All results documented in this chapter have already been reported in the master thesis. Therefore, only a summary will be presented here, in order to act as comparison for the rest of the unsaturated dicarboxylic acids investigated, namely fumaric and maleic acid. Detailed analysis and discussion of these results can be found in [114]. The molecule was investigated with XPS, RAIRS, TPD, LEED and STM. However, the two latter methods offered no viable results, since the molecules did not seem to self-assemble in any ordered structures and will therefore not be presented here. The rest of the results will be presented as a whole in this chapter.

5.1 XPS

Upon adsorption ACDC forms a chemical bond with the surface and as in the case of the other dicarboxylic acids discussed previously, a saturation point is reached after a certain time of exposure, as shown in Figure 5.2.

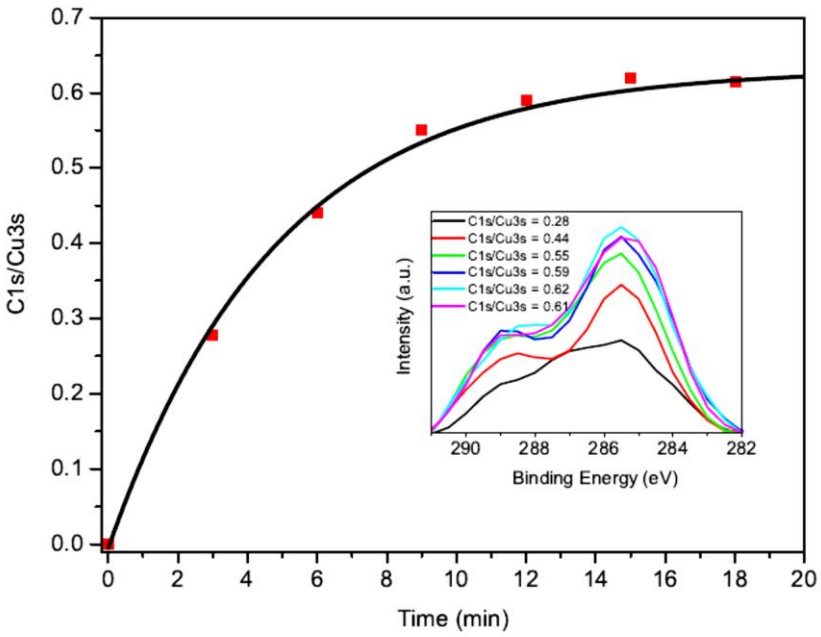

Figure 5.2: XPS coverage calibration of the adsorption of ACDC on Cu(110). The inset shows the C1s signal of a series of different amounts of molecules on the surface.

The ratio of the C1s/Cu3s signals at the saturation point was 0.61 and was reached after approximately 15 minutes of evaporation, with the crystal held at RT and the evaporation cell containing the molecules at 323 K.

In order to determine if there is a second layer of physisorbed molecules, a multilayer experiment was performed by cooling the sample to 80 K prior to the adsorption of the molecules. Subsequently, a TPD experiment was performed in which the crystal was flash heated to approximately 850 K and the mass of the molecule (114 amu) was investigated.

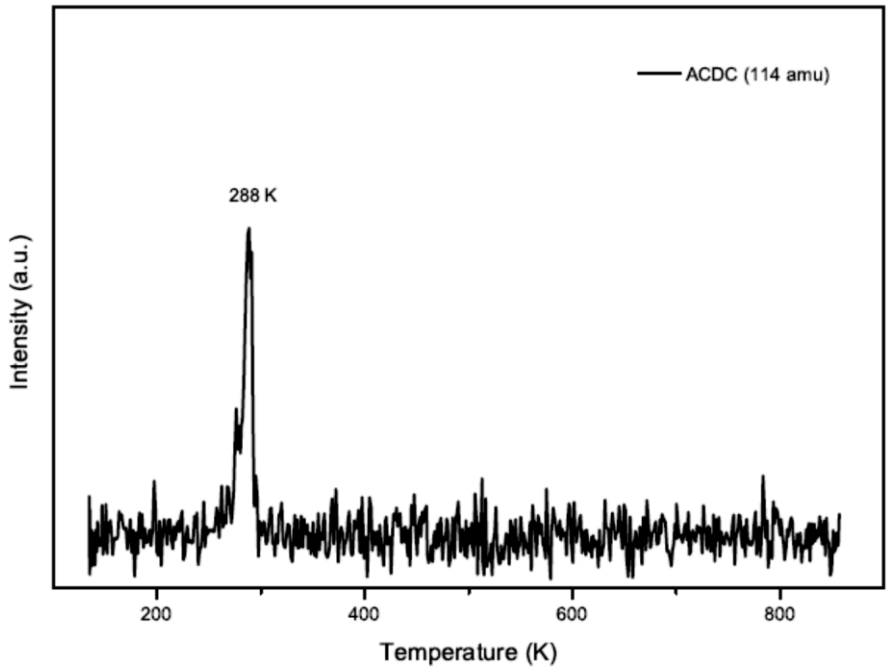

Figure 5.3: TPD spectrum of a multilayer coverage of ACDC on the surface. The 114 amu investigated corresponds to the molecular mass and can be detected at 288 K.

It is made clear from Figure 5.3 that since the molecular mass is detected at 288 K, i.e. slightly lower than RT, there is no second layer of molecules on the surface when the evaporation of the molecules is performed at RT. Additionally, the multilayer TPD experiment is an indication that the molecule exits the evaporation cell as a whole and does not decompose due to the heating applied for the evaporation.

According to the XPS results for fumaric and maleic acid the C1s/Cu3s value at the saturation point for both was 0.43, in contrast to the 0.61 value identified for ACDC. This is an indication that the slightly smaller size of ACDC allows for more molecules to be adsorbed on the surface at RT.

Unfortunately, fitting of the XPS spectra could not help with the identification of the type of adsorbates on the surface. A fitting of the C1s XPS spectrum at the multilayer coverage, as shown in Figure 5.4, could however help to identify the binding energies of the different parts of the molecule.

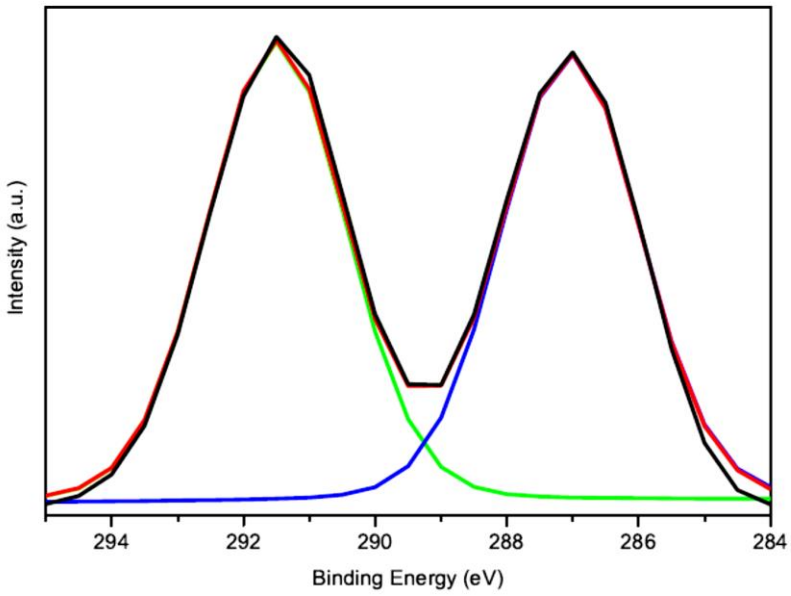

Figure 5.4: Fitted C1s XPS spectra for a multilayer coverage of ACDC. The black line represents the spectrum as measured, whereas the red line depicts the sum of the fitted peaks. The spectrum is fitted with 2 peaks with a 1:1 ratio, corresponding to the –COOH and –C≡ parts of the molecule.

The C1s peak for the multilayer coverage of ACDC was fitted with 2 peaks having a 1:1 ratio and corresponding to the signals obtained by the –COOH and –C≡ parts of the molecule. According to the fitting, the carbon involved in the triple bond has a C1s binding energy of 287 eV, whereas for the carboxylic acid groups the binding energy is 291.5 eV.

5.2 RAIRS

In order to identify the configuration of the adsorbates, RAIRS experiments were performed for a series of increasing amounts of ACDC on the crystal and at the multilayer coverage.

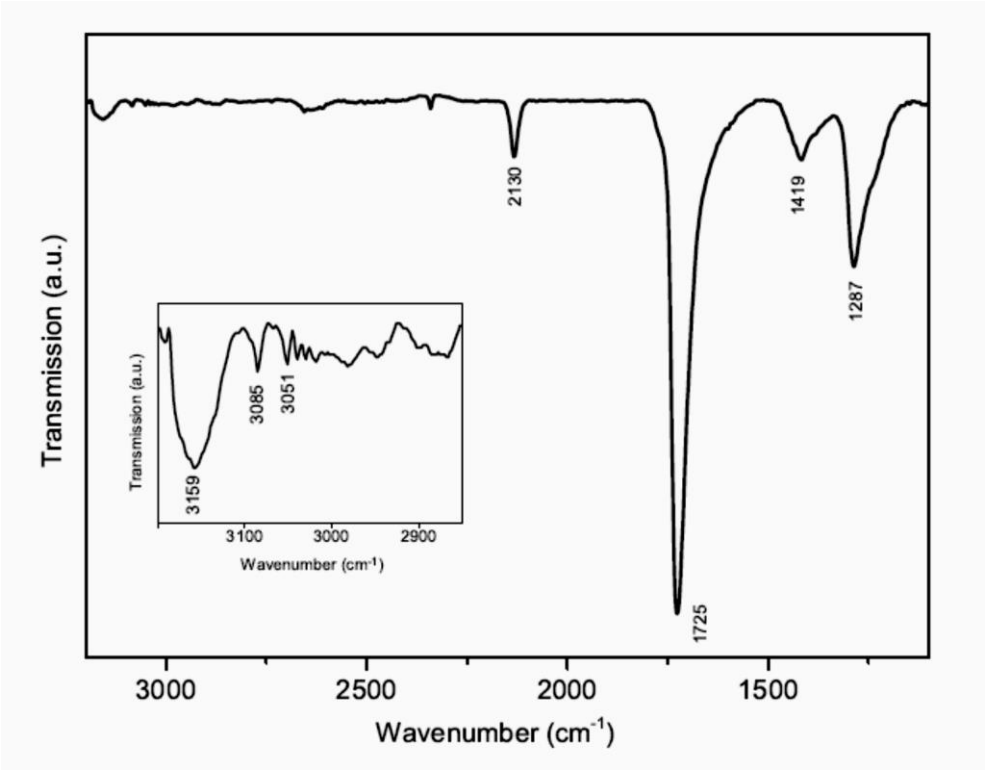

Figure 5.5: RAIR spectrum of a multilayer coverage of ACDC. The band at 2130 cm^{-1} corresponds to the C≡C stretching vibration, indicating the presence of neutral, unsaturated ACDC molecules on the surface.

The spectrum at the multilayer coverage is depicted in Figure 5.5 and is in agreement with the coexistence of both chemisorbed and physisorbed species of ACDC. The first layer is attached to the surface by the formation of a chemical bond, which is expressed by the symmetric stretching vibration of the carboxylate group at 1419 cm^{-1}. It is however unclear whether the molecules in the first layer have a mono- or a bi-ACDC configuration. This is due to the fact that the physisorbed additional layers are in their neutral forms and therefore give rise to a very intense carbonyl stretching vibration at 1725 cm^{-1}. This could potentially overshadow any features due to the molecules in the first layer. An important observation stemming from the RAIR multilayer spectrum is the band at 2130 cm^{-1}, which corresponds to the stretching vibration of the C≡C, further confirming that the molecules leave the evaporation cell intact and without any protonation of the triple bond.

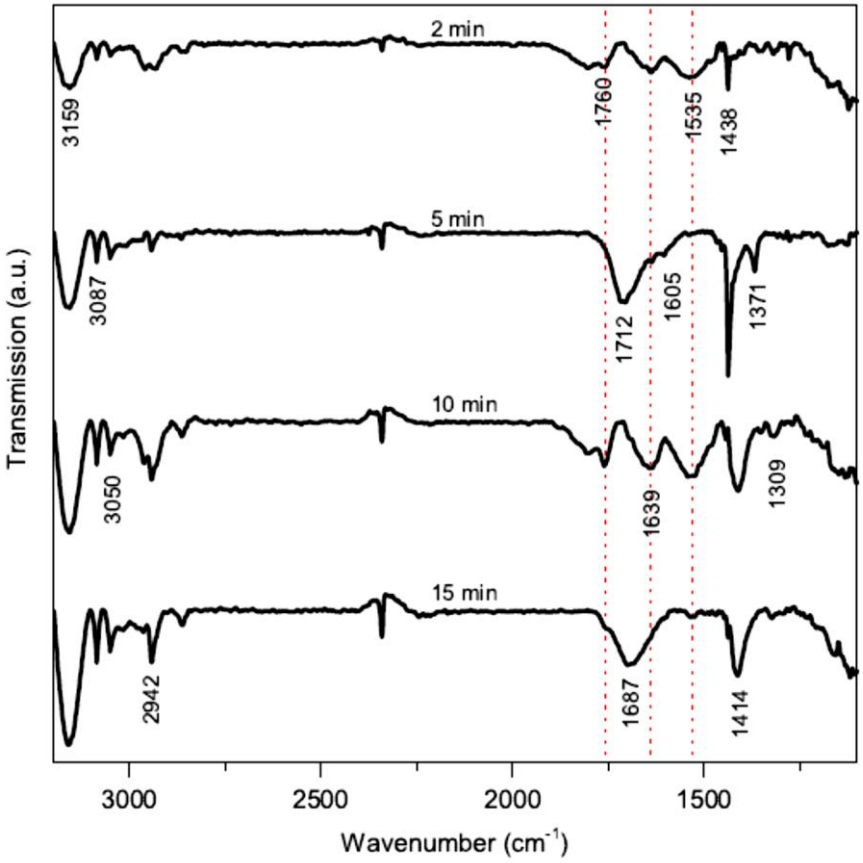

Figure 5.6: RAIRS spectra showing the transmission of a coverage series of ACDC adsorbed at RT. All spectra indicate inhomogeneity in the molecular layer, with the bands around 2350 cm^{-1} being artifacts due to the misalignment of the spectrometer mirrors.

The spectra obtained by the series of increasing amounts of ACDC on the surface are shown in Figure 5.6, with the spectrum after 15 minutes of exposure corresponding to the saturation coverage. It is evident from Figure 5.6 that the molecular layer exhibits severe inhomogeneity, depicted here by the splitting of the C=O stretching vibration around 1700 cm^{-1}, the shoulders observed at the symmetric OCO stretching vibration around 1400 cm^{-1} and the existence and disappearance of the asymmetric OCO vibration around 1530 cm^{-1} with the change of the coverage. It can be concluded however, that at least a percentage of the adsorbates is arranged in a mono-ACDC configuration. An important feature of the spectra depicted in Figure 5.6 is the total absence of a stretching vibration for the C≡C, at around 2100 cm^{-1}. This could either indicate that the molecular backbone is parallel to the surface, therefore making the vibration IR inactive, or it could signify that upon adsorption on the surface the C≡C becomes protonated by the H atoms leaving the carboxylic acid groups that bind to the substrate, becoming in this way a C=C. Unfortunately, this cannot be

unequivocally proven by the results at hand, is supported however by the existence of a weak band around 1640 cm^{-1}, which could correspond to the stretching vibration of the C=C. It should be noted that the bands around 2940 cm^{-1} could simply be artifacts of the measurement, as described in chapter 3, instead of real bands describing a vibrational mode.

5.3 TPD

The desorption mechanism of different amounts of the molecule on the crystal was investigated by TPD and the resulting CO_2 (44 amu) fragment is shown in Figure 5.7.

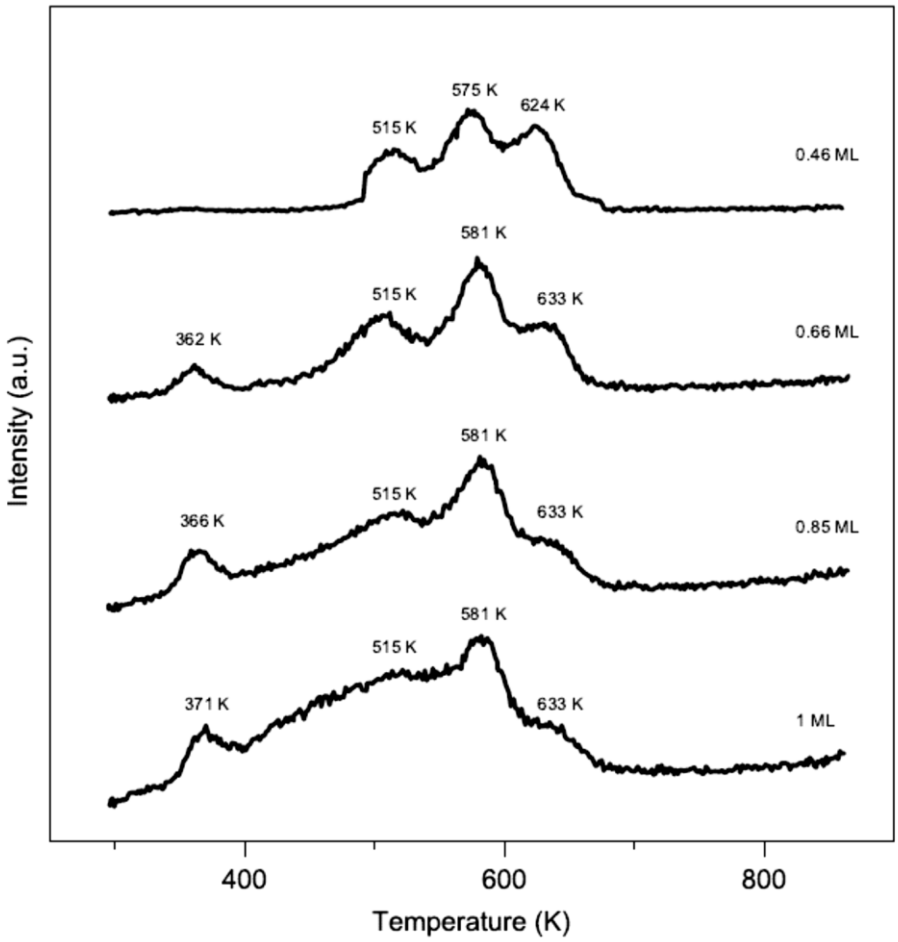

Figure 5.7: TPD spectra for a series of different coverages of ACDC. The molecule exhibits three desorption peaks at low coverages which merge into one broad peak at the saturation coverage with a maximum at 581 K, as well as an additional peak around 365 K.

At low coverage the TPD spectrum shows the existence of three distinct peaks between 515 K and 624 K. As the coverage increases these three peaks begin to merge with each other, resulting in a very broad peak with a maximum at 581 K and two shoulders at 515 K and 633 K at the saturation coverage. At the same time a peak starts to appear at 362 K and with increasing coverage it increases in intensity and shifts to slightly higher temperatures, ending up at 371 K at the saturation coverage. The TPD experiments further confirm the inhomogeneity in the molecular layer suggested by the RAIRS results, with the peaks observed here corresponding to the fragmentation and desorption of the different molecular species present on the surface.

5.4 Conclusions

The investigation of ACDC on Cu(110) showed that, upon reaching the surface, the molecule forms a strong chemical bond with the copper atoms. As with other dicarboxylic acids, the amount of molecules being adsorbed on the surface at RT decreases with increasing exposure time, until it reaches a saturation point after which no more molecules can stick to the surface. When the sample temperature is decreased below RT prior to evaporation, multilayer coverages can be obtained, with the first molecular layer chemisorbed onto the surface and with weakly physisorbed molecules in any additional layers. RAIRS depicted an inhomogeneity in the molecular layer, but also revealed a possible hydrogenation of the C≡C. LEED and STM offered no viable results, since even after extended heating treatment, the molecules did not form any ordered structures.

Although ACDC is another C_4 dicarboxylic acid, it showed a very different behavior than other molecules in the same family. In spite of the fact that the RAIRS results suggest a possible protonation of the C≡C, the behavior of the new hydrogenated molecule, which would now include a C=C in its molecular backbone, is far from that observed for both FUA and MAL. The molecule shows a completely different desorption mechanism and does not form any ordered structures, similar to those reported for FUA and MAL, or otherwise. It is possible that the triple bond is still intact but IR inactive, creating such a steric hindrance in the molecular backbone that makes the formation of an ordered structure impossible.

6: 2,3-Dimethyl succinic acid on Cu(110)

Dimethyl succinic acid (DMSU) exists in an achiral meso configuration and a left or right handed enantiomer. The structural formulas of the achiral and chiral forms of the molecule are shown in Figure 6.1.

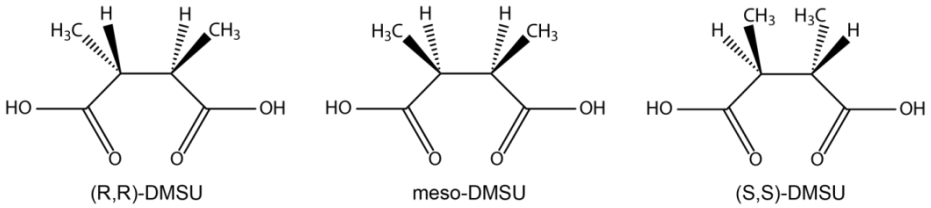

Figure 6.1: Structural formulas of the different DMSU stereoisomers. From left to right: (*R,R*)-DMSU, meso-DMSU and (*S,S*)-DMSU.

The molecule is very similar to succinic acid in its backbone, however the bulky substituents give it an increased volume. This could potentially give it a unique self-assembly configuration upon adsorption on the crystal. As described for the molecules investigated in previous chapters, DMSU can bind in the usual mono- and bi-DMSU deprotonated configurations.

Both the achiral and the racemic mixture of the chiral moieties of the molecule were investigated. The results for both are documented here and compared to one another, with the XPS experiments for both available in the Appendix.

6.1 LEED

The LEED results are the same for both molecules with the only difference being the quality of the resulting structures. Upon adsorption on the surface no ordered structure can be observed. Subsequent heating leads to the arrangement of the molecules into ordered structures, with a starting coverage of a full monolayer. A phase diagram of these structures is shown in Figure 6.2 and the LEED patterns for both molecules are depicted in Figure 6.3.

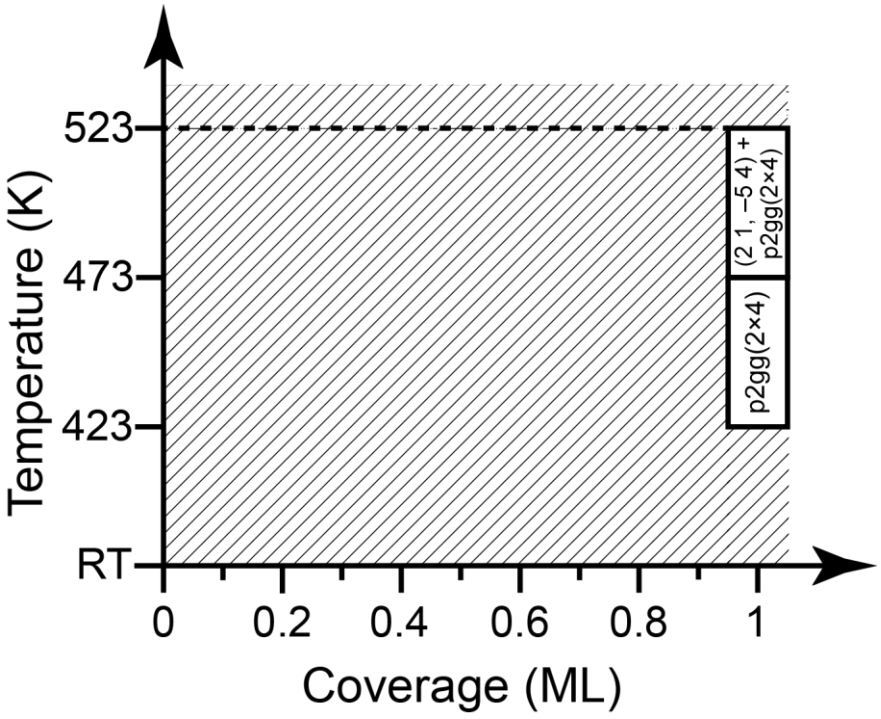

Figure 6.2: Phase diagram for DMSU on Cu(110). No ordered structures were observed at conditions represented by the shaded areas.

Of the two distinct structures observed, one, which can be obtained after annealing of the sample at 423 K for 15 minutes, is a well-ordered p(2×4) structure with missing (0,n) spots, n = 1/2 , 3/2, etc and missing (n,0) spots, n = 1/4, 3/4, etc (Figure 6.3a and c). Changing the intensity of the electron beam or the angle of incidence does not make the missing spots visible, leading to the conclusion that glide planes exist parallel to the [001] and [1$\bar{1}$0] directions of the crystal, as already reported for SU [71] and FUA in Chapter 3. Consequently, this structure will henceforth be named p2gg(2×4). Models for the p(2×4) structures of both meso- and rac-DMSU are shown in Figures 6.2e and f. The presence of the glide planes is presented in the models by mirroring the molecules and shifting them in the [001] and [1$\bar{1}$0] directions of the crystal in every second row. The models depicted show only some of the possible configurations in which the molecules can be arranged on the surface.

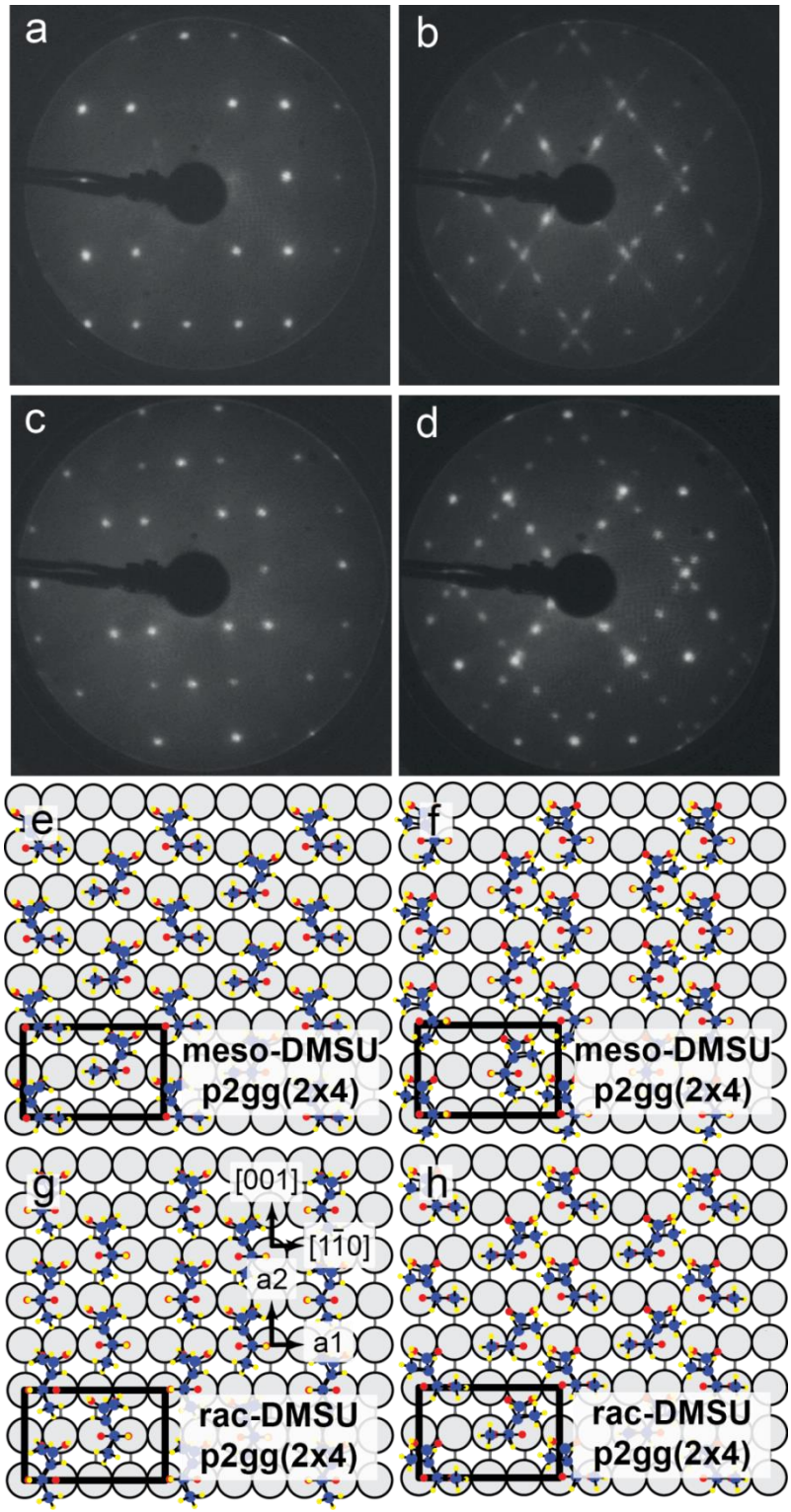

Figure 6.3: LEED patterns of DMSU on Cu(110). a) meso-DMSU p2gg(2×4) structure, E_p = 30 eV; b) meso-DMSU (2 1, –5 4) structure coexisting with the p2gg(2×4), E_p = 27 eV. The diffraction pattern exhibits stripes and faint spots, indicating the lack of long-range order; c) rac-DMSU p2gg(2×4) structure, E_p = 55 eV; d) rac-DMSU (2 1, –5 4) structure coexisting with the p2gg(2×4), E_p = 26 eV. Here sharp diffraction spots can be observed, signifying a well-ordered structure; e-f) tentative models of the p2gg(2×4) structure of meso-DMSU; g-h) tentative models of the p2gg(2×4) structure of rac-DMSU.

In the meso-DMSU model in Figure 6.3e an additional configuration would be with the methyl groups facing in the opposite direction from which they are depicted. In the case of the rac-DMSU model in Figure 6.3f it is assumed that the structure is composed of heterochiral domains, i.e. of a mixture of (*R*,*R*)- and (*S*,*S*)-DMSU, with the molecular backbone assuming a certain zigzag twist. However, the LEED structure would still be the same if the twist of the backbone was facing in the opposite direction, or even if there was no twist at all (see Appendix for additional models).

6.2 RAIRS

RAIRS experiments were performed for both molecules on a series of increasing coverages as well as when the two structures were observed on the crystal. The coverage series experiments for the meso compound and the racemic mixture are depicted in Figures 6.3 and 6.4 respectively.

When comparing the RAIR spectra of the non-tempered meso- and racemic-DMSU the situation is very similar. In both cases, the band around 3160 cm^{-1} can be attributed to the stretching vibration of the OH group, indicating that one of the carboxyl groups is not interacting with the surface, but is rather facing away from it. This is reinforced by the presence of the carbonyl stretching vibration around 1680 cm^{-1}, suggesting that the molecules are bound to the surface in a mono-DMSU configuration. The fact that the band of the carbonyl vibration shows a shoulder around 1710 cm^{-1} indicates that there is inhomogeneity in the molecular layer, something that is supported by the LEED measurements, which show blunt spots. The band around 1420 cm^{-1} corresponds to the symmetric stretching vibration of the carboxylate, but the lack of the asymmetric OCO vibration implies that both oxygen atoms are equidistant from the surface, therefore rendering the vibration inactive. The band around 1460 cm^{-1} is assigned to the stretching vibration of the C–O component of the carboxylic acid, further corroborating the assumption of a mono-DMSU configuration.

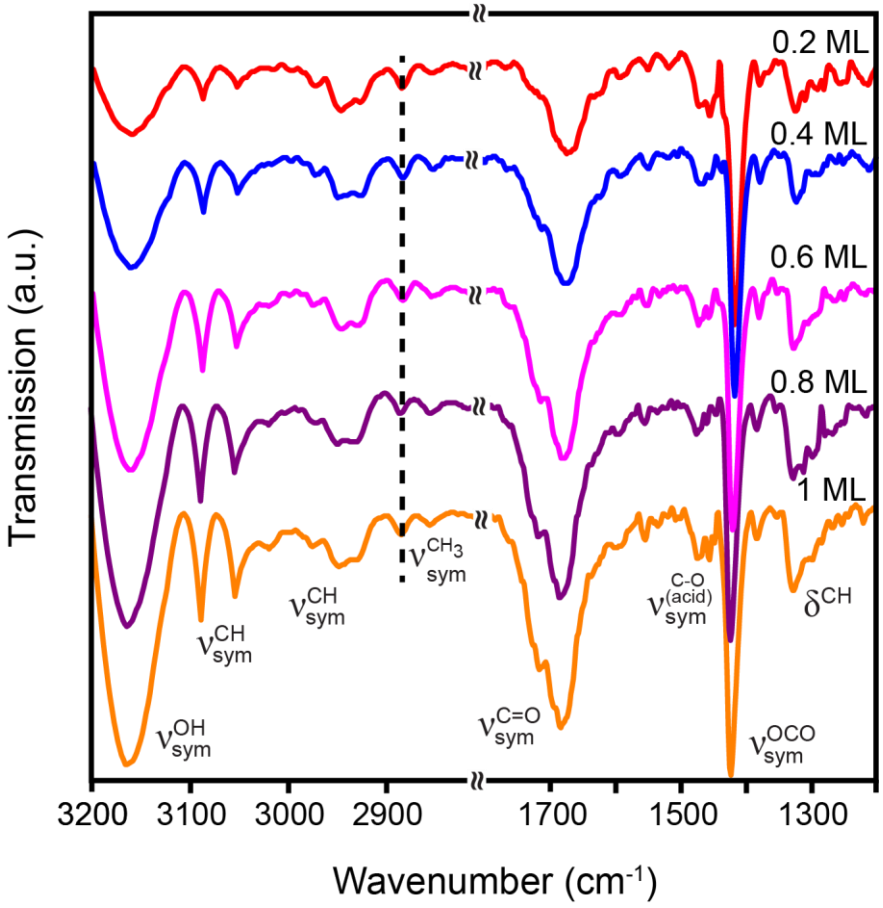

Figure 6.4: RAIRS spectra showing the transmission of a coverage series of meso-DMSU adsorbed at RT. All spectra show a strong OCO vibration band around 1400 cm^{-1} and a C=O vibration band around 1700 cm^{-1}, which indicates a mono-DMSU configuration.

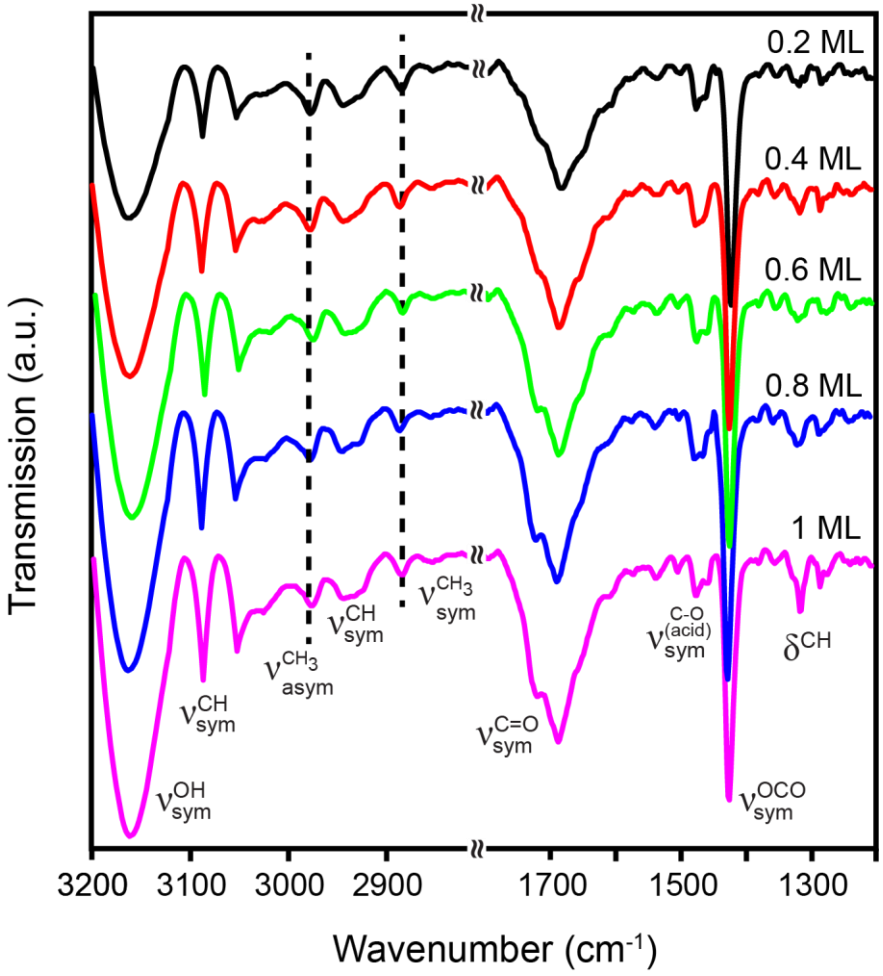

Figure 6.5: RAIRS spectra showing the transmission of a coverage series of rac-DMSU adsorbed at RT. The spectra are similar to those observed for meso-DMSU, with the most pronounced difference being the existence of the asymmetric component of the CH_3 vibration here.

Upon investigating the spectra of the p2gg(2×4) structures for both meso and racemic DMSU (Figure 6.6), it becomes evident that most of the bands are in the same positions and with relative intensities as before the heating treatment. The only differences are observed in the 1700 cm^{-1} region for both molecules and at around 1320 cm^{-1} for the racemate. The stretching vibrations of the carbonyl groups are now found at a slightly higher wavenumber than before the heating treatment and especially for the racemate, the band itself is much smoother with no shoulders, indicating homogeneity in the adsorbate layer. Also, in the case of the racemate the CH deformation vibration can no longer be observed, indicating that the hydrogens at carbons 2 and 3 of the molecule are now lying parallel to the surface, making the vibration invisible to the RAIRS.

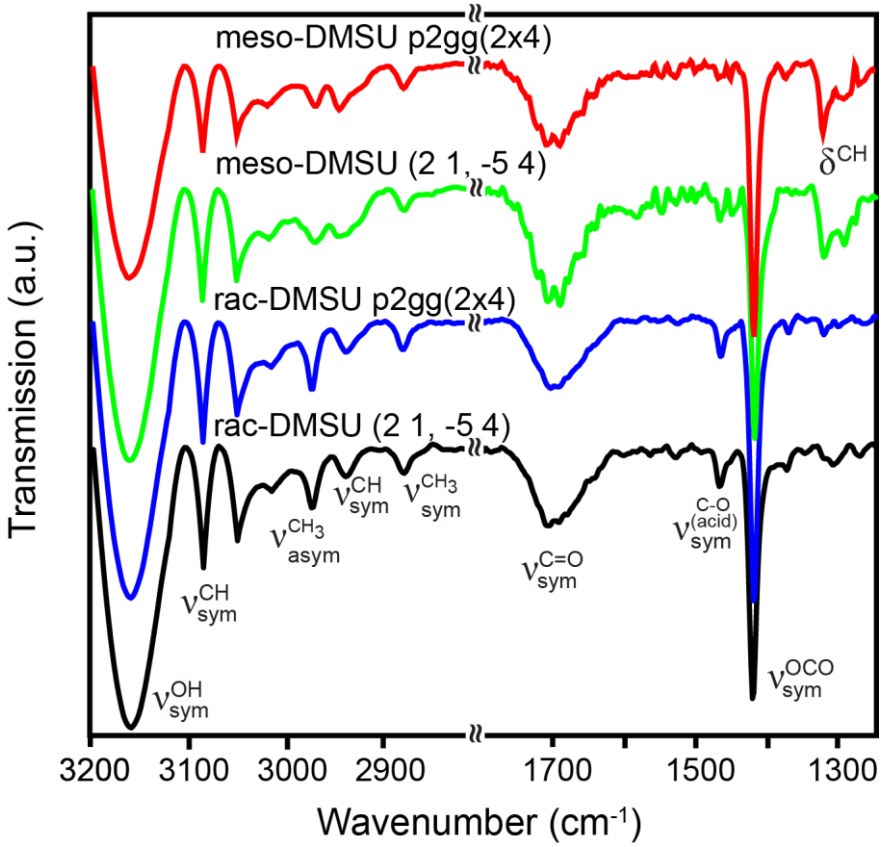

Figure 6.6: RAIRS spectra showing the transmission of the (2 1, –5 4) and p2gg(2×4) structures for both molecules. All spectra exhibit similar behavior, apart from the deformation vibration of the CH group which is present in the meso-DMSU samples, but not in the racemic ones.

In the case of the RAIR spectra of the (2 1, –5 4) structures (Figure 6.6) the situation is similar as before, with differences in band positions around 1700 cm^{-1} and 1320 cm^{-1}, when compared to the non-tempered samples. The spectra for each molecule follow the trend set by the p2gg(2×4) structures, with the bands appearing in the same positions. In both cases for meso and racemic DMSU however, the bands for the carbonyl vibrations show a decrease in intensity with respect to their p2gg(2×4) equivalents. On the other hand, the bands for the carboxylate vibrations around 1420 cm^{-1} show an analogous increase in intensity, indicating that an amount of molecules has become doubly deprotonated and has assumed a bi-DMSU configuration. The main difference between the spectra for the meso- and rac-DMSU is the existence and absence of the CH deformation vibration around 1320 cm^{-1}, respectively.

Unfortunately, the fact that both p2gg(2×4) and (2 1, –5 4) structures coexist on the surface, with the p2gg(2×4) being the dominant one, makes it impossible to determine experimentally the configuration that the molecules in the (2 1, –5 4) unit cell assume on the surface. The

vibrations for the saturation coverages and the structures for both molecules, along with their assignments are listed in Table 5.1.

Table 5.1: Frequencies and assignment of vibrational modes identified for the saturation coverages and the (2 1, –5 4) and p2gg(2×4) structures for both meso- and rac-DMSU (sh: shoulder, w: weak, b: broad, s: strong, m: medium).

Mode	Meso-DMSU			Racemic-DMSU		
	1 ML	**p2gg(2×4)**	**(2 1, –5 4)**	**1 ML**	**p2gg(2×4)**	**(2 1, –5 4)**
ν_{sym}^{OH}	3160 b,m	3160 b,m	3160 b,m	3161 b,m	3160 b,m	3160 b,m
ν_{sym}^{CH}	3087 s,m	3087 s,m	3087 s,m	3081 s,m	3087 s,m	3087 s,m
	3053 b,w	3051 b,w	3051 b,w	3053 b,w	3051 b,w	3051 b,w
$\nu_{asym}^{CH_3}$		2973 w	2973 w	2976 w	2976 w	2976 w
ν_{sym}^{CH}	2945 b,w	2945 w	2945 w	2943 w	2941 w	2941 w
$\nu_{sym}^{CH_3}$	2881 w	2881 w	2881 w	2884 w	2884 w	2884 w
$\nu_{sym}^{C=O}$	1713 sh		1722 sh	1715 sh	1700 b	1708 b
		1710 b	1708 b			
	1679 b	1692 b	1692 b	1681 b		1692 sh
		1664 sh	1664 sh			
$\nu_{sym}^{C-O(acid)}$	1470 w		1468 w	1463 b,w	1468 sh	1468 sh
ν_{sym}^{OCO}	1415 s	1419 s	1419 s			
δ^{CH}	1321 b	1324 b,w	1324 b,w	1422 s	1420 s	1420 s
		1292 sh	1292 sh	1310 w	1308 w	1321 w

6.3 STM

STM was used to investigate the enantiomorphous and achiral structures of both chiral and achiral DMSU. The experiments reveal the same results for both meso- and rac-DMSU but the quality of the rac-DMSU images is much better than that of its achiral analogue. This is in accordance with the LEED results, which exhibited stripes instead of sharp diffraction spots for the (2 1, –5 4) structure of meso-DMSU. Therefore, only the images for rac-DMSU will be presented here.

Figure 6.7a depicts a long-range image of the crystal when both (2 1, –5 4) and p2gg(2×4) structures are observed for rac-DMSU with LEED. They are all well-ordered and high resolution insets of the (2 1, –5 4) and p2gg(2×4) structures are shown in Figures 6.6b and c, respectively.

The p2gg(2×4) structure presents very well long-range order with islands bigger than 25×25 nm. Closer inspection of the structure (Figure 6.7c) displays the existence of two molecules within the unit cell, creating in this way rows of differently oriented molecules. The same effect has already been reported for SU both by LEED and STM [71]. A tentative model of this structure can be seen in Figure 6.3f.

In the STM images of the (2 1, –5 4) structure of rac-DMSU three distinct features can be detected within the unit cell. Of these features, two have an oval shape and are positioned at the same distance above the surface, whereas the third has a round shape and lies slightly lower than the other two. The difference in physical appearance and distance from the substrate is a strong indication that the two oval features are similar to each other, but different from the third one. More specifically the features are assumed to represent molecules and reconstructed copper atoms, respectively. Of the two molecules in the unit cell, one is a lying parallel to the [110] direction of the crystal, measured along the longest dimension of the oval shape, whereas the other one is lying along the <2,1> direction of the crystal and parallel to one of the molecules in the p2gg(2×4) structure. In the case of the mirrored configuration, the second molecule described above now lies along the <-2,1> direction of the crystal and parallel to the second molecule in the p2gg(2×4) structure.

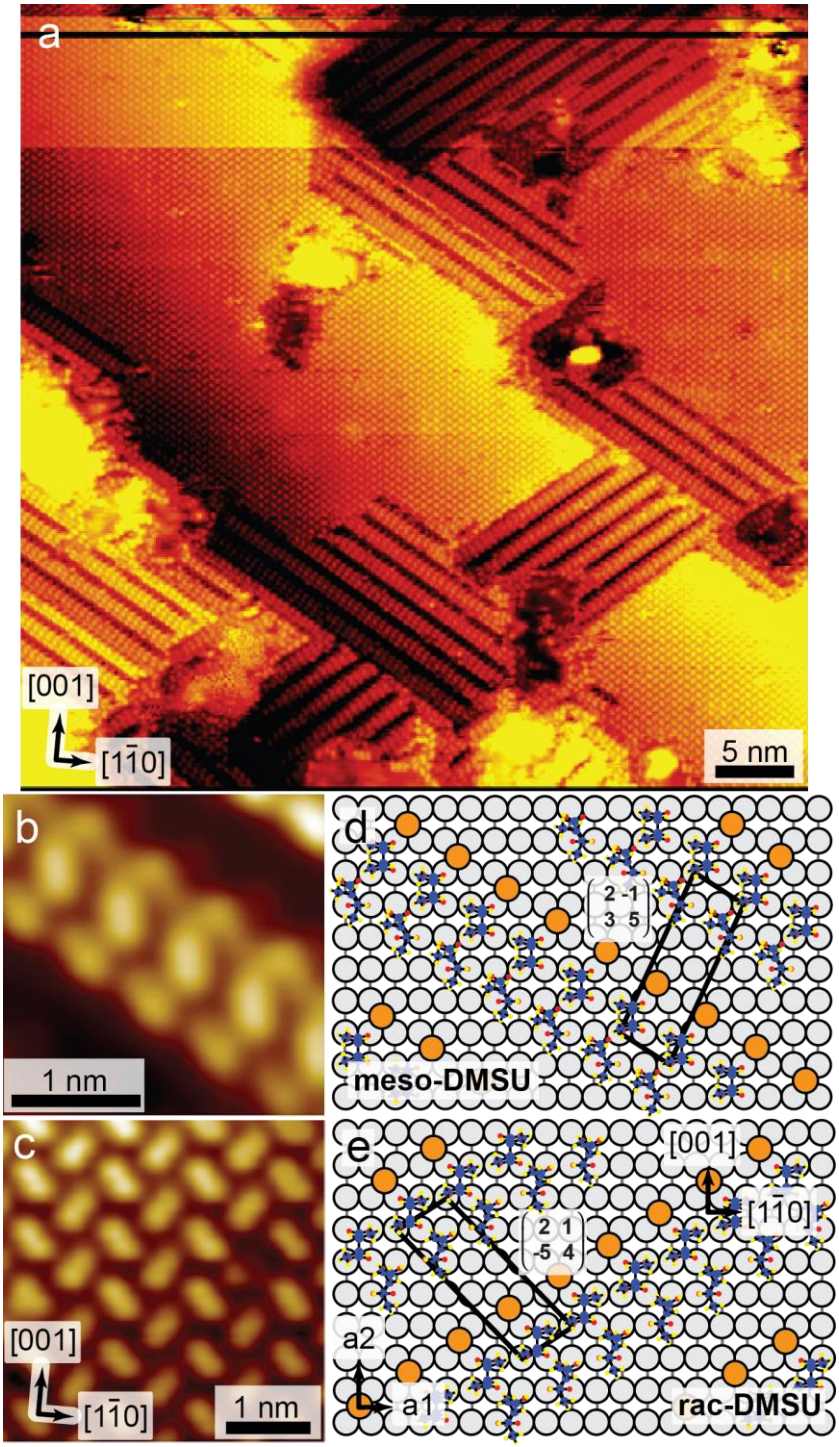

Figure 6.7: STM images of the achiral and enantiomorphous structures of rac-DMSU on Cu(110). a) Long range STM image (50 nm × 50 nm, I = -590 pA, U = -611 mV) showing the coexistence of the p2gg(2×4) structure and both mirrored domains of the (2 1, –5 4); b) close-up STM image (2.5 nm × 2.5 nm, I = 430 pA, U = 611 mV) of the (2 –1, 3 5) structure, which is the enantiomorph of the (2 1, –5 4) structure. The elongated features represent the molecules within the unit cell, whereas the round ones represent copper adatoms; c) STM image (3.8 nm × 3.8 nm, I = 430 pA, U = 611 mV) of the p2gg(2×4) structure. The molecules exhibit different orientations between adjacent rows and lines; d) tentative model of the (2 –1, 3 5) structure for meso-DMSU; e) tentative model of the (2 1, –5 4) structure for rac-DMSU.

A tentative model for this structure is shown for meso-DMSU in Figure 6.7d and for rac-DMSU in Figure 6.7e. Faint features are also observed behind the reconstructed copper atoms in Figure 6.7b, most likely depicting the copper atoms of the second layer of the crystal. As in the case of the p2gg(2×4) structure there are different configurations that the molecules could assume within the (2 –1, 3 5) unit cell and which would not alter the LEED or STM results. In the model in Figure 6.7e it is assumed that the molecules lying along the [110] direction of the crystal are (*R,R*)-DMSU, whereas the ones along the <2,1> direction are (*S,S*)-DMSU, with the former assuming a bi-DMSU configuration and the latter a mono-DMSU configuration, respectively. However, the arrangement of the molecules could be reversed, i.e. the former could be (*S,S*)- and the latter (*R,R*)-DMSU, leading to the same result. Alternatively, the structure could be composed of homochiral domains of only (*R,R*)- or (*S,S*)-DMSU. A preferred configuration due to energetic differences could potentially be identified by DFT calculations.

6.4 Conclusions

The adsorption behavior of chiral and achiral DMSU on Cu(110) was studied with a variety of methods. As with other dicarboxylic acids investigated previously, DMSU forms a chemical bond with the surface upon adsorption and after a certain amount of evaporation time the surface gets saturated.

After annealing of the crystal at the saturation coverage, LEED showed the existence of an achiral p2gg(2×4) structure. When the annealing temperature was increased, a (2 1, –5 4) structure appeared, which coexisted with the aforementioned p2gg(2×4) structure. In the case of rac-DMSU sharp diffraction spots could be observed, in contrast to the situation for meso-DMSU, where only faint diffraction spots with stripe-like appearance could be detected. This indicated a lower degree of order for meso-DMSU than for the racemate, something that was confirmed by STM results.

According to the RAIRS results both meso- and rac-DMSU were bound to the substrate in a mono-DMSU configuration with the oxygen atoms of the carboxylate group positioned equidistant from the surface. The inhomogeneity of the molecular layer in the case of meso-DMSU was again evident in the form of several shoulders in the carboxylate vibration around 1700 cm^{-1}. The molecules were bound in a mono-DMSU configuration when only the p2gg(2×4) structure was present on the crystal. Unfortunately, it was not possible to propose

an indisputable configuration for the molecules in the (2 1, –5 4) structure, since its coexistence with the p2gg(2×4) structure could possibly be clouding the presence of molecules in a bi-DMSU configuration.

STM imaging of both structures showed the distinct existence of glide planes in the p2gg(2×4) structure with the molecules arranged in rows running along the [001] direction of the crystal. Within the p2gg(2×4) unit cell two different molecules could be observed, one with its backbone lying along the <2,1> direction of the crystal and a second one with a configuration perpendicular to that of the first one. The islands of the (2 1, –5 4) structure displayed bright elongated features for the molecules and round features for reconstructed copper atoms that were positioned a little lower than the molecules. The second layer of the copper substrate could also be seen in this structure, albeit with a lower quality.

Although DMSU is a molecule with a larger volume than those reported in the previous chapters, due to the methyl groups in carbons 2 and 3, it is evident that its bigger size does not hinder it from creating ordered structures on the crystal. It is interesting that of those structures, the achiral p2gg(2×4), which exhibits very well long-range order, has been now observed for several dicarboxylic acids with differences in their molecular backbones. The enantiomorphous structure created by DMSU induces a reconstruction of the copper substrate, although in a different periodicity than that reported for FUA and MAL. The fact that meso-DMSU exhibits lower quality ordering, apparent both in LEED and STM, is probably due to the fact that the methyl groups are positioned on the same side of the molecule, creating in this way a steric hindrance.

7: *Trans*-1,2-cyclohexane dicarboxylic acid

Trans-1,2-cyclohexane dicarboxylic acid (CHDCA) is a chemical compound with the structural formula shown in Figure 7.1. It shares a similar configuration with the rest of the dicarboxylic acids already investigated, i.e. two carboxylic acid groups that can form chemical bonds with the copper substrate. Its molecular backbone is composed of one side of a hexane ring, with the rest of the ring acting as a bulky substituent.

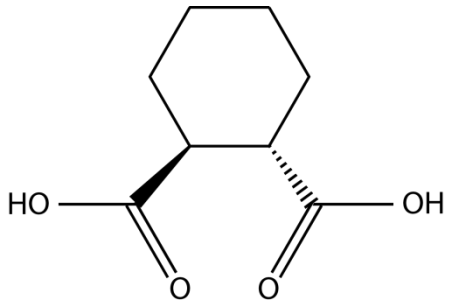

Figure 7.1: Structural formula and ball-and-stick model for CHDCA.

Due to the hexane ring, this molecule is much larger than the ones already investigated, which could potentially lead to steric hindrance in the self-assembly, thus creating interesting new configurations.

The molecule was investigated with all the methods typically used in this research work, with the XPS results available in the Appendix. Unfortunately, no ordered structures could be prepared in System B containing the STM and RAIRS facilities. Therefore, no results will be presented for the former method and only results for the non-tempered samples for the latter method.

7.1 LEED

Upon adsorption of CHDCA on the crystal at RT only a low quality c(2×4) structure is observed at monolayer saturation. However, annealing the crystal after adsorption of the

molecules, or keeping the crystal at elevated temperatures during evaporation leads to several well-ordered structures, which are depicted in Figure 7.2.

When evaporation is performed at RT and after annealing the saturated crystal at 373 K for 15 to 30 minutes a well ordered p(2×4) structure with missing (0,n) spots, n = 1/2 , 3/2, etc and missing (n,0) spots, n = 1/4, 3/4, etc, can be observed (Figure 7.2a). This is the same structure with those already identified for FUA, MAL and DMSU and will hereby be referred to as p2gg(2×4). Further annealing at 423 K leads to the appearance of a (1 1, –5 2) enantiomorphous structure, which is shown in Figure 7.2b. Additionally, weak stripes can be observed running along the <1,1> and <1,–1> directions of the crystal, suggesting an additional (2,±2) periodicity in real space, similar to the one reported for FUA and MAL (chapters 3 and 4, respectively).

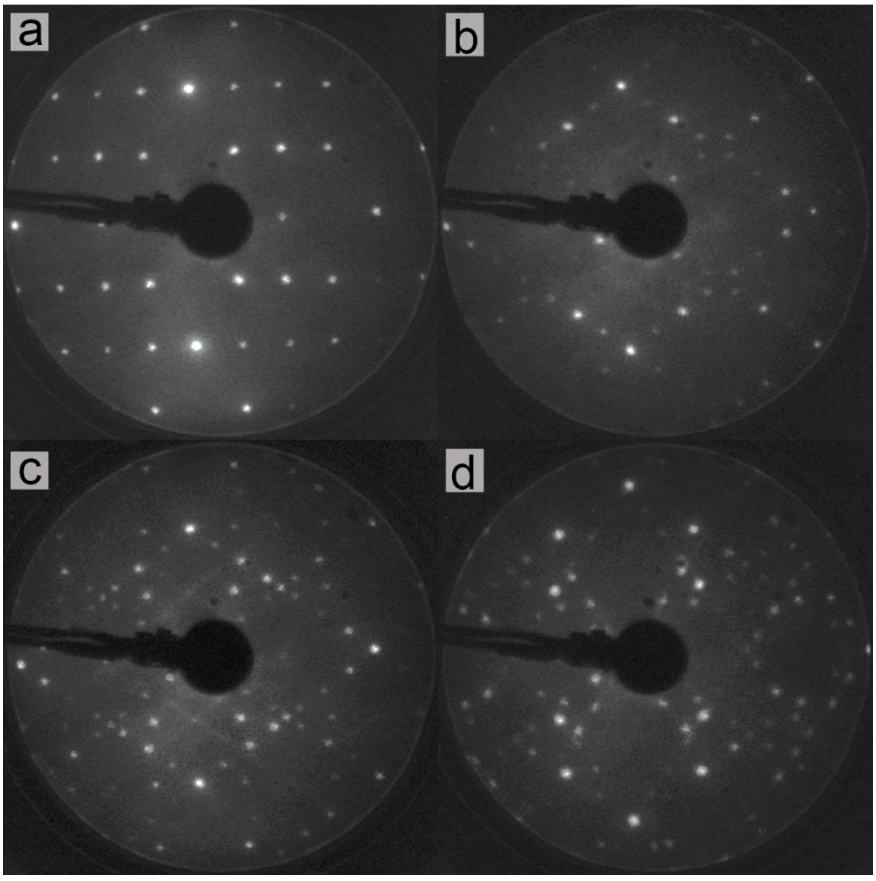

Figure 7.2: LEED patterns of CHDCA on Cu(110). a) p2gg(2×4) structure, E_p = 54 eV; b) (1 1, –5 2), E_p = 51 eV, the faint lines in the background suggest an additional (2,±2) periodicity instead of just the (1,±1); c) p2gg(2×4) structure coexisting with a (1 1, –5 2) and a (1 2, –5 4) structure, E_p = 55 eV; d) closer look of the structure in c), E_p = 32 eV.

When evaporation is performed with the temperature of the crystal at 423 K and after the saturation coverage has been reached, additional diffraction spots appear with 3 different structures now coexisting on the surface (Figure 7.2c and d). These can be identified as an achiral p2gg(2×4) structure and two enantiomorphous (1 1, –5 2) and (1 2, –5 4) structures.

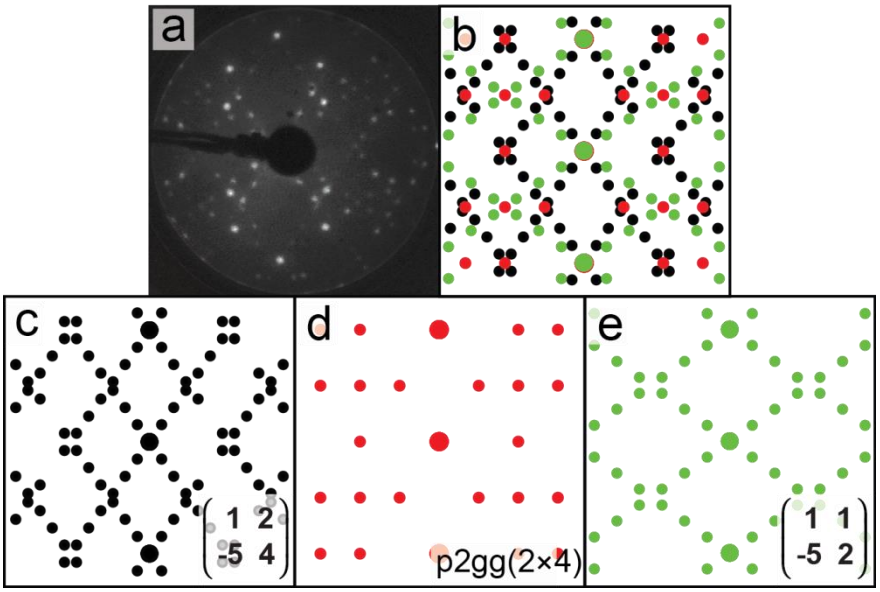

Figure 7.3: LEED pattern of the mixed structure of CHDCA with simulated LEED patterns of the individual structures composing it. a) p2gg(2×4) structure coexisting with a (1 1, –5 2) and a (1 2, –5 4) structure, E_p = 32 eV; b) simulated LEED pattern of all three superimposed structures with missing (0,n) spots, n = 1/2 , 3/2 in the case of the p2gg(2×4) structure; c) simulated LEED pattern of the (1 2, –5 4) structure, d) simulated LEED pattern of the p2gg(2×4); e) simulated LEED pattern of the (1 1, –5 2) structure.

Simulated LEED patterns of the three isolated structures, as well as the result of their superposition can be seen in Figure 7.3. It should be noted that the p2gg(2×4) structure has been discovered for FUA, MAL and DMSU, whereas the (1 1, –5 2) structure for FUA and MAL and the (1 2, –5 4) for DMSU. It appears that upon adsorption on the crystal CHDCA behaves in a similar way as all three of these molecules. The steric hindrance in the molecular backbone created by the cyclohexane ring mimics that created by the C=C in FUA and MAL, therefore forming the (1 1, –5 2) structure, whereas the existence of the bulky $–CH_3$ substituents of DMSU is simulated in the case of CHDCA by the presence of the hexane ring, consequently forming the (1 2, –5 4) structure. Models for all the structures observed for CHDCA can be found in previous chapters.

7.2 RAIRS

A series of different amounts of CHDCA adsorbed on the crystal at RT was investigated by RAIRS in order to obtain information about the configuration of the molecules, with the results depicted in Figure 7.4. For all spectra an intense band around 1416 cm^{-1} is detected, which is assigned to the symmetric stretching vibration of the OCO group. This suggests that at least one of the carboxylic acid groups is deprotonated and bound to the Cu substrate. The fact that the asymmetric OCO vibration appears only weakly around 1530 cm^{-1} indicates that the oxygen atoms are positioned almost completely equidistant from the surface.

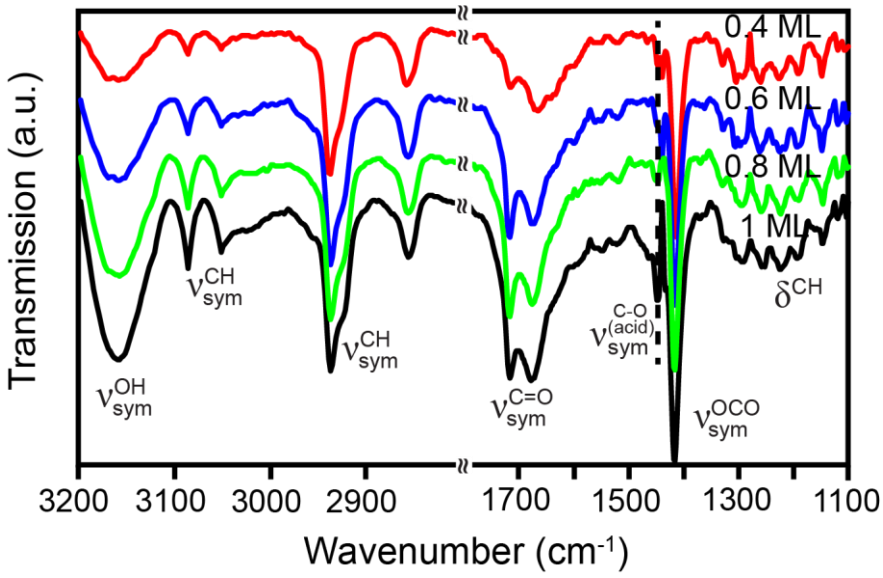

Figure 7.4: RAIRS spectra showing the transmission of a coverage series of CHDCA adsorbed at RT, with no additional heating treatment. All spectra show a strong C=O vibration band around 1700 cm^{-1}, which is indicative of mono-CHDCA configuration. The splitting of the band, however, suggests the presence of an additional molecular species.

The bands around 1700 cm^{-1} and 1447 cm^{-1} assigned to the stretching vibration of the C=O and the C-O of the acid group respectively, lead to the conclusion that the second carboxylic acid group is intact and does not form a chemical bond with the surface. The splitting of the carbonyl band around 1700 cm^{-1} suggests inhomogeneity in the adsorbate layer, indicating that there might be more than one molecular species present. However, due to the results, a mono-CHDCA arrangement is proposed as the dominating molecular configuration. This is also confirmed by the existence of a broad band around 3160 cm^{-1}, associated with the

symmetric stretching vibration of the OH entity in the carboxylic acid group. It should be noted, however, that an additional bi-CHDCA configuration cannot be dismissed.

Table 7.1: Frequencies and assignment of vibrational modes identified for the saturation coverage of CHDCA without further heating treatment (sh: shoulder, w: weak, b: broad, s: strong, m: medium).

Mode	**1 ML**
ν_{sym}^{OH}	3159 b,m
ν_{sym}^{CH}	3086 s,m
	3051 b,w
ν_{sym}^{CH}	2937 w
	2920 sh
	2856 w
$\nu_{sym}^{C=O}$	1716 b
	1675 b
	1629 sh
ν_{asym}^{OCO}	1535 b,w
	1518 b,w
$\nu_{sym}^{C-O(acid)}$	1447 w
ν_{sym}^{OCO}	1416 s
δ^{CH}	1297 b,w
	1254 b,w
	1221 b,w
	1190 w
	1145 w

The rest of the bands observed in the spectra are associated with the symmetric vibrations of the several CH groups of the hexane ring. Unfortunately the characteristic vibration of the hexane ring itself cannot be detected since it is outside of the measurement limits of the spectrometer. A detailed report of the observed bands with their respective assignments is given in Table 7.1.

It should be noted that, as mentioned in Chapter 3 for FUA, the bands around 2930 cm^{-1} could possibly be measurement artifacts due to dirt in the spectrometer.

7.3 Conclusions

LEED and RAIRS results of the adsorption of *trans*-1,2-cyclohexane dicarboxylic acid were presented here. LEED investigation of annealed samples led to the discovery of three different structures, an achiral p2gg(2×4), an enantiomorphous (1 1, –5 2) and the superposition of both of these and an enantiomorphous (1 2, –5 4) structure, with faint stripes in the background suggesting the existence of an additional (2,±2) periodicity.

It is noteworthy that when the same structure appeared in the case of FUA and MAL with the coexistence of the faint stripes, STM indicated the presence of two different unit cells, one defined by the arrangement of the molecules and one due to a reconstruction of the underlying copper substrate. Although no STM investigation has been performed for CHDCA it can be assumed that the situation is similar here, with the molecule forcing the crystal surface to rearrange its uppermost atomic layer. This result indicates that the nature of the chemical bond between the carboxylic acid groups of the molecules and the substrate is what drives this reconstruction, with the specific structure of the molecular backbone having little or no influence in the process.

RAIRS uncovered a dominant mono-CHDCA configuration for the molecules when no heating was applied to the crystal. However, splitting of the band describing the stretching vibration of the carbonyl group suggested that another molecular species might be present on the surface.

8: Phthalic acid

Phthalic acid (PHTA) is a chemical compound with the structural formula shown in Figure 8.1. It is another member of the dicarboxylic acid family, very similar in configuration with CHDCA, with the only difference being that its backbone is composed of a benzene ring.

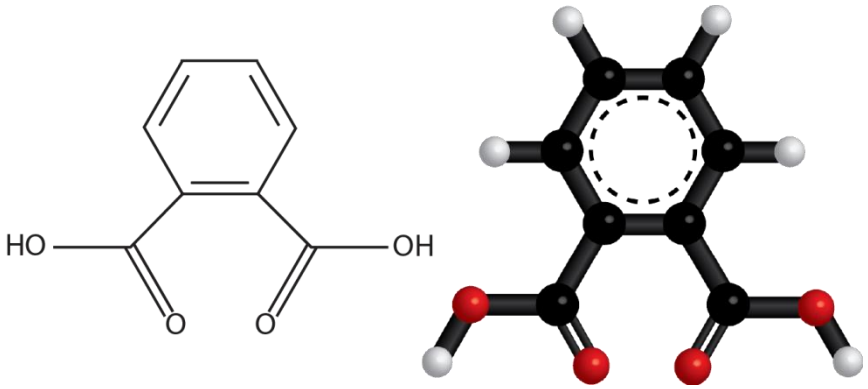

Figure 8.1: Structural formula and ball-and-stick model for PHTA.

The presence of the benzene ring makes the molecular backbone more rigid and immune to twisting, giving an additional degree of steric hindrance to the molecule.

The coverage calibration and general XPS investigation of the molecule can be found in the Appendix.

8.1 LEED

Upon adsorption of PHTA on the surface no ordered structures are observed at room temperature or with annealing of the sample. When the evaporation is performed with the sample at elevated temperatures and after the crystal is allowed to cool back down to RT, two achiral and three enantiomorphous structures are observed, as shown in Figure 8.2. However, not all structures could be detected in both UHV systems used. In system A (see Chapter 2), when evaporation was performed with the crystal temperature held at 373 K, and after the saturation coverage had been reached, an achiral p(3×2) structure with missing (0,n) spots, n

= 1/3 , 4/3, etc and missing (n,0) spots, n = 1/4, 3/4, etc. was observed (Figure 8.2a). The missing spots suggest the existence of glide planes parallel to the [001] and $[1\bar{1}0]$ directions of the crystal, as observed for several of the dicarboxylic acids described in previous chapters, as well as for SU [71]. This structure will henceforth be referred to as p2gg(3×2), with a tentative model for it shown in Figure 8.3d. Upon increasing the temperature of the crystal prior to evaporation to 398 K and with a coverage of about 0.63 ML, an enantiomorphous (2 –3, 5 3) pattern was detected. This consisted of the superposition of two chiral mirrored domains, as shown in Figure 8.2b, with a simulated pattern for the structure presented in Figure 8.3a. With the crystal temperature at 423 K during evaporation and at saturation coverage, another structure was discovered (Figure 8.2c). The LEED pattern was a p(10×2) with missing (0,n) spots, n = 1/2 , 1, etc and missing (n,0) spots, n = 1/4, 1/2, etc. The missing spots suggest the existence of glide planes parallel to the [001] and $[1\bar{1}0]$ directions of the crystal. Hence, the structure is named p2gg(10×2), with a tentative model for it shown in Figure 8.3e.

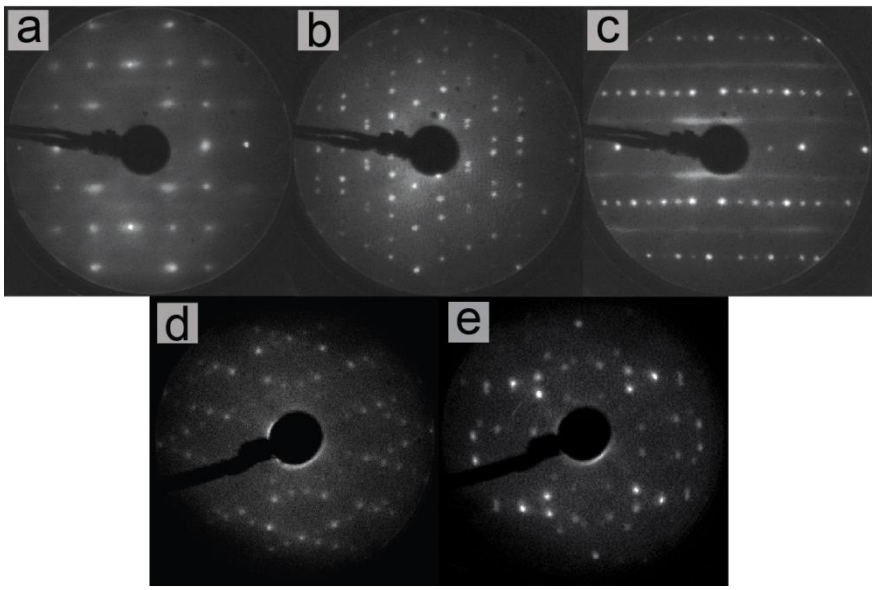

Figure 8.2: LEED patterns of PHTA on Cu(110). a) p2gg(3×2) structure, E_p = 60 eV; b) (2 –3, 5 3) structure, E_p = 27 eV; c) p(10×2) structure, E_p = 34 eV, faint stripes running along the $[1\bar{1}0]$ direction of the crystal indicate the existence of an additional double periodicity; d) (1 2, –8 2) structure, E_p = 48 eV; e) (1 3, –6 1) structure, E_p = 36 eV.

Two additional enantiomorphous structures were observed in System B. The first was obtained at a coverage of about 0.4 ML of PHTA on the crystal, with the surface temperature

held at 373 K during evaporation. The structure, which is shown in Figure 8.2d, is a (1 2, –8 1) structure, composed of two mirror domains. It should be noted that it is similar to the (9 0, 1 2) structure reported for (*R*,*R*)-TA on Cu(110) [54] and the (1 2, –8 2) structure reported for (*R*)-MA on Cu(110) [67]. A simulated pattern of this structure depicting both mirrored domains is shown in Figure 8.3b.

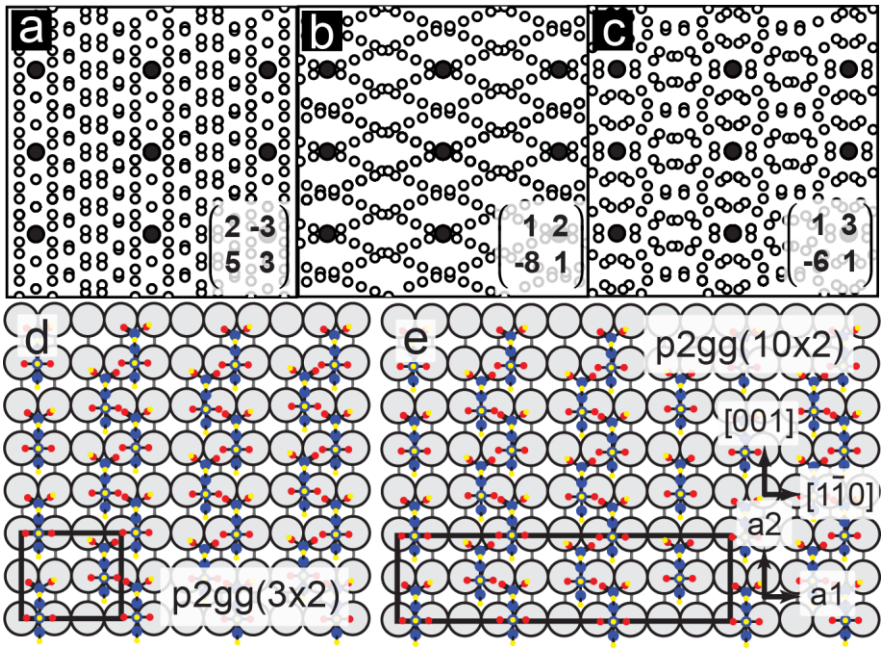

Figure 8.3: LEED pattern simulations representing the LEED images of the enantiomorphous structures of PHTA on Cu(110). The Cu diffraction spots are represented by black dots. a) (2 –3, 5 3) structure; b) (1 2, –8 1) structure; c) (1 3, –6 1) structure; d) tentative model of the p2gg(3×2) structure. It is assumed that the molecules adopt a monophtalate configuration; e) tentative model of the p2gg(10×2) structure. Also here it is assumed that the molecules adopt a monophtalate configuration.

The second structure discovered in System B was a (1 3, –6 1) structure which was obtained when approximately 0.85 ML of PHTA molecules were adsorbed on the substrate with the crystal temperature during evaporation held at 423 K. The LEED pattern of this structure and a simulated pattern for it are shown in Figures 8.2e and 8.3c, respectively.

8.2 RAIRS

A series of different amounts of PHTA adsorbed on the crystal at RT were investigated with RAIRS, with the results depicted in Figure 8.4.

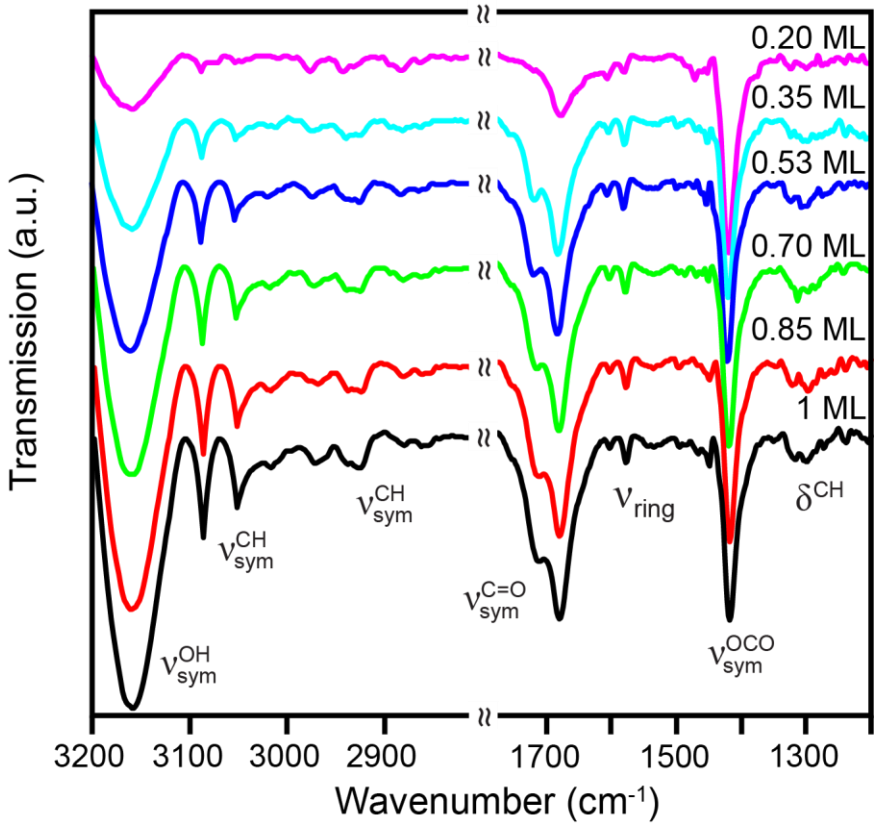

Figure 8.4: RAIRS spectra showing the transmission of a coverage series of PHTA adsorbed at RT, with no additional heating treatment and with no ordered structures detected by LEED. All spectra show a strong C=O vibration band around 1680 cm^{-1}, which is indicative of monophthalate configuration, whereas the shoulder around 1710 cm^{-1} suggests inhomogeneity in the molecular layer.

For all coverages an intense band is detected around 1420 cm^{-1}, which describes the symmetric stretching vibration of the carboxylate group, indicating that at least one carboxylic acid group is deprotonated and bound to the substrate. The fact that the asymmetric OCO vibration at around 1530 cm^{-1} cannot be detected suggests that the oxygen atoms in the carboxylate group are equidistant from the surface. The configuration of the second carboxylic acid group is revealed by the band around 1680 cm^{-1}, assigned to the stretching vibration of the carbonyl group. The existence of this vibration indicates that the molecule is bound in a monophthalate configuration. This is further supported by the existence of the band around 3160 cm^{-1} assigned to the OH group in the carboxylic acid group not bound to

the substrate. The fact that the band for the carbonyl group displays the existence of a shoulder around 1720 cm^{-1} suggests inhomogeneity in the molecular layer and the presence of at least two different molecular species on the crystal. Both of these molecular species are bound in a monophthalate configuration but within different chemical environments, possibly due to the interaction of the benzene rings with their neighbors or with the substrate. The rest of the bands detected are associated with the various vibrations occurring due to the benzene ring. Specifically, the weak band around 1460 cm^{-1} is assigned to the "ring mode" or otherwise known as "breathing mode" of the ring, which has to do with the stretching and contracting of the C-C bonds in it. The vibrations associated with the in- and out-of-plane bending of the ortho-di-substituted benzene ring in PHTA, would normally be detected between 770-735 cm^{-1}. They are, however, outside of the resolution of the IR-spectrometer used in this work.

RAIRS experiments were also performed when the (1 2, –8 1) and (1 3, –6 1) structures were present on the surface, the results of which are shown in Figure 8.5.

The main bands detected in the spectrum for the (1 2, –8 1) structure were already present for the non-tempered samples. However, a closer inspection of the band for the carbonyl vibration around 1700 cm^{-1} reveals that its intensity is now much lower than that of the carboxylate around 1420 cm^{-1}. Moreover, the existence of a shoulder around 1400 cm^{-1}, and the fact that the quality of the LEED image is not perfect, suggests that there are two different types of molecules accommodated on the surface, one arranged in a biphthalate configuration and another in a monophthalate configuration. No ring mode vibrations can be detected between 1450 cm^{-1} and 1600 cm^{-1}.

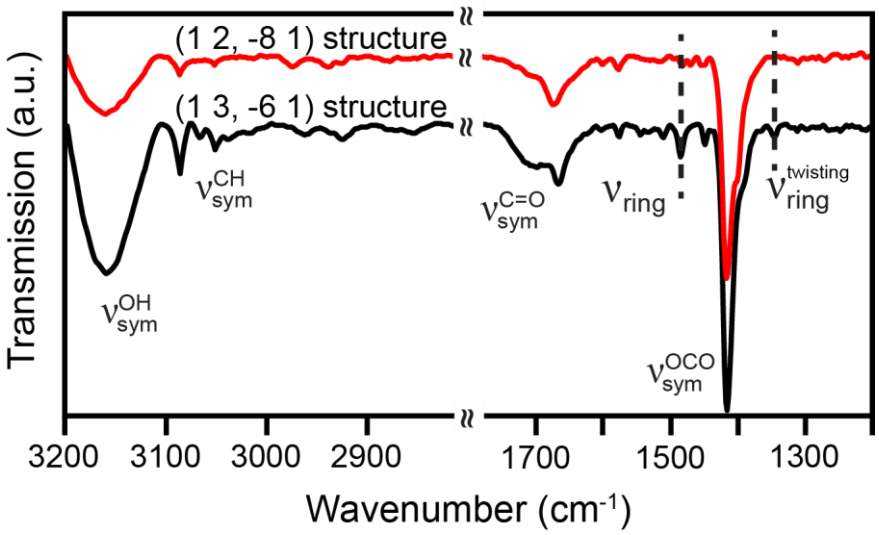

Figure 8.5: RAIRS spectra showing the transmission of two of the enantiomorphous structures of PHTA. Compared to the non-tempered samples, here a much smaller intensity of the C=O stretching mode can be observed. The shoulder in the (1 3, –6 1) structure indicates the existence of two distinct molecular species on the crystal with different configurations.

The situation is slightly different when the (1 3, –6 1) structure is present on the surface, with the main differences being the shape of the band for the carbonyl vibration and the existence of two ring mode vibrations around 1480 cm^{-1} and 1350 cm^{-1}. The wide band for the carbonyl group around 1700 cm^{-1} and the existence of a shoulder for the carboxylate band at 1390 cm^{-1} suggests, also in this case, the existence of two different molecular species on the crystal. Of these, one is arranged in a biphthalate configuration and the other is bound in an unidentate arrangement. In the unidentate case only one oxygen atom of each carboxylic acid group is chemically bound to the copper substrate, thus forcing the benzene ring to tilt in an orientation different than in the biphthalate case.

All vibrations for the saturation coverage and the two structures along with their assignments are listed in Table 8.1.

Table 8.1: Frequencies and assignment of vibrational modes identified for the saturation coverage of the non-tempered samples and two of the enantiomorphous structures (sh: shoulder, w: weak, b: broad, s: strong, m: medium).

Mode	1 ML	(1 2, –8 1)	(1 3, –6 1)
ν_{sym}^{OH}	3159 b,m	3157 b,m	3157 b,m
ν_{sym}^{CH}	3085 s,m	3085 s,m	3085 s,m
	3051 b,w		3051 b,w
	2969 b,m		
ν_{sym}^{CH}	2928 w		
$\nu_{sym}^{C=O}$	1712 sh		1704 sh
	1680 s	1671 b,m	1664 b,m (unidentate)
ν_{ring}	1576 w	1574 w	1574 w
			1484 w,s
ν_{sym}^{OCO}	1417 b	1415 s	1415 s
		1396 sh	1391 sh (unidentate)
$\nu_{ring}^{twisting}$			1344 w
δ^{CH}	1306 w		

8.3 STM

STM experiments were performed for the (1 2, –8 1) and (1 3, –6 1) structures, with the results, along with tentative models for each, shown in Figures 8.6 and 8.7 respectively.

In Figure 8.6 the (1 2, –8 1) structure and its enantiomophous (1 –2, 7 3) domain are shown. The molecules are arranged in lines running along the <±1,2> direction of the crystal, with three adjacent molecules creating thick lines which are isolated from each other from an atom-wide gap. Of the three molecules in each line, the middle one appears to be higher than its neighbors, expressed in the STM by much brighter features. A tentative model for both enantiomorphous domains is shown in Figure 8.6c. The STM result is in agreement with the RAIRS experiments, which suggested a biphthalate configuration, with only a few molecules assuming a monophthalate arrangement. Long-range STM images showed that there is good order for the most part, with only small areas exhibiting disorder. It is therefore assumed that

the molecules in the (1 2, –8 1) structure are arranged in a biphthalate configuration and those in the disordered areas assume the monophthalate configuration.

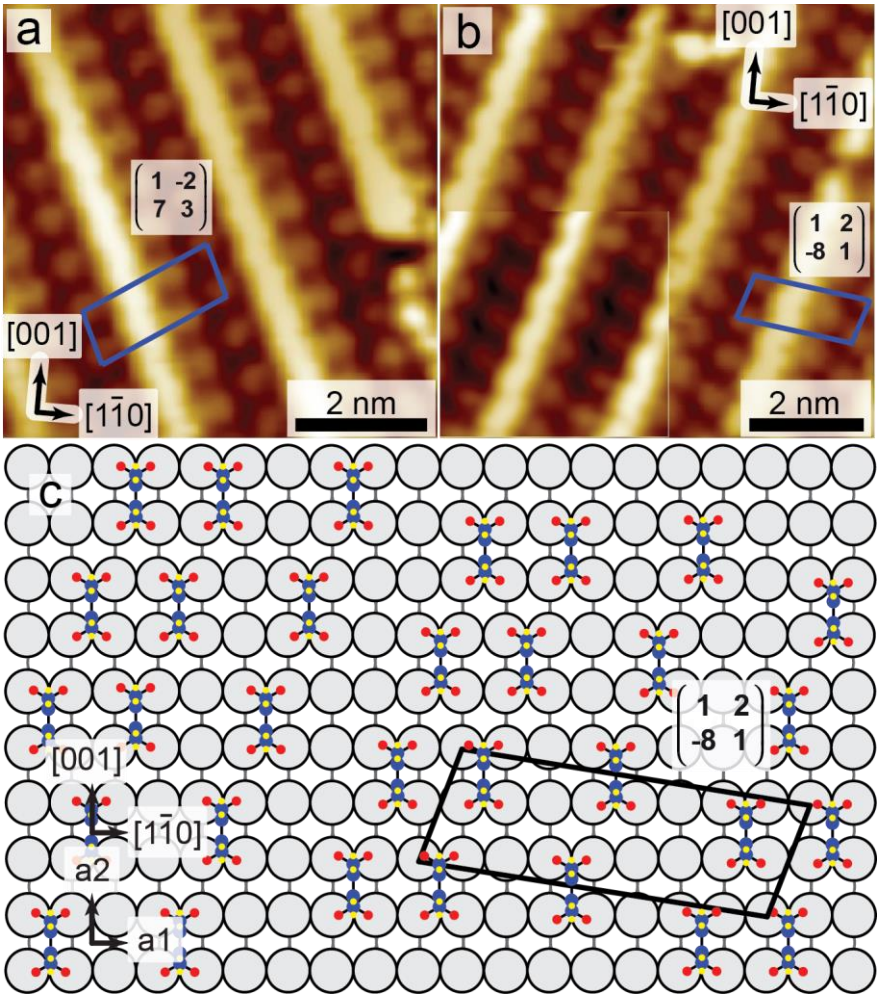

Figure 8.6: STM images of the (1 2, –8 1) domains of PHTA on Cu(110). a) STM image (6.6 nm × 6.6 nm, I = – 440 pA, U = – 423 mV) of the (1 –2, 7 3) domain, which is the enantiomorph of the (1 2, –8 1) structure. The blue parallelogram denotes the unit cell; b) STM image (7.6 nm × 7.6 nm, I = – 440 pA, U = – 423 mV) of the (1 2, –8 1) structure. A part of the image is shown in higher resolution in the inset (4 nm × 4 nm, I = – 440 pA, U = – 423 mV, inset averaged 5×); c) tentative model of the (1 2, –8 1) unit cell, which is denoted by the black parallelogram.

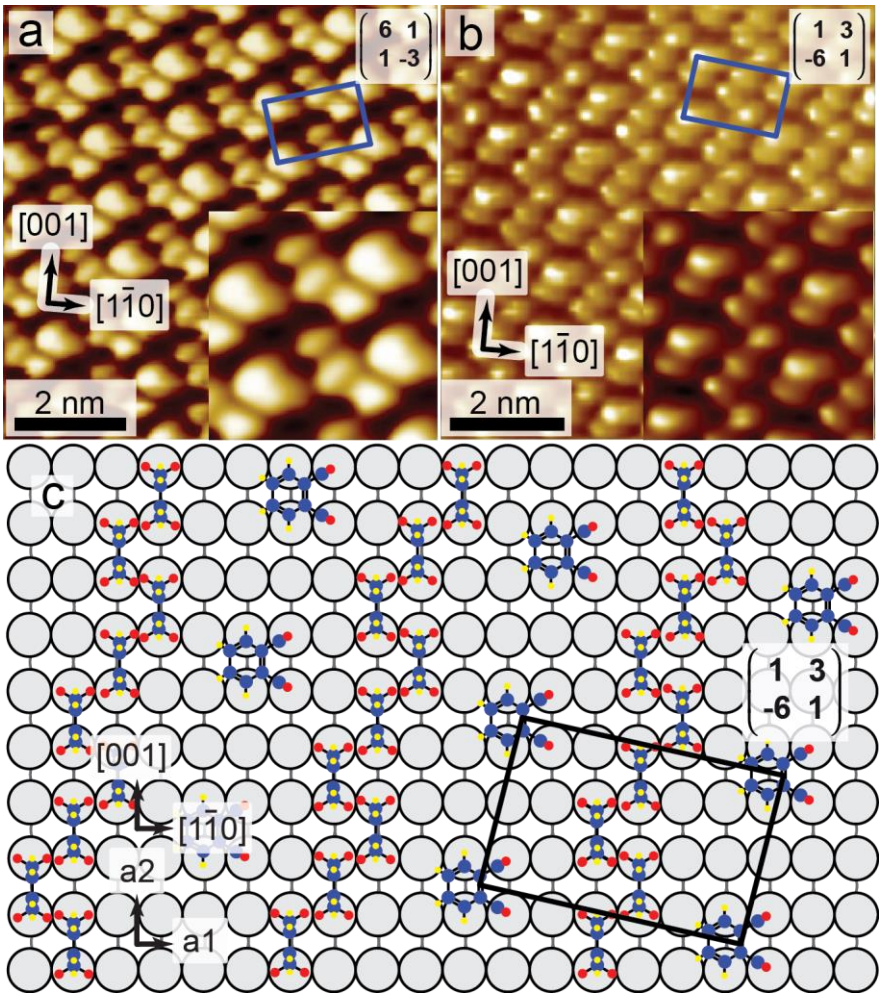

Figure 8.7: STM images of the (1 3, –6 1) domains of PHTA on Cu(110). a) STM image (7.8 nm × 7.8 nm, I = – 370 pA, U = – 782 mV) of the (6 1, 1 –3) domain, which is the enantiomorph of the (1 3, –6 1) structure. A part of the image is shown in higher resolution in the inset (2.6 nm × 2.6 nm, I = – 370 pA, U = – 782 mV, inset averaged 5×). The blue rectangle denotes the unit cell; b) STM image (7.6 nm × 7.6 nm, I = 430 pA, U = 857 mV) of the (1 3, –6 1) structure. A part of the image is shown in higher resolution in the inset (3 nm × 3 nm, I = 430 pA, U = 857 mV, inset averaged 5×); c) Model of the (1 3, –6 1) structure, with the black rectangle denoting the unit cell.

The (1 3, –6 1) structure was also investigated with STM and the results for both enantiomorphs, as well as a tentative model are shown in Figure 8.7. It is evident from the STM results that there are two different types on molecules present on the surface, one that appears brighter and slightly bigger in the STM images and a second type depicted by smaller, more subdued features. The slightly bigger features are better resolved in the (1 3, –6 1) structure than in its mirror domain, as shown in Figures 8.7b and a, respectively. The higher resolution of the (1 3, –6 1) structure helps to clarify that the big feature is actually composed of a set of three smaller features. It is therefore concluded that this set of features depicts the molecules in the unidentate configuration that was identified in the RAIRS. The

fainter features in the set correspond to the two carboxylic acid groups bound to the substrate, whereas the middle brighter feature is assigned to the benzene ring, which is tilted with respect to the surface normal. An illustration of the way the molecules are bound to the substrate for unidentate-, bi- and monophthalate configurations is shown in Figure 8.8.

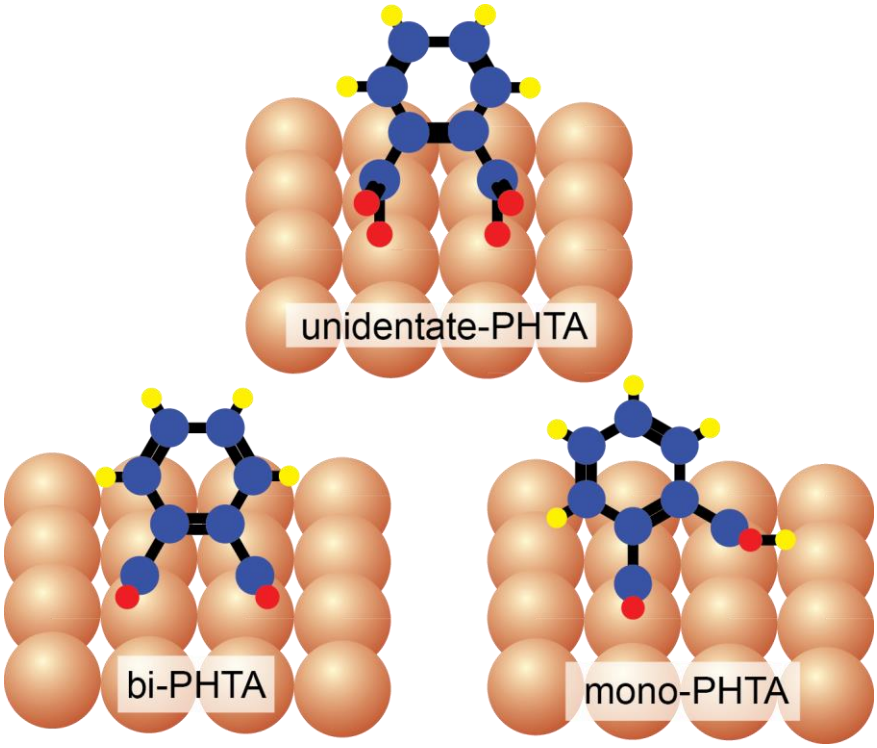

Figure 8.8: Models of the different adsorption modes of PHTA on Cu(110).

The rest of the molecules appear in a triplet formation running parallel to the <±1,1> direction of the crystal. Each triplet is positioned to the left or right of its neighboring triplet, depending on the enantiomorphous domain. The last molecule of each triplet is lying 4.4 Å away from the first molecule in the next triplet, which is equivalent to the distance of one Cu atom to the next in the <±1,1> direction.

8.4 Conclusions

After evaporation of PHTA on the heated substrate LEED revealed five well-ordered structures, two achiral, p2gg(3×2) and p2gg(10×2), and three enantiomorphous, (2 –3, 5 3), (1 2, –8 1) and (1 3, –6 1).

The binding mode of the molecules was investigated by RAIRS for a series of non-tempered samples, when no ordered structures were present, as well as when two of the enantiomorphous structures could be observed. This revealed that, in the absence of an ordered structure, the molecules assumed a monophthalate configuration, being chemically bound to the substrate via the two oxygen atoms of one of the carboxylic acid groups. The situation changed when two of the enantiomorphous structures were present on the surface. In the case of the (1 2, –8 1) structure the molecules were bound in a biphthalate configuration with the plane of the benzene ring positioned perpendicular to the surface. A small amount of molecules in the disordered areas on the surface were still in a monophthalate configuration. In the case of the (1 3, –6 1) structure two distinct molecular species were present, one assuming a biphthalate orientation and one arranged in an unidentate configuration, being bound to the surface with only one oxygen atom of both carboxylic acid groups. This configuration therefore forced the benzene ring to be tilted away from the surface normal.

STM investigation of the two aforementioned structures confirmed the RAIRS results, with the STM images of the (1 2, –8 1) structure exhibiting lines of three equivalent molecules, with the middle molecule in each row arranged slightly higher than its neighbors. These lines were separated from each other by atom-wide gaps, strongly resembling the results already reported for TA and MA. STM investigation of the (9 0, 1 2) and (1 2, –8 1) structures of TA [54] and MA [67], respectively, revealed the existence of rows of three molecules separated from each other by gaps, which were referred to as “troughs” [57, 58]. The middle of the three molecules in each row appeared brighter in the STM and RAIRS investigation revealed a bi-tartrate and bi-malate configuration, respectively. In spite of the fact that the molecular structure of PHTA is quite dissimilar to both TA and MA, the molecule still forms a very similar self-assembly configuration. This could possibly be due to the fact that the plane of the benzene ring is most likely perpendicular to the surface, thus not adding any further volume in the footprint of the molecule onto the surface. Additionally, the benzene rings themselves might interact with one another.

The STM results for the (1 3, –6 1) structure were also consistent with the RAIRS findings, clearly revealing the presence of two types of molecular species on the surface. The unidentate-bound molecule was characterized by a set of one bright and two more subdued features, corresponding to the benzene ring and the two carboxylic acid groups respectively. The molecules in the biphthalate configuration were organized in a triplet formation along the <±1,1> direction of the crystal, creating in this way zigzag rows along the [001] direction of the substrate.

9: Thermal decomposition of dicarboxylic acids

In order to investigate the desorption mechanism of the dicarboxylic acids in this work, TPD experiments were performed. The crystal was held at room temperature while adsorption of the molecules took place. During the decomposition experiment the crystal was held perpendicular to the line-of-sight of the mass spectrometer and heated with a heating rate of 4 K/sec. The coverage was determined with XPS before the decomposition experiment, whereas further XPS measurements after the desorption experiment revealed a complete absence of oxygen on the surface and only a minimal amount of carbon. The molecular mass could never be detected, meaning that the intramolecular bonds break before the metal-molecule bonds, causing the molecules to decompose in fragments. The fragments with the highest intensities were CO_2, CO and H_2, with only the results for CO_2 being presented here, with the desorption signals for CO and H_2 being very similar.

9.1 Fumaric acid

Figure 9.1 shows the TPD spectra obtained for different amounts of FUA on the crystal, without any further heating treatment. All spectra show characteristics of surface explosion decomposition, as discussed in Chapter 1.3.7, i.e. the position of the peak shifts with increasing coverage and at saturation a very narrow peak is observed.

For all coverages shown in Figure 9.1 two main peaks are observed. The first peak is narrow and shifts from 463 K at lower coverage to 508 K at saturation. The second peak is wide and is always be observed around 650 K, but with its intensity increasing with increasing coverage. A third weak signal is observed for all spectra around 565 K, with its intensity being almost similar for all coverages. The existence of the higher temperature peaks indicates that the first decomposition step at 463-508 K creates more stable molecular species on the crystal. A similar observation has been made for MA on Cu(110) [75]. The specific peak temperatures for all TPD spectra are listed in Table 9.1.

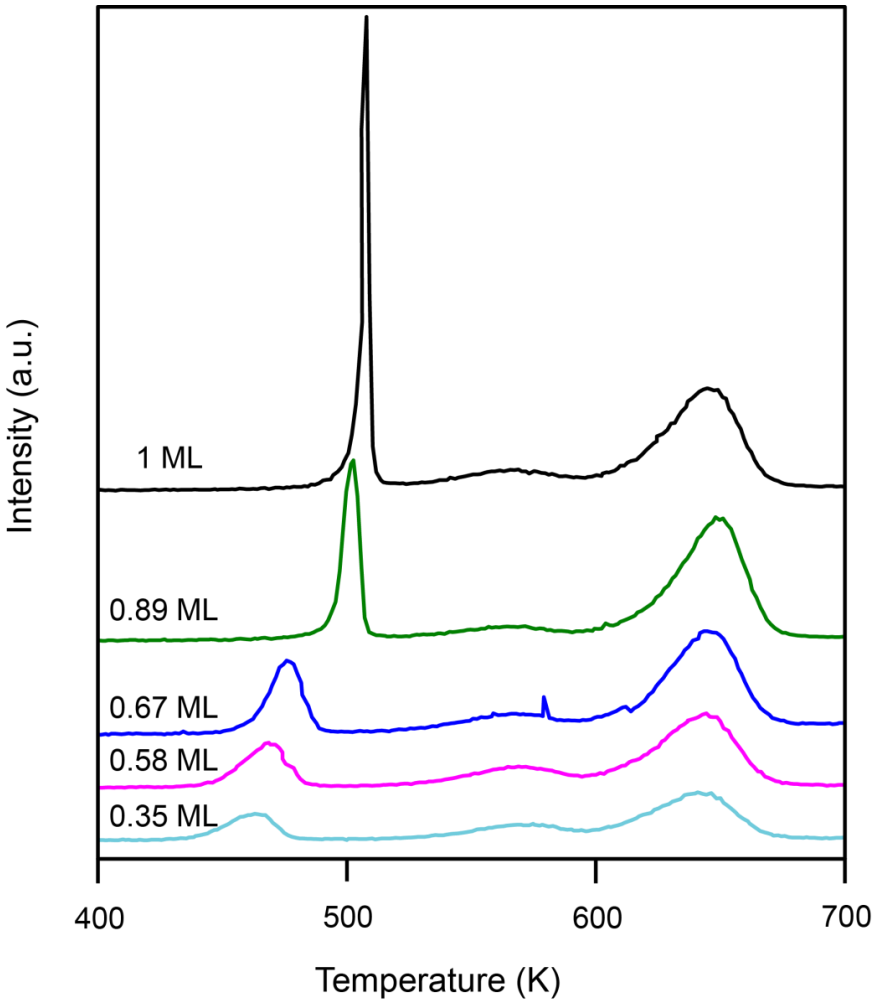

Figure 9.1: TPD spectra for a series of different coverages of FUA. The molecule exhibits explosion decomposition with a sharp peak that shifts from 463 K to 508 K with increasing coverage. The peak at 650 K indicates either the creation of a more stable species in the first desorption step, or the presence of a more stable species before the "explosion".

The explosive decomposition described here for the non-tempered samples is not observed when the (1 1, –5 2) and (1 1, –6 3) structures are present on the crystal. As shown in Figure 9.2 the main feature in both cases is a wide peak around 640 K.

This indicates that the molecules responsible for the explosion peak are either rearranged in a more stable configuration or are no longer present on the crystal. This is in accordance with XPS experiments showing a slight decrease in coverage after both structures are detected. Also, the small peak at 494 K observed in the spectrum of the (1 1, –6 3) structure is assigned to the decomposition of the c(2×4) structure that coexists on the surface. The molecules in the structures that cause the reconstruction of the crystal seem to be more stable and decompose at higher temperatures.

Table 9.1: Desorption temperatures for a series of non-tempered samples with different coverages and the two enantiomorphous structures.

Coverage (ML)/ Structure	Temperature (K)		
	Peak 1	Peak 2	Peak 3
0.35	463	570	643
0.58	469	571	645
0.67	475	566	645
0.89	501	564	649
1	508	565	646
(1 1, –5 2)		560	650
(1 1, –6 3) and c(2×4)	494		638

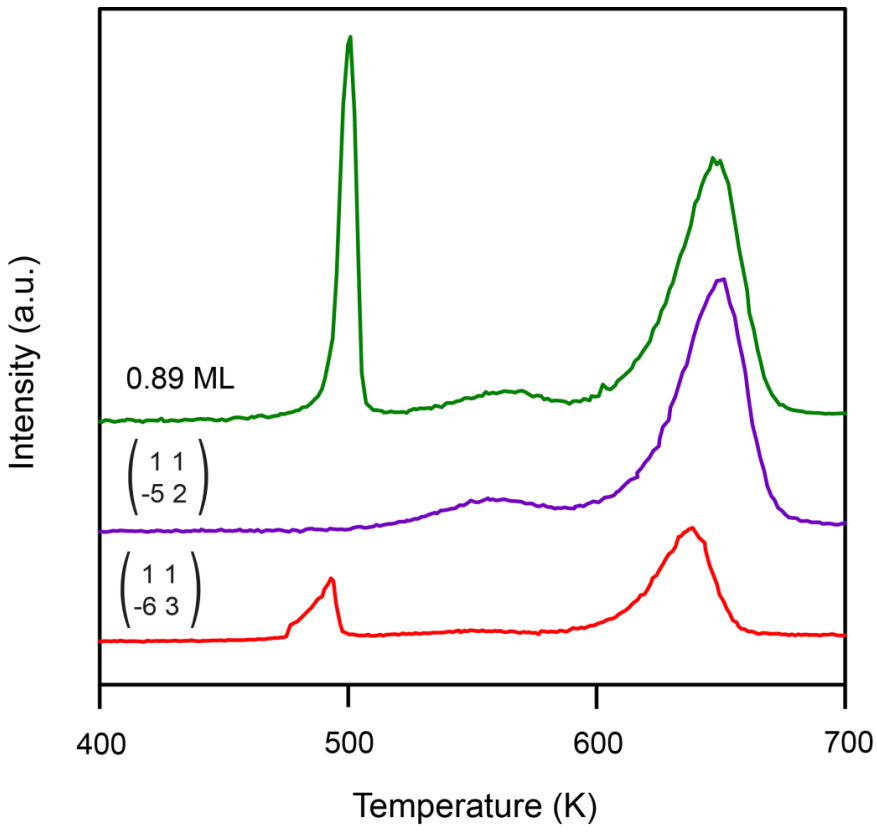

Figure 9.2: TPD spectra of two enantiomorphous structures of FUA and the spectrum of the non-tempered sample of similar coverage for comparison. The explosion peak is not observed for the annealed samples and the small peak discovered at 494 K is assigned to the decomposition of the c(2×4) structure coexisting with the (1 1, –6 3).

9.2 Maleic acid

Both non-tempered samples and the two enantiomorphous structures of MAL were investigated. Figure 9.3 shows the desorption spectra for different amounts of MAL on the crystal.

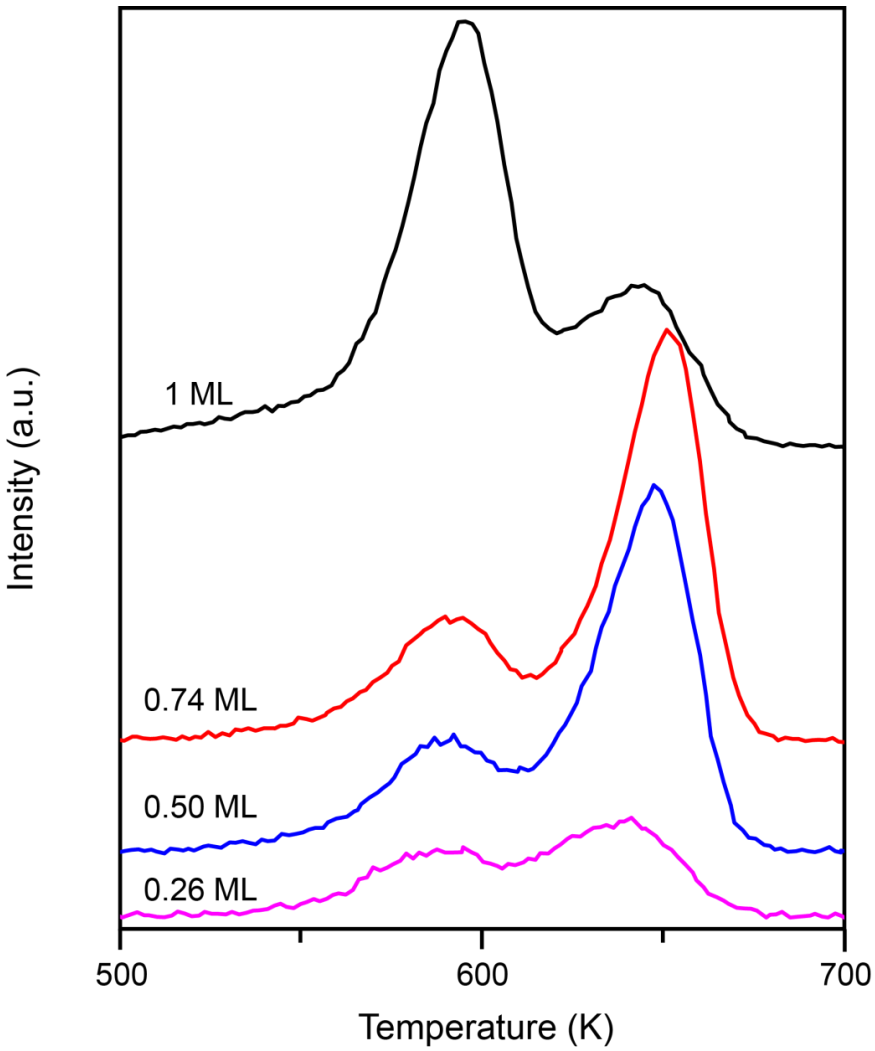

Figure 9.3: TPD spectra for a series of different coverages of MAL. The molecule exhibits explosion decomposition with a sharp peak that shifts from 639 K to 651 K with increasing coverage. The peak at 593 K indicates the first desorption step of a less stable species.

All TPD spectra exhibit two distinct peaks. For all coverages below saturation the first peak observed at 593 K is broad and lower in intensity. The second peak around 647 K is sharper and more pronounced, shifting slightly to higher temperatures with increasing coverage. These are both typical characteristics of surface explosion decomposition. This could indicate

that upon heating of the sample an amount of the molecules decompose early, creating a more stable species that requires more heat before it decomposes. The situation is reversed at the full monolayer coverage, with the intense peak observed at a lower temperature of 596 K and the weaker peak at a higher temperature of 645 K. This could be due to the fact that the molecules are so closely packed that the heating creates a domino effect for the decomposition, with a smaller amount of the more stable species being produced now. The specific positions for all the desorption peaks are listed in Table 9.2.

Table 9.2: Desorption temperatures for a series of non-tempered samples with different coverages and the two enantiomorphous structures.

Coverage (ML)/ Structure	**Temperature (K)**	
	Peak 1	**Peak 2**
0.26	590	639
0.50	590	648
0.74	592	651
1	596	644
(1 1, –5 2)	582	635
(1 1, –6 3) and c(2×4)	582	637

The decomposition mechanism described for the non-tempered samples is similar when the enantiomorphous structures are present on the crystal. For both structures a broad peak with lower intensity is observed at 582 K, followed by a more intense peak around 636 K, as shown in Figure 9.4.

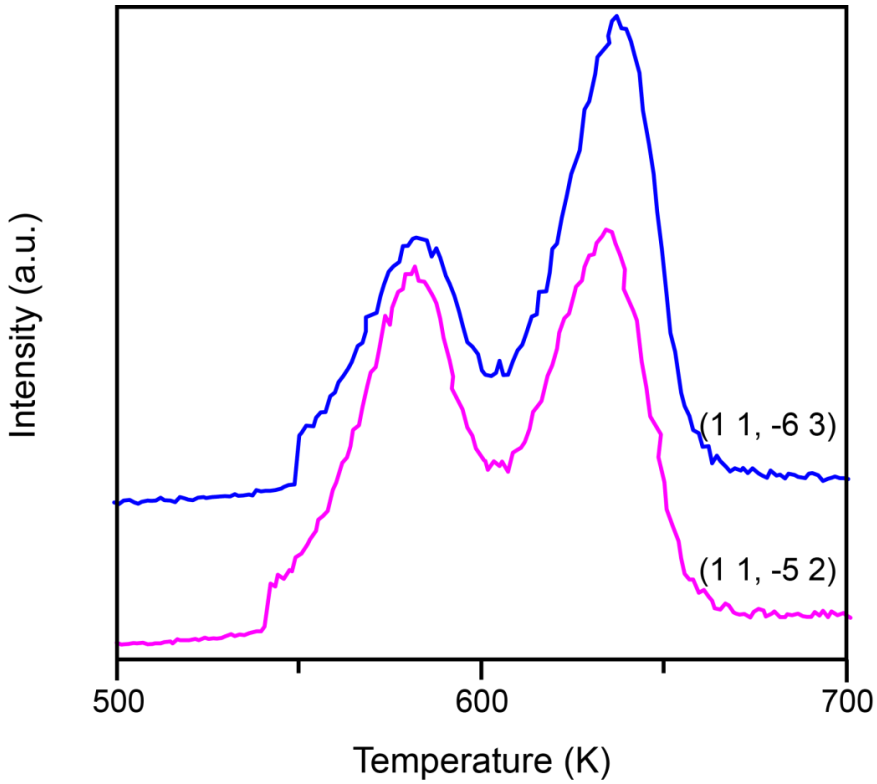

Figure 9.4: TPD spectra for the CO_2 fragment of the two enantiomorphous structures of MAL. Two peaks are also observed here for both structures, at 582 K and 636 K.

Both desorption peaks for the structures appear at a slightly lower temperature than that of their non-tempered analogues of the same coverage, but are otherwise similar in shape. This could indicate that the flash heating of the non-tempered samples during the desorption experiment is in fact sufficient to induce the formation of the enantiomorphous structures and therefore their desorption behavior is alike. In the case of the saturation coverage, the situation is reversed. This could probably be because of the large amount of molecules on the surface, making it difficult for them to self-assemble before they desorb.

9.3 2,3-dimethyl succinic acid

In order to study the desorption mechanism of DMSU, TPD experiments were performed on a series of different amounts of meso- and rac-DMSU on the crystal, as well as their respective structures.

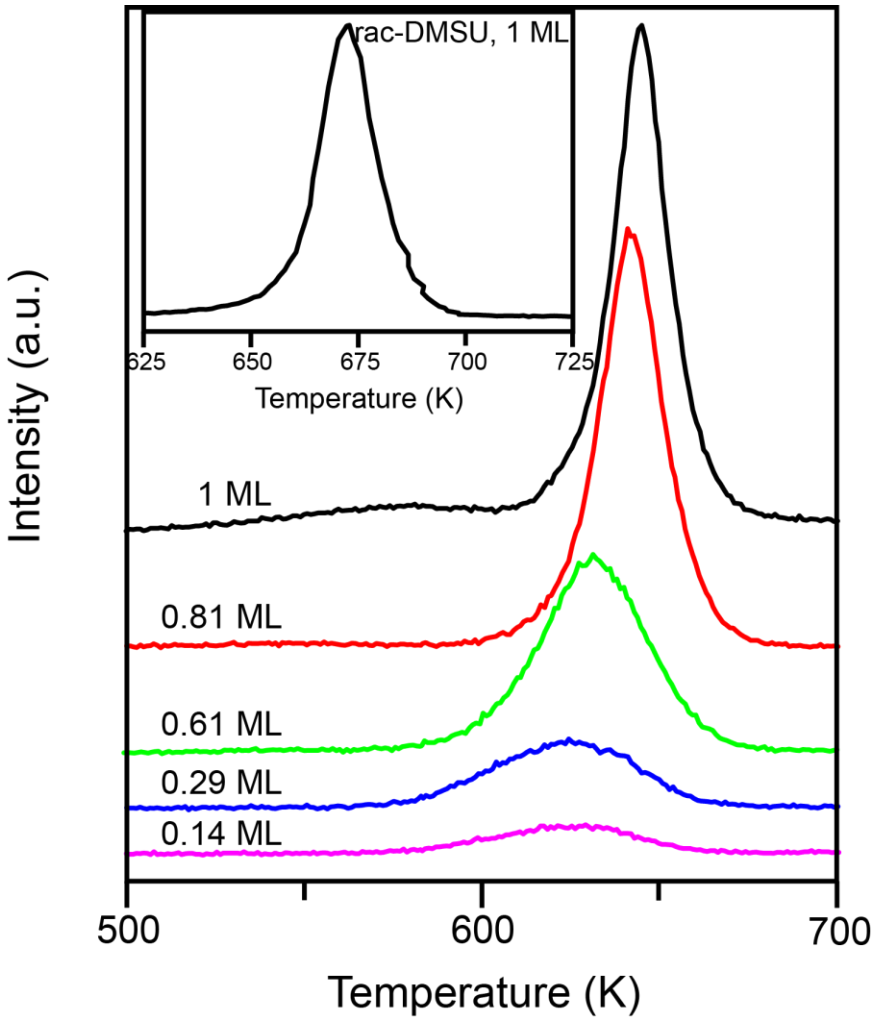

Figure 9.5: TPD spectra for a series of different coverages of meso-DMSU. The molecule exhibits explosion decomposition with a sharp peak that shifts from 624 K to 645 K with increasing coverage. The inset shows the TPD spectrum for rac-DMSU at the saturation coverage, with the peak observed at 674 K.

The results for the non-tempered samples are shown in Figure 9.5 for meso-DMSU, with the desorption experiment of the saturation of rac-DMSU presented in the inset. In the case of meso-DMSU the peaks shift to higher temperatures as the coverage increases, with the peak at saturation recorded at 645 K. The desorption peak is sharp and intense, characteristic of explosive decomposition and no additional peaks are observed. In the case of rac-DMSU the situation is similar. However, the desorption temperature for the saturation coverage is 674 K, almost 30 K higher than that observed for meso-DMSU. The fact that meso-DMSU is less thermally stable than rac-DMSU could be an indication that when the methyl groups are on the same side of the molecule more stress exists within the molecular layer, therefore making the binding of the adsorbates less stable.

The situation is similar when the structures are present on the crystal for both molecules (Figure 9.6), with both structures of meso-DMSU desorbing at lower temperatures than those of rac-DMSU. In the case of meso-DMSU, both structures desorb at the same temperature of 651 K. However, in the case of rac-DMSU there is a small difference in desorption temperature between the two structures. The (2 1, –5 4) structure desorbs at 669 K and the p2gg(2×4) decomposition peak is detected at 674 K, indicating that the latter is more stable than the former.

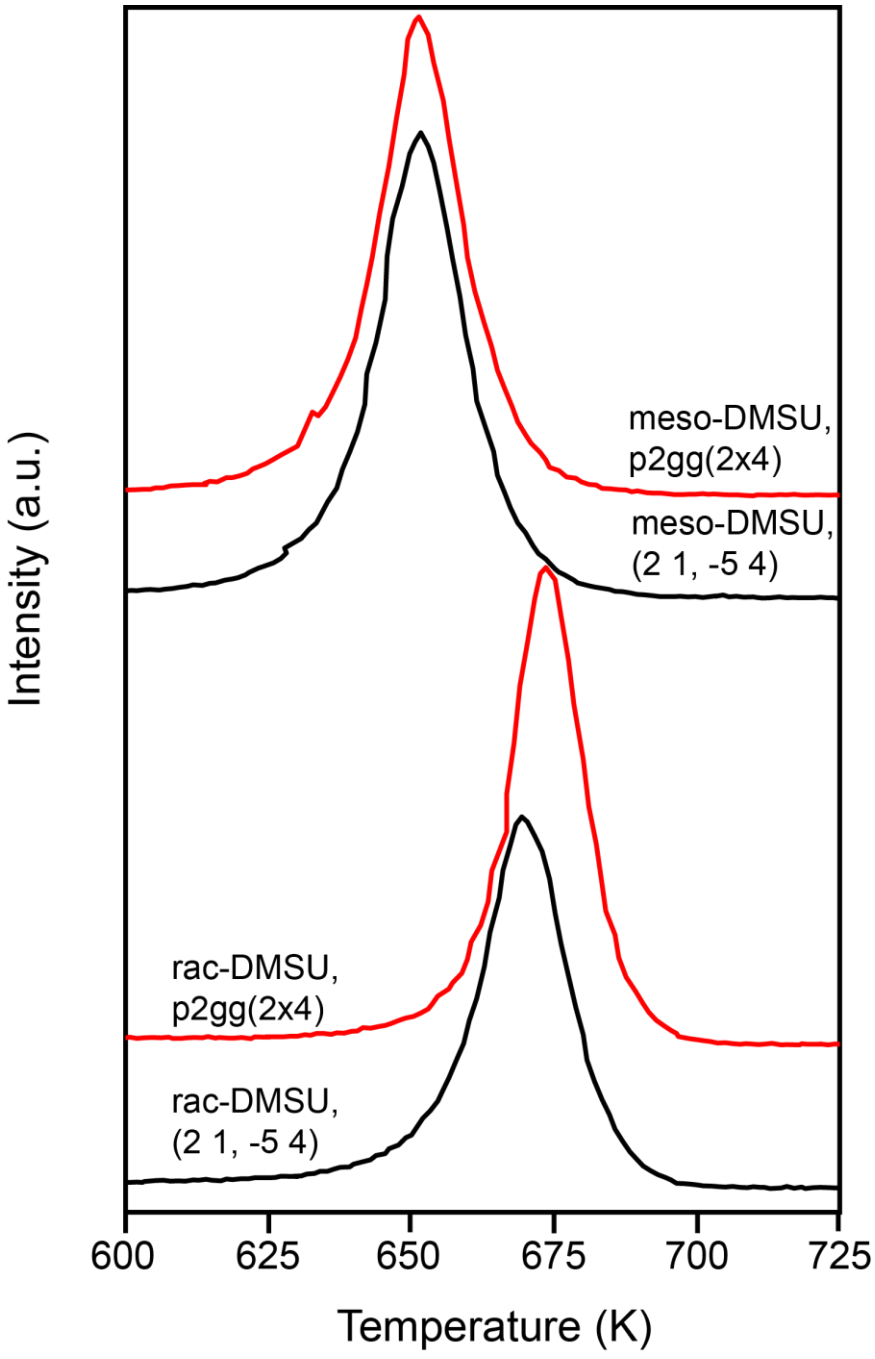

Figure 9.6: TPD spectra for the CO_2 fragment of the two structures of both meso- and rac-DMSU.

9.4 *trans*-1,2-cyclohexane dicarboxylic acid

The desorption mechanism of CHDCA was investigated by TPD for a series of different amounts of molecules on the surface.

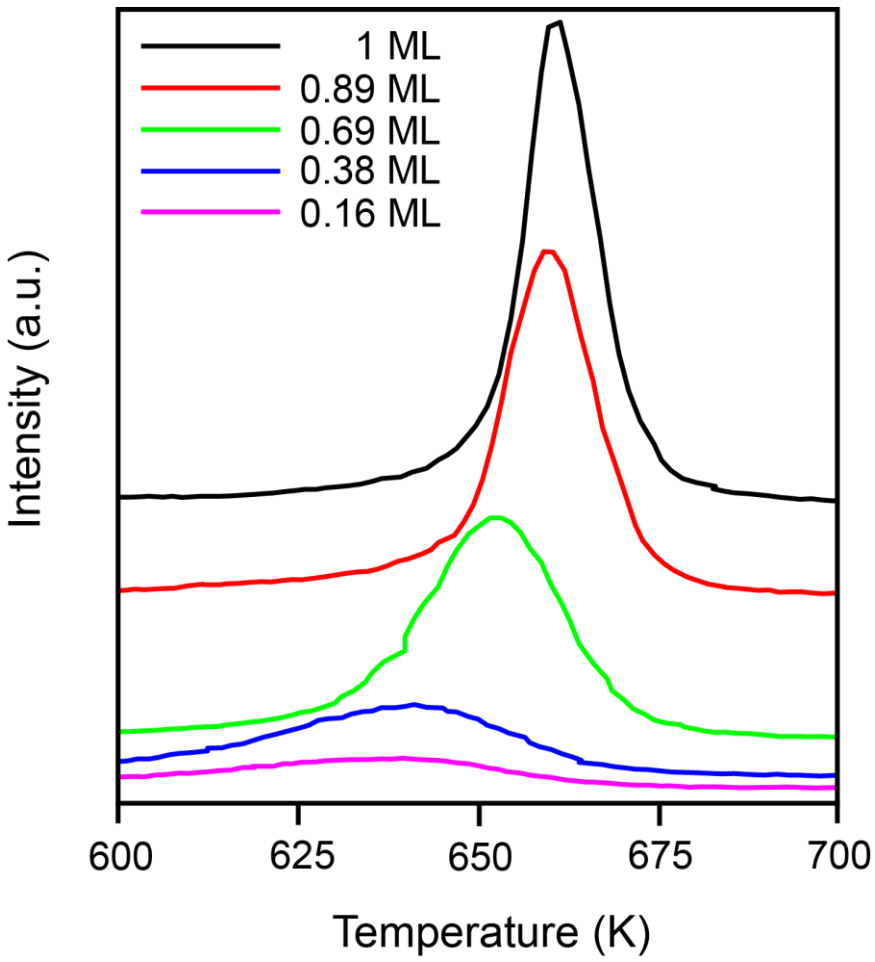

Figure 9.7: TPD spectra for a series of different coverages of CHDCA. The molecule exhibits explosion decomposition, with a sharp peak that shifts from 638 K to 661 K with increasing coverage.

All spectra depicted in Figure 9.7 exhibit characteristics of surface explosion decomposition. Only one sharp peak can be observed, with its position shifting from 638 K to 661 K as the saturation coverage is reached. The fact that there is only one desorption peak indicates that there is a single decomposition step for CHDCA, which is also thermally stable to higher temperatures than those observed for FUA, MAL and meso-DMSU but lower than rac-DMSU.

9.5 Phthalic acid

The desorption mechanism of PHTA was investigated with TPD when different amounts of the molecule were present on the surface, as shown in Figure 9.8.

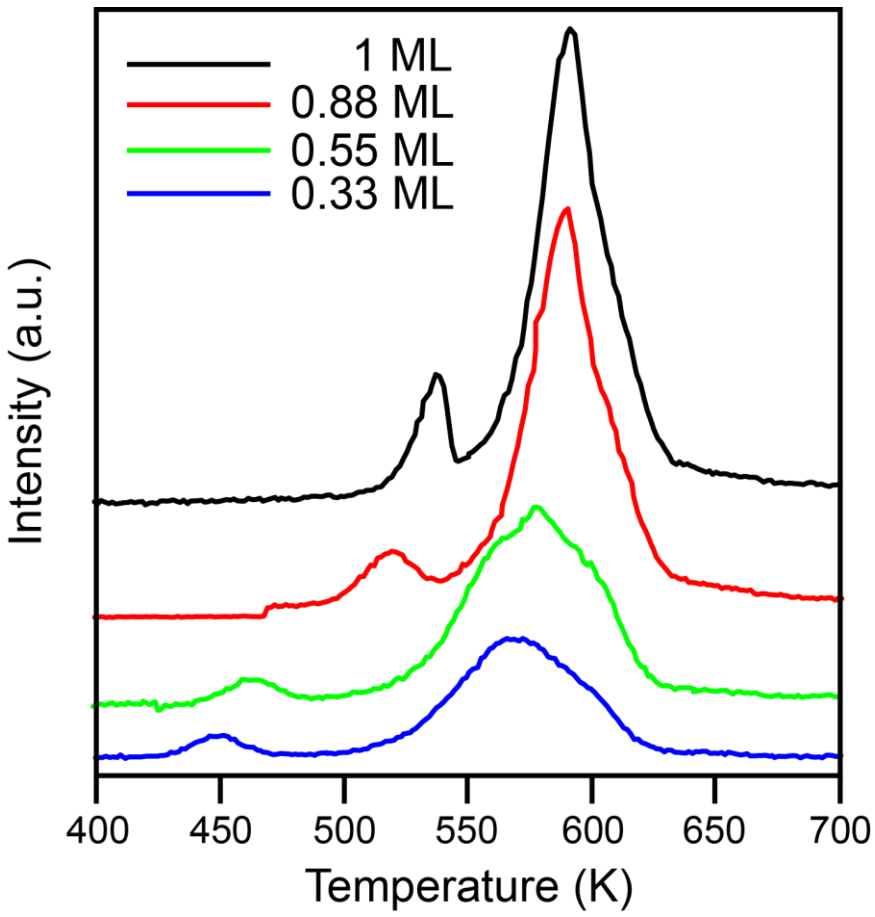

Figure 9.8: TPD spectra for a series of different coverages of PHTA. The desorption spectrum of the molecule exhibits the presence of two peaks for all coverages, which shift to higher temperatures as the coverage increases.

The spectra for all coverages of PHTA on the crystal show the existence of two different peaks. The first peak, which is weaker in intensity, shifts from 449 K to 537 K as the saturation coverage is reached. The second peak has higher intensity and shifts from 566 K to 592 K with increasing coverage. The presence of two different peaks suggests that the decomposition mechanism takes place in two steps. During the first step a small amount of molecules decomposes, creating a more stable species on the crystal.

9.6 Conclusions

The thermal desorption mechanism of the dicarboxylic acids studied in this work was described in this chapter. All molecules decompose in fragments, such as CO_2, CO, H_2 and H_2O. This indicates that the metal-molecule bond is stronger than the intramolecular bonds, causing the latter to break first during the flash heating of the sample. Both DMSU stereoisomers and CHDCA desorb in one single step, with a similar mechanism to that described for explosive decomposition, i.e. increasing desorption temperature for an increasing coverage. However, the FWHM for these molecules is quite high (~25 K), as compared to other molecules that exhibited similar decomposition routes. In the case of the explosive decomposition of TA the FWHM was 4 K [72], whereas for MA it was as low as 2.3 K [60]. The remaining 3 molecules, FUA, MAL and PHTA, show a different behavior, with the presence of two peaks in their TPD spectrum. The relative intensity between the two peaks varies between the molecules. The presence of multiple desorption peaks indicates that the decomposition of these molecules takes place in different steps, with a more stable molecular species created after the first decomposition step. This has already been reported for MA on Cu(110), with the peak at lower temperature exhibiting explosion-desorption characteristics and the peak at higher temperatures getting saturated already at low coverages [75].

Conclusions and outlook

The self-assembly of six different 1,4-dicarboxylic acids and their influence on a Cu(110) surface was investigated. A variety of structures were observed, several of which were the same between the various molecules. Some of these structures had previously been reported for other members of the 1,4-dicarboxylic acid family, as well. STM revealed that the molecules force a reconstruction of the surface, creating in this way a topmost atomic layer that is truly chiral, although the underlying substrate is achiral.

More specifically, the molecules investigated in this work were classified in two distinct categories. FUA, MAL and ACDC were achiral molecules with a steric hindrance in their backbone in the form of a double and triple carbon bond, respectively. DMSU, CHDCA and PHTA had bulky substituents in carbons 2 and 3, therefore making the molecular footprint larger. Despite their different structures, all the molecules investigated exhibited similar binding configurations upon adsorption on the crystal. They were bound to the substrate via chemical bonds between the oxygen atoms of one or both of the carboxylic acid groups and the uppermost atomic layer of the surface. Similar configurations have already been reported for other 1,4-dicarboxylic acids investigated before, like SU [60], TA [54-56] and MA [67, 68]. The desorption mechanism of all the molecules studied here was also similar. Upon flash heating of the substrate all the molecules decomposed into smaller fragments and subsequently left the surface.

Of the molecules in the first category, ACDC gave the least information about the self-assembly of 1,4-dicarboxylic acids on Cu(110), since it did not form any ordered structures upon adsorption. On the contrary, FUA and MAL offered new insight regarding the interaction of such molecules with the copper substrate. Specifically, both molecules formed the same ordered structures on the surface, which had previously been reported for SU [60, 69]. STM investigation of both FUA and MAL revealed a reconstruction of the underlying copper substrate and the existence of two unit cells with different periodicities, describing the arrangement of the molecules and the copper adatoms, respectively. Whereas such a reconstruction had been reported previously for racemic MA [68], this work showed that no intra-, intermolecular bonding or functional groups are needed as substituents for such an effect to be induced. The simple interaction of the molecules with the surface is enough.

Of the molecules in the second category, STM investigation of DMSU also revealed a reconstruction of the substrate. This reconstruction had a different periodicity than the one induced by FUA and MAL, which could possibly be due to the disubstituted methyl groups in carbons 2 and 3. In the case of CHDCA, although no STM results were available, its LEED results showed the co-existence of three different structures, which were observed for MAL, FUA and DMSU. STM investigation of these molecules revealed a reconstruction of the substrate, which is probably also present for CHDCA. It seems, therefore, that upon adsorption on the copper surface, CHDCA combines the rigid-backbone quality of FUA and MAL, as well as the presence of a large substituent, as in the case of DMSU. The adsorption of PHTA on the Cu(110) surface did not seem to force a reconstruction of the copper substrate, but it revealed a structure similar to one that had previously been reported for TA [54] and (*R*)-MA [67]. This is an indication that although the molecules are structurally different from each other, upon adsorption on the surface they behave in a similar way.

In order to try to gain further insight as to what really drives the self-assembly, the influence of the molecule and in particular its substituents was studied in this work. It is possible that the existence of a functional group and its interaction with the neighboring molecules or with other atoms within the same molecule might have an influence on the periodicity of the resulting structure. However, the exact influence of the potential functional groups has not yet been identified. To this end molecules with different functional groups, like sulfur (for example 2,3-dimercapto-succinic acid, $C_4H_6O_4S_2$) could be investigated and compared to other butanedioic acids, with and without functional groups.

Additionally, although several examples have now been exhibited of 1,4-dicarboxylic acids inducing a reconstruction of the underlying copper substrate, the exact reason that drives this reconstruction is still unclear. The particular influence of the molecules on the surface should be further investigated so that the next step can be made, which would be the creation of chiral surfaces when starting from an achiral crystal.

Appendix

A.1 Coverage calibration

Upon adsorption on the surface all the molecules investigated in this work form a chemical bond with the substrate. With increasing coverage the available sites on the crystal for the molecules to adsorb on decrease and eventually saturation coverage is reached. By checking the ratio of the C1s and Cu3s signals after background subtraction, this saturation point can be identified.

In order to perform a calibration of the coverage of the molecules on the crystal, it is necessary to have a well-ordered, well-defined structure that covers the entire surface. For this purpose, the p2gg(2×4) structure of DMSU will be used, which, as seen by STM, covers the entire crystal (see Chapter 6).

In the p2gg(2×4) structure of DMSU it is known that 2 molecules are arranged within the unit cell, which in turn is defined by 8 copper atoms. There is therefore 1 molecule per 4 copper atoms, which amounts to an absolute coverage θ of 0.25 and corresponds to a relative coverage of 1 monolayer (ML). Since the molecule has 6 carbon atoms and the C1s/Cu3s value for the p2gg(2×4) structure is 0.62, by looking at the structures of the remaining molecules studied in this work, a prediction can be made regarding their C1s/Cu3s values. In the case of FUA, MAL and ACDC which have only 4 carbon atoms per molecule, the expected C1s/Cu3s value would then be 0.42, whereas in the case of CHDCA and PHTA, which have 8 carbon atoms per molecule, the expected C1s/Cu3s value would be 0.83.

This approach, although helpful in giving an indication of what to expect, is also flawed, since some assumptions have to be made. There are several parameters which could change the C1s/Cu3s value. A reason why the theoretically calculated C1s/Cu3s value might be different from the one experimentally determined is the fact that the dicarboxylic acid molecules investigated here do not form ordered structures upon adsorption on the surface, but they remain disordered until a sufficient amount of heating has been applied. During this heating process the initial coverage might decrease slightly, since some of the molecules desorb from the surface. Another reason for a potential difference between the experimental and theoretical C1s/Cu3s value is the structural configuration of the molecules. DMSU, which was used here as the calibration standard, has two bulky methyl groups attached to its

backbone, either on one or on both sides of the molecule, depending on its chirality. This creates a bigger footprint on the surface, since the entire volume of the molecule has to be accommodated. In contrast, ACDC for example, with its sp hybridized carbon backbone, is a linear molecule, much smaller than DMSU. Therefore, it creates a much smaller footprint on the surface, meaning that at saturation coverage more molecules can be adsorbed on the same area, when compared to DMSU. The opposite is valid in the case of CHDCA, which is intrinsically chiral due to the conformation of the cyclohexane ring. This probably results in a larger footprint than DMSU, especially if the cyclohexane ring is not perpendicular to the surface but has a tilt. Finally, a distinction has to be made in the case of the absolute coverage, between local and global. The global absolute coverage describes the amount of molecules adsorbed on the entire crystal surface, whereas the local absolute coverage demonstrates the amount of molecules of an ordered structure. These two are only the same when a certain structure covers the entire crystal and since in most cases the overlayer structures described in this work coexist with areas of disordered molecules, it is very rarely the case that local and global absolute coverage are identical.

A.2 XPS of 1,4-dicarboxylic acids

The coverage calibration of the molecules investigated in this work is presented here, determined as the C1s/Cu3s value with increasing exposure time. Additionally, the shapes of the C1s curves for different amounts of each adsorbate on the surface are also shown.

A.2.1 Maleic acid

Figure A.1 shows the relation between the C1s/Cu3s ratio and the evaporation time of the maleic acid molecules, with the evaporation cell held at 323 K and the crystal at RT. For maleic acid the C1s/Cu3s ratio at saturation coverage is 0.43 and it is reached approximately after 50 seconds of evaporation.

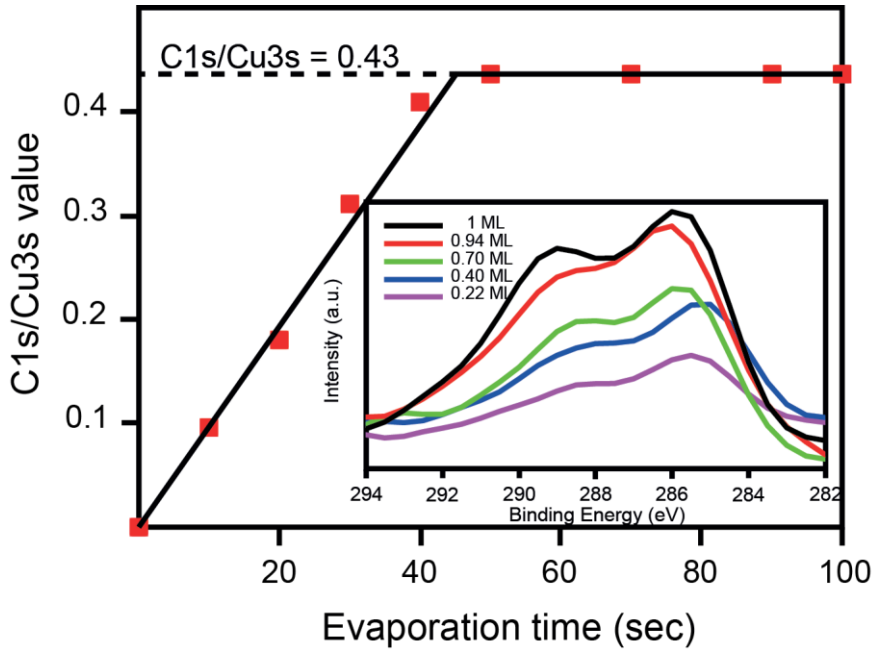

Figure A.1: Coverage versus evaporation time for MAL. In the inset, the C1s signal for different amounts of MAL on the crystal is shown.

In order to establish that there is no second layer of molecules on the crystal for evaporation at room temperature, a low temperature experiment was performed, at 80 K using liquid nitrogen, so that multilayers could be adsorbed on the crystal. The C1s/Cu3s ratio was determined as usual and in this case was found to be 3, clearly indicating the presence of more than one layer of molecules on the surface, in particular 6.98 ML. The C1s peak is shown in Figure A.2, fitted with two peaks in a 1:1 ratio corresponding to the signals obtained by the two –CH and the two –COOH groups.

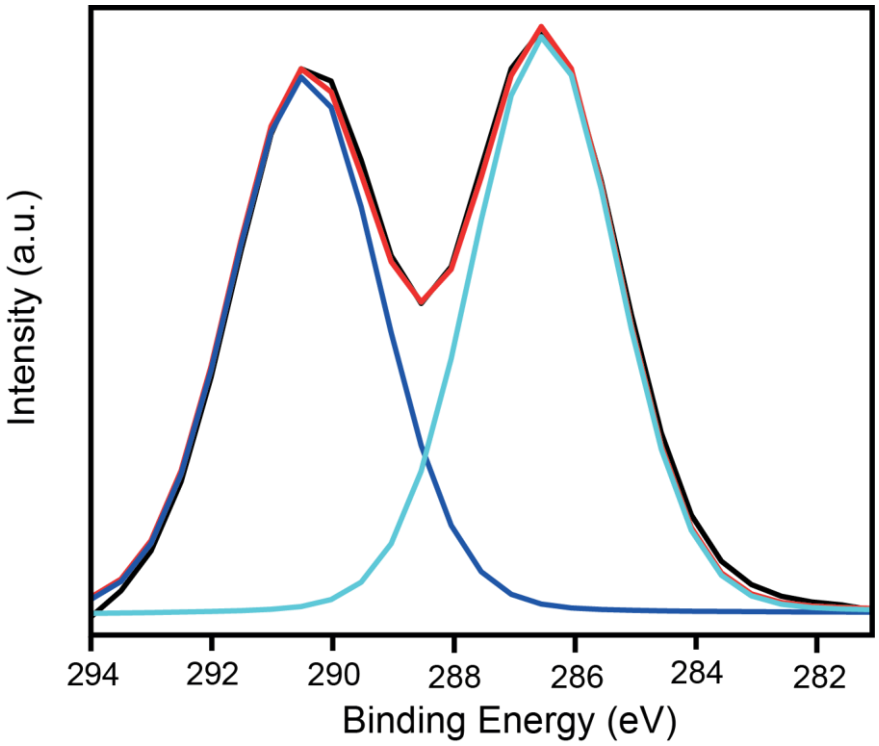

Figure A.2: Fitted C1s XPS spectra for a multilayer coverage of MAL. The black line represents the spectrum as measured, whereas the red line depicts the sum of the fitted peaks. The peak at 286.5 eV represents the –CH parts of the molecule, whereas the one at 290.4 eV is assigned to the –COOH groups.

From the fitting of the multilayer coverage of maleic acid it is possible to determine the binding energies of the carbon atoms for the two different parts of the molecule. For the two carbons involved in the double bond the C1s binding energy is 286.5 eV, whereas for the carboxylic acid groups it is 290.4 eV.

In order to examine the thermal stability of the additional physisorbed layers on the crystal, a TPD experiment was performed and masses 116 and 71 were inspected, corresponding to the molecular mass and the –CH=CH-COOH fragment of the molecule, respectively. The motivation behind the investigation of the –CH=CH-COOH fragment came from the possible fragments that the molecule could produce during decomposition. The results of the multilayer TPD experiment are shown in Figure A.3.

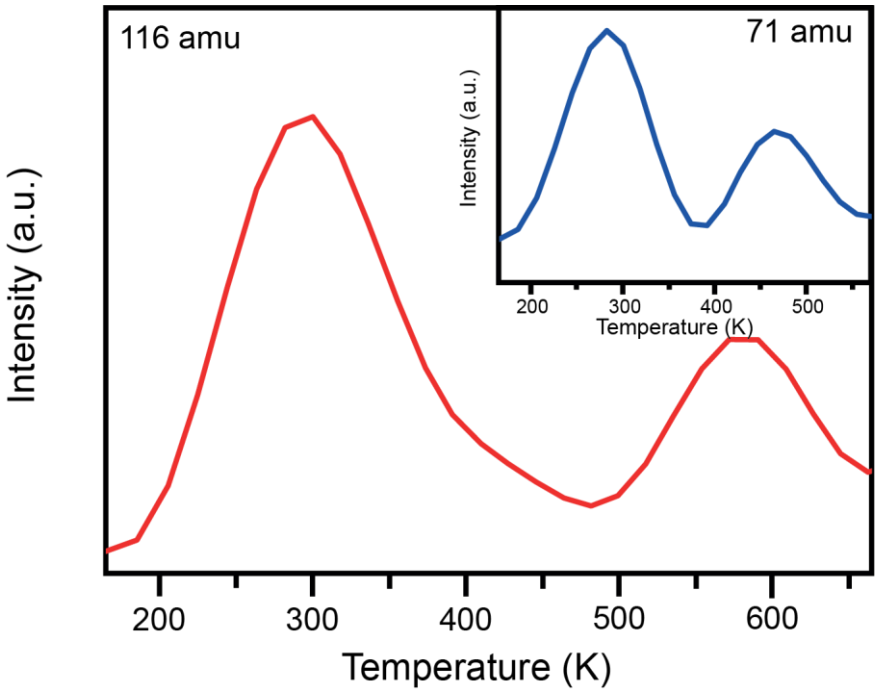

Figure A.3: TPD spectra of a multilayer coverage of MAL on the surface. The 116 amu corresponds to the molecular mass, whereas 71 amu describes the –CH=CH-COOH fragment of the molecule.

The results of both spectra indicate that the physisorbed molecules desorb at 288 K, which is lower than the temperature of the crystal during evaporation without cooling. The second peak observed at 576 K and 465 K for the 116 amu and the 71 amu respectively, could possibly correspond to the desorption of the first layer of molecules chemisorbed on the surface. However, the intensity of the latter peak is miniscule compared to that for the CO_2 fragment, which is an indication that only a small percentage of molecules fracture in such a way.

An attempt was made to gain further information regarding the binding mechanism of MAL when the (1 1, –5 2) structure was detected on the surface by fitting its C1s XP spectrum (Figure A.4). The same assumptions for the fittings were used as in the case of fumaric acid (Chapter 3.2).

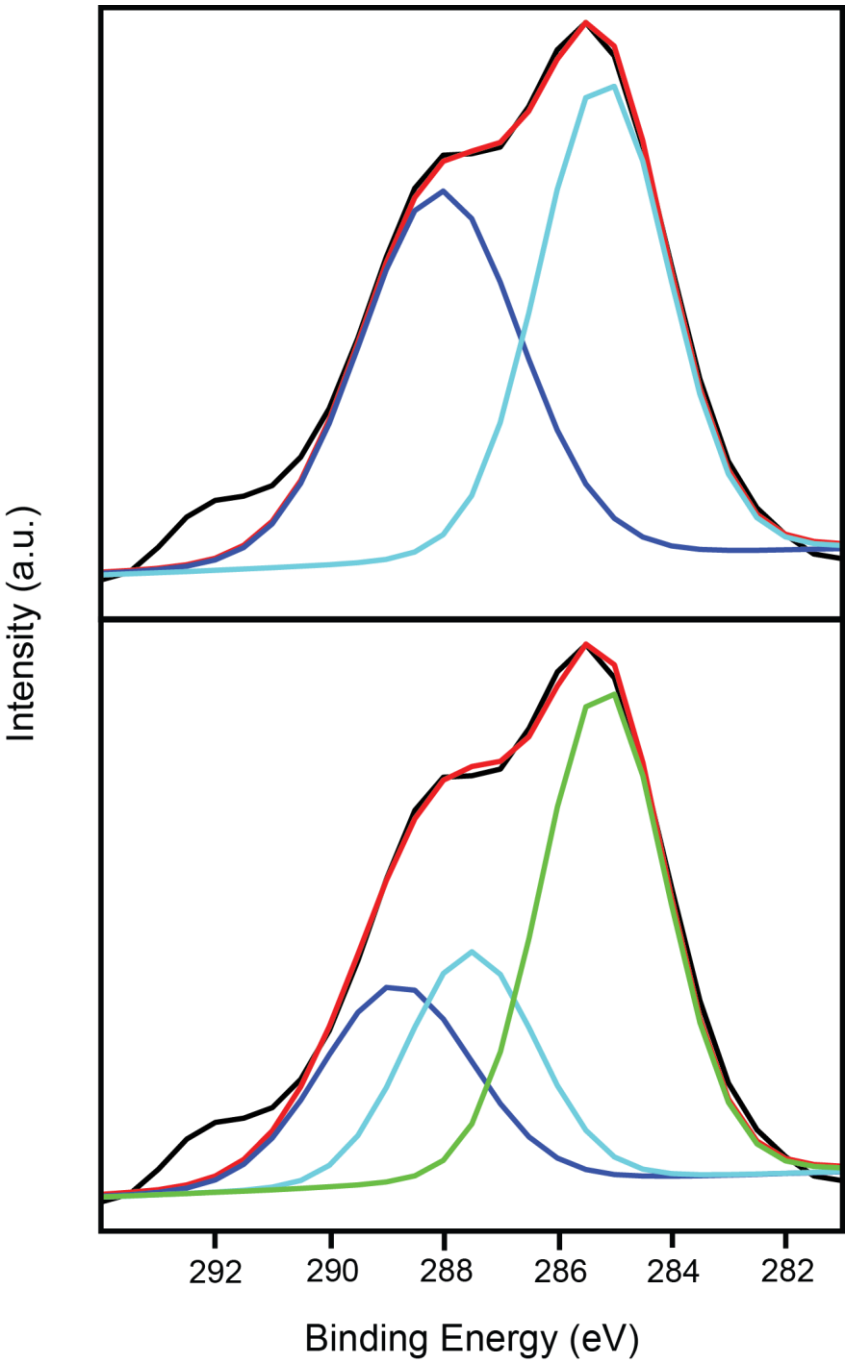

Figure A.4: Fitted C1s XPS spectra of the (1 1, –5 2) structure of MAL fitted with 2 and 3 peaks respectively. The black line depicts the spectrum as measured, whereas the red line represents the sum of the fitted peaks.

Unfortunately, as in the case of FUA, it is possible to fit the spectra for both mono- and bimaleate configurations, meaning that XPS cannot help with the identification of the bonding mechanism. RAIRS was used, instead, to deduce the molecular configuration.

A.2.2 2,3-dimethyl succinic acid

Upon adsorption on the surface DMSU forms a chemical bond with the substrate, with the sticking probability decreasing with increasing coverage. Eventually a saturation point is reached, after which, no more molecules can be accommodated on the surface.

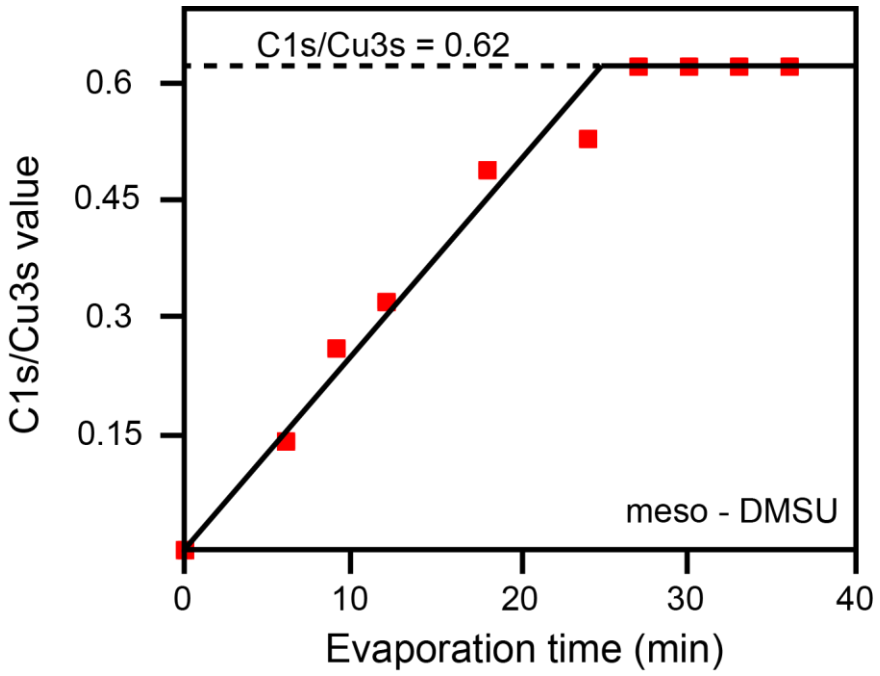

Figure A.5: Coverage versus evaporation time for meso-DMSU: the ratio is 0.62 and is reached after 30 minutes of evaporation at 333 K.

As depicted in Figures A.5 and A.6, both the meso- and racemic DMSU reach their respective saturation points after about 30 minutes of evaporation, with the C1s/Cu3s value at that coverage being 0.62 for the meso compound and 0.61 for the racemic mixture. The C1s/Cu3s value for DMSU is higher than that observed for FUA and MAL, which is in accordance to the fact that DMSU has 2 more carbon atoms per molecule than FUA and MAL.

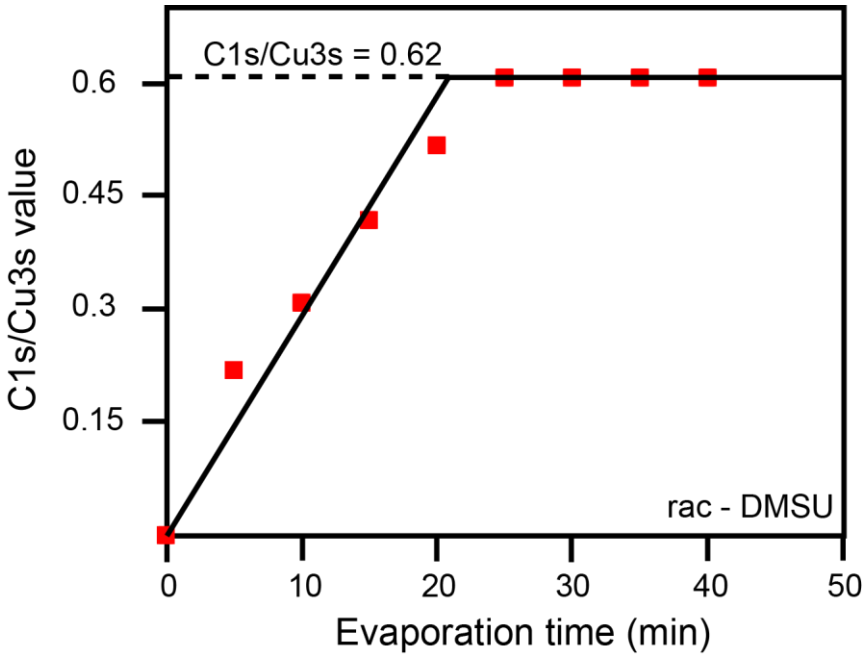

Figure A.6: Coverage versus evaporation time for rac-DMSU: the ratio is 0.61 and is reached after 25 minutes of evaporation at 318 K.

The C1s spectra for a series of different amounts of molecules on the crystal for both meso- and racemic DMSU are shown in Figure A.7. The spectra are very similar between the two molecules. The main difference is that at the saturation coverage meso-DMSU has two distinct peaks in its spectrum, whereas for rac-DMSU the second peak at higher energy is much less pronounced. It can be therefore concluded that both meso- and rac-DMSU adsorb on the surface in similar configurations judging by the resemblance of the shape of their XPS spectra.

XPS investigation of the p2gg(2×4) and (2 1, –5 4) structures observed for DMSU showed a similar shape for the C1s signal with that observed for the non-tempered samples (Figure A.8). Two peaks are identified in all cases, one intense and well defined at 285 eV and a second with a shoulder-like appearance at 287.5 eV. The existence of two structures on the crystal, the lack of information about the extend of one in respect to the other and the relative configuration of the molecules within each structure, makes fitting of the XP spectra difficult.

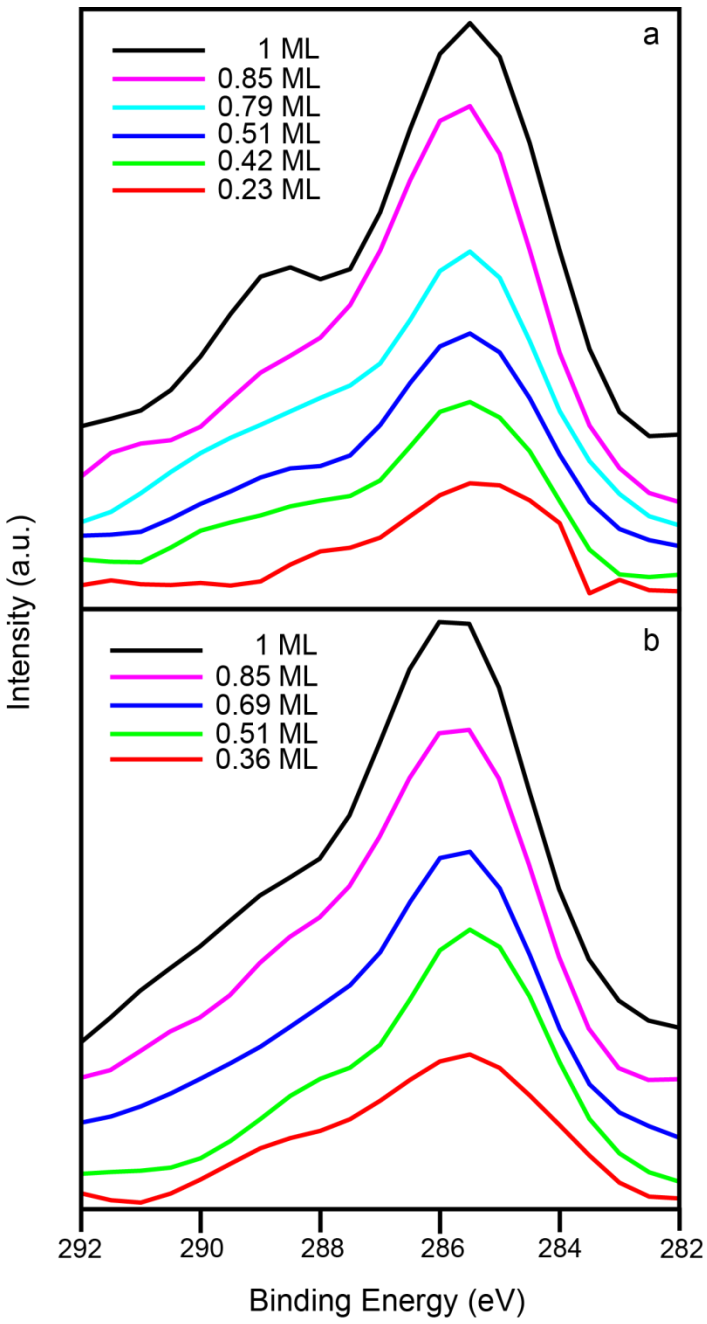

Figure A.7: C1s spectra for different amounts of a) meso-DMSU and b) rac-DMSU on the crystal.

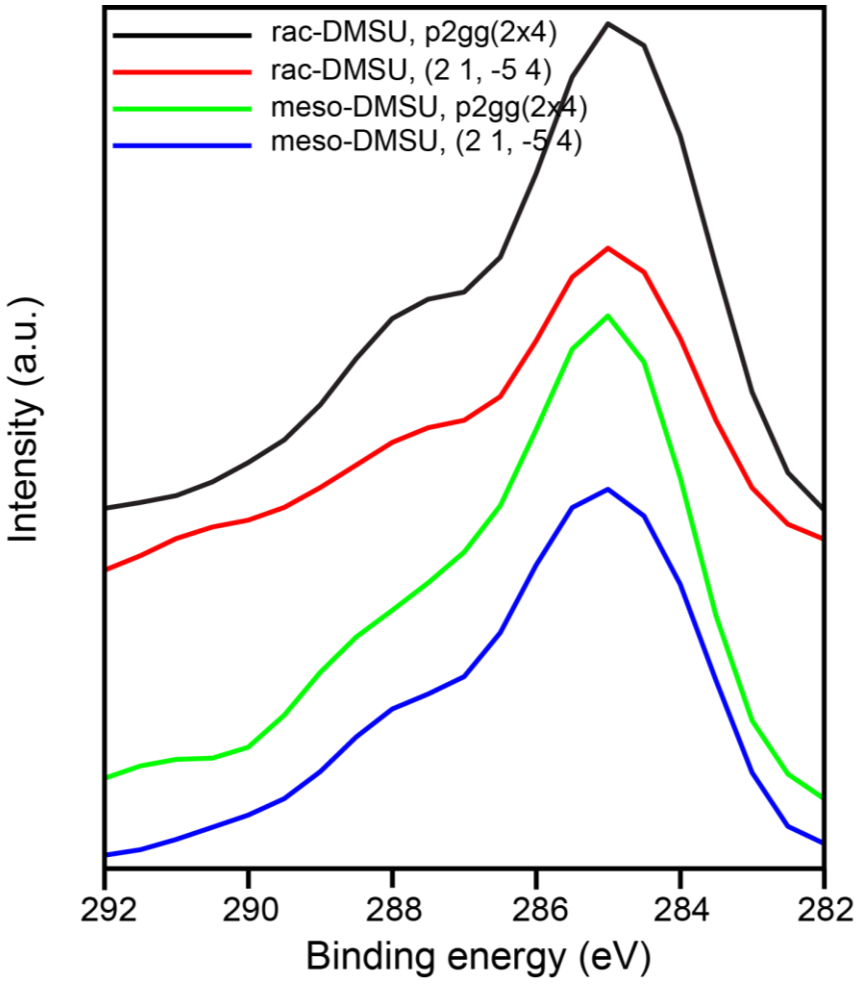

Figure A.8: C1s spectra the p2gg(2×4) and (2 1, –5 4) structures of meso-DMSU rac-DMSU.

A.2.3 *trans*-1,2-cyclohexane dicarboxylic acid

XPS helped to determine the saturation point of the CHDCA molecules on the surface. It also revealed that evaporation with the crystal held at elevated temperatures didn't have any influence on the resulting C1s/Cu3s value or the exposure time needed to reach the saturation point.

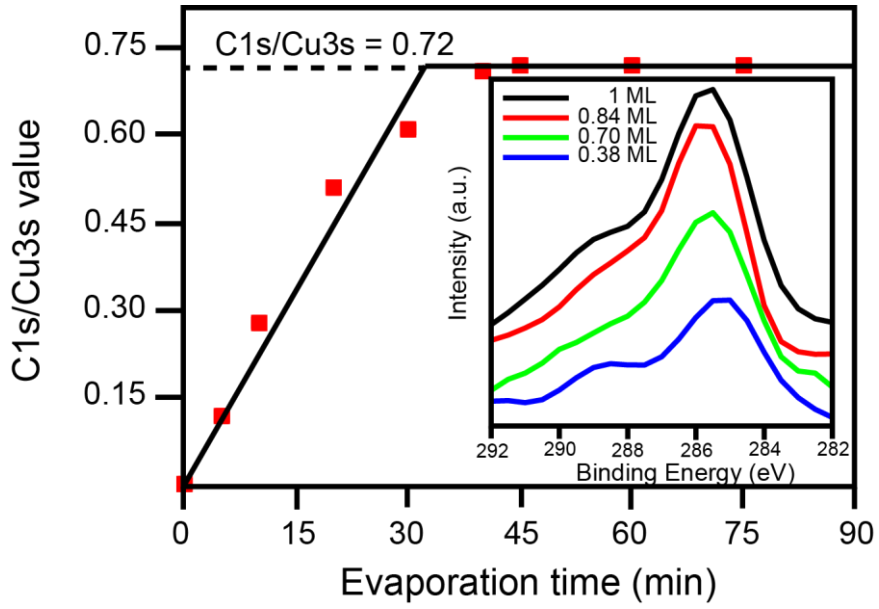

Figure A.9: Coverage versus evaporation time for CHDCA. The C1s/Cu3s ratio was calculated after Shirley background subtraction for binding energies between 282-291 eV. The inset shows the C1s spectra for different coverages of CHDCA on the crystal.

As depicted in Figure A.9, the saturation coverage is reached after approximately 45 min of evaporation with the crystal held at RT and the molecules at 353 K. The C1s/Cu3s value at the saturation coverage is in the case of CHDCA 0.72, which is higher than the values identified for the molecules investigated previously. This difference can be explained by the fact that CHDCA contains more carbon atoms per molecule, therefore causing an increase in the area of the C1s peak. In the inset of Figure A.9 the C1s spectra of a series of different amounts of CHDCA on the crystal are shown. One main peak is observed around 285 eV, with a shoulder around 289 eV.

In order to determine whether an increase of the crystal temperature would lead to a difference in the saturation point, evaporation of the molecules with the crystal held at 423 K and 473 K was investigated as well. The difference in temperature had no influence in the time needed to reach the saturation point, or in the C1s/Cu3s value when that coverage was reached.

A.2.4 Phthalic acid

The coverage of PHTA molecules on the Cu(110) surface was also investigated by XPS, as shown in Figure A.10.

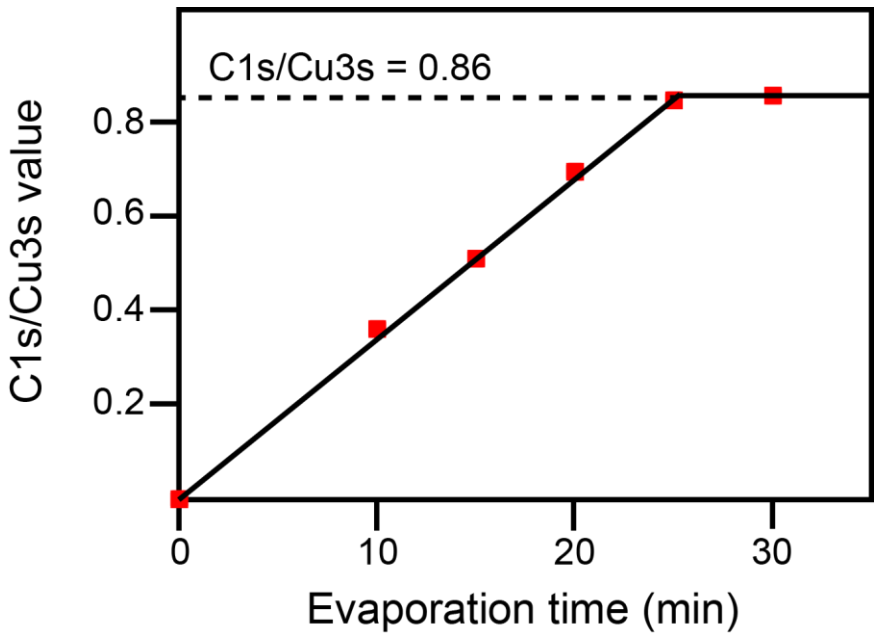

Figure A.10: Coverage versus evaporation time for PHTA. The C1s/Cu3s ratio was calculated after Shirley background subtraction for binding energies between 282-291 eV.

The C1s/Cu3s value at saturation was 0.86. This point was reached after approximately 30 min of evaporation with the crystal at RT and the molecules at 373 K. Although CHDCA and PHTA have the same amount of carbon atoms per molecule, the C1s/Cu3s ratio identified here is higher, indicating that more molecules are accommodated on the surface, implying a more closely-packed arrangement. This could be due to the smaller size of the benzene ring, with respect to the cyclohexane ring, or even due to the fact that the benzene ring is planar, therefore creating less bulk above the dicarboxylic acid backbone of the molecule.

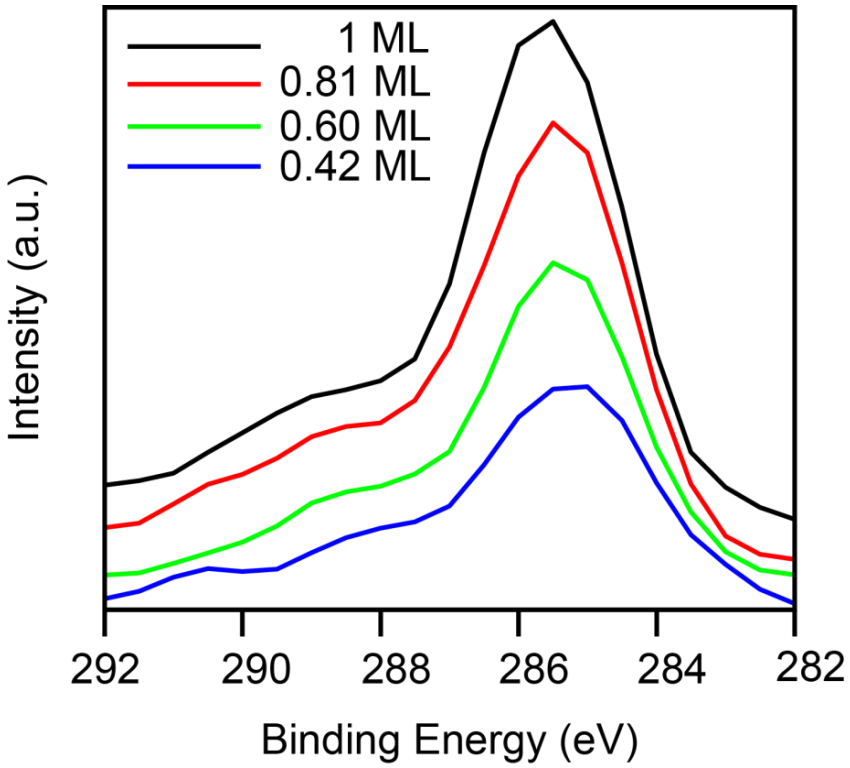

Figure A.11: C1s spectra for different amounts of PHTA on the surface, with the crystal held at RT during evaporation.

In Figure A.11 the C1s spectra of different amounts of PHTA on the crystal are shown. One main peak is observed for all coverages around 285 eV with a shoulder around 289 eV, which becomes more pronounced as the amount of adsorbed PHTA molecules increases.

Two additional experiments were performed, evaporation with the crystal temperature held at 383 K and 423 K, in order to determine if an elevated temperature on the surface would have an influence. However, neither the time needed to reach the saturation point, nor the C1s/Cu3s value at saturation were affected.

A.3 Molecular models

In Chapters 3, 4 and 6 tentative models are presented for several of the structures that were detected by LEED and STM. However, they depict only a top-view of the molecules in their several arrangements. Here, side views of the same models are presented, to act as a helpful tool. Figures A.12 to A.16 show the different molecules in their mono- and bi- configurations.

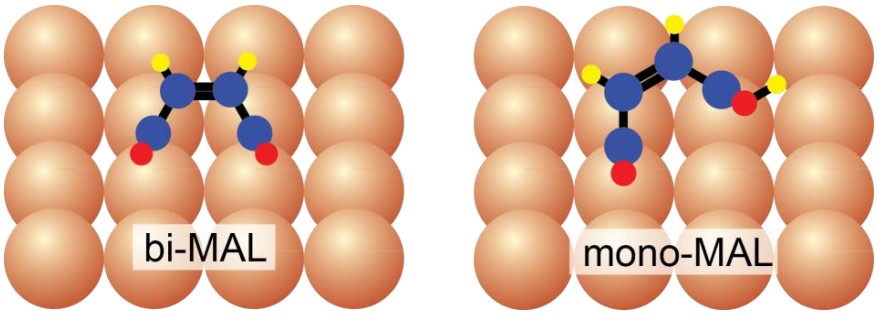

Figure A.12: Side-view models of the mono- and bi- configurations of maleic acid. In the mono-MAL case it is assumed that the C-C bond between the carboxylate and the backbone is perpendicular to the surface.

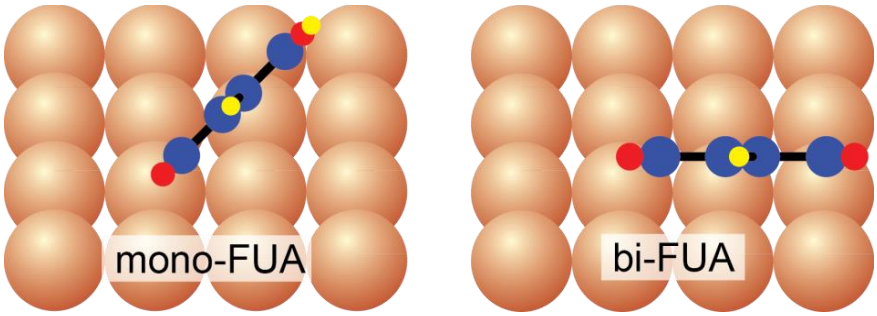

Figure A.13: Side view models of the mono- and bi- configurations of fumaric acid. In the mono-FUA case a 45° tilt from the surface is assumed, whereas in the bi-FUA case, the molecule lies with its backbone parallel to the surface.

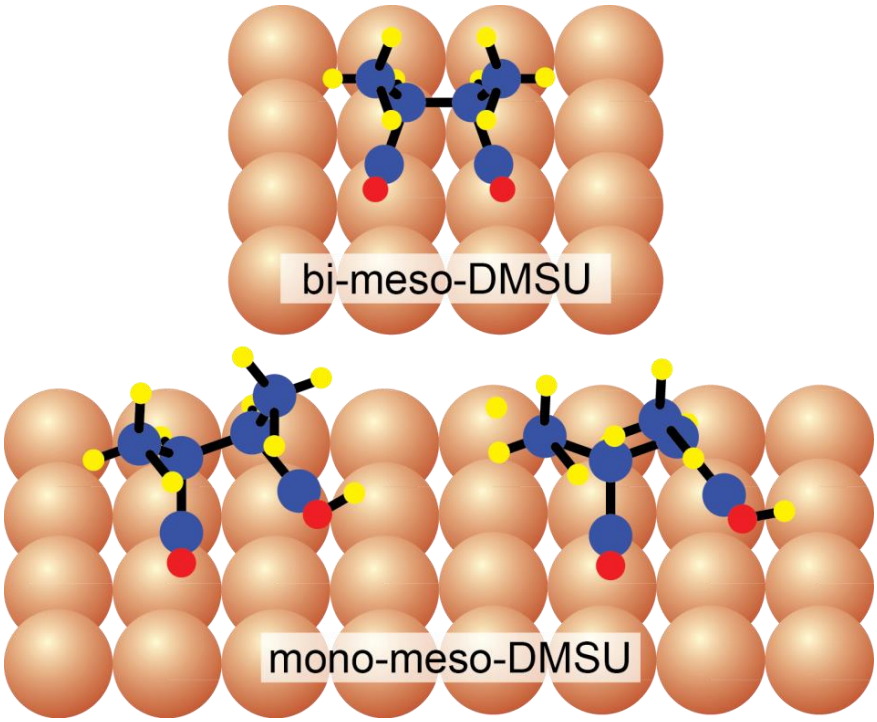

Figure A.14: Side view models of the mono- and bi- configurations of meso-DMSU. In the mono-DMSU case two zigzag distortions of the molecular backbone are assumed and presented here.

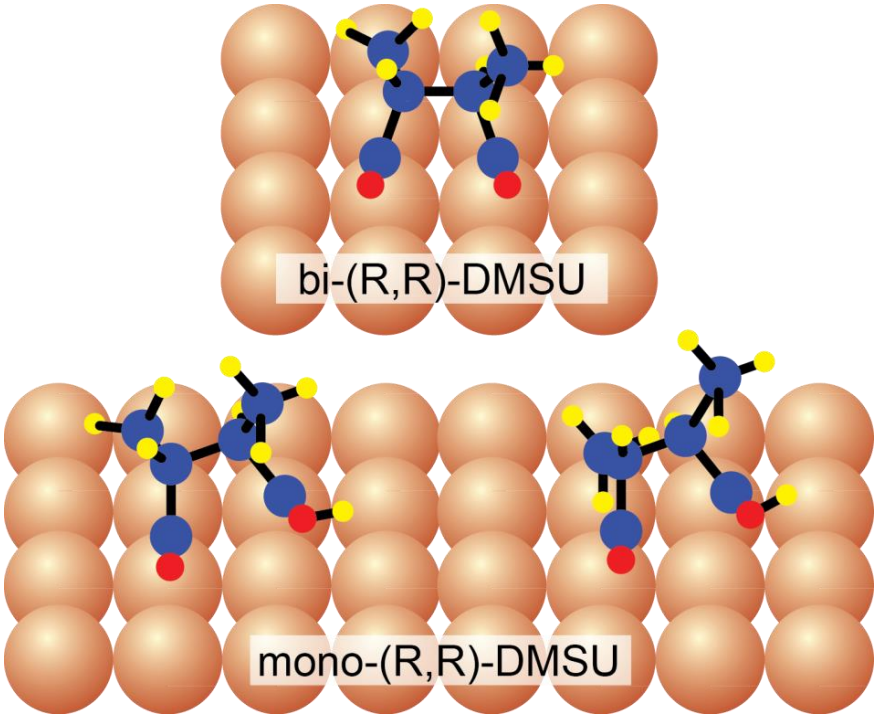

Figure A.15: Side view models of the mono- and bi- configurations of (R,R)-DMSU. In the mono-DMSU case two zigzag distortions of the molecular backbone are assumed.

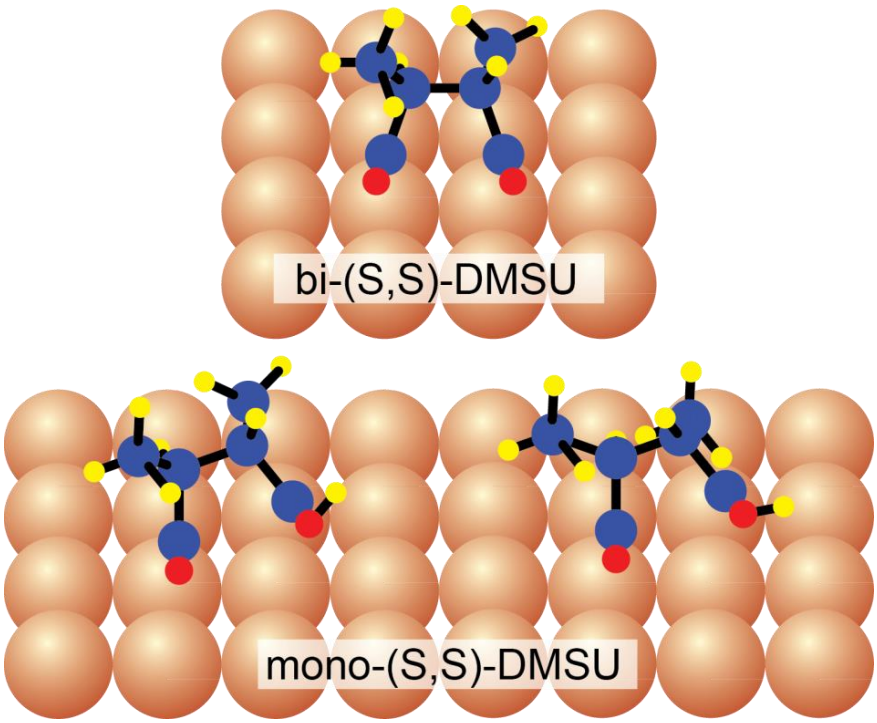

Figure A.16: Side view models of the mono- and bi- configurations of (S,S)-DMSU. As for its stereoisomer, in the mono-DMSU case two zigzag distortions of the molecular backbone are assumed.

Curriculum Vitae

Personal Data

Last name:	Karageorgaki
First name:	Chrysanthi
Address:	Aprikosenstrasse 28, 8051, Zürich
Telephone:	+41 (0)76 544 10 85
E-mail:	chkarage@gmail.com
Nationality:	Greek
Date of birth:	21.10.1985
Marital status:	Married

Work experience

01/2015 – present **Postdoctoral work**

EMPA / University of Zürich

Study and characterization of size-selected nanoparticle clusters on different substrates

Keywords: Ultra High Vacuum (UHV), X-ray Photoelectron Spectroscopy (XPS), Mass Spectrometry (MS), Reflection Absorption Infrared Spectroscopy (RAIRS), Scanning Tunneling Microscopy (STM), Magnetron Sputtering, Nanoparticles

07/2010 – 10/2014		**Doctoral thesis** EMPA / University of Zürich "Interaction of 1,4 – Dicarboxylic Acids with a Cu(110) Surface" in Molecular Surface Science
	Keywords:	Ultra High Vacuum (UHV), Self-assembly of molecules on surfaces, X-ray Photoelectron Spectroscopy (XPS), Low Energy Electron Diffraction (LEED), Temperature Programmed Desorption (TPD), Mass Spectrometry (MS), Reflection Absorption Infrared Spectroscopy (RAIRS), Scanning Tunneling Microscopy (STM), Surface Science
11/2009 – 06/2012		**Master thesis** Aristotle University of Thessaloniki Master thesis: "Study of an analytical method for the determination of platinum in carboplatin-containing biological liquids, by inductively coupled plasma atomic emission spectrometry."
	Keywords:	Inductively Coupled Plasma - Atomic Emission Spectroscopy (ICP-AES), Solid Phase Extraction (SPE), Platinum based drugs
11/2009 – 05/2010		**Laboratory assistant** Aristotle University of Thessaloniki Institute for analytical chemistry
	Responsibilities:	Supervision of students in experiments in analytical chemistry, as well as demonstration of spectrophotometric analysis

07/2008 – 09/2008		**Internship**
		Water Supply and Sanitation Company of Thessaloniki
	Responsibilities:	Chemical analysis of everyday water samples, including conductivity and pH measurements

Education

10/2003 – 11/2009		**Diploma in Chemical Engineering**
		Aristotle University of Thessaloniki
		Diploma thesis: "Structural study of polymer/layered silicate nanocomposites"
	Keywords:	X-Ray Diffraction (XRD) , Differential Scanning Calorimetry (DSC), Thermogravimetric Analysis (TGA), Polymers, Nanocomposites

Languages

Greek:	Mother tongue
English:	Written and oral fluent (Proficiency Degree Cambridge & Michigan)
German:	Written and oral good (Mittelstufenprüfung)
French:	Written and oral good (C1 Diploma)

Skills and Competences

- team oriented
- creative
- eager to learn
- well organized
- motivated
- patient
- accustomed to an international working environment

Hobbies

Cooking / baking, movies, music, traveling, books, knitting

Publications

- C. Karageorgaki, D. Passerone and K.-H. Ernst, Chiral reconstruction of Cu(110) after adsorption of fumaric acid, *Surf. Sci.*, 629: 75-80, 2014

- C. Karageorgaki, K.-H. Ernst, A metal surface with chiral memory, *Chem. Commun.*, 50, 1814-1816, 2014

- C. Karageorgaki, D. Passerone and K.-H. Ernst, On the interaction of chiral and achiral dimethylsuccinic acid with a Cu(110) surface *(in preparation)*

- S. Fotiadou, C. Karageorgaki, K. Chrissopoulou, K. Karatasos, I. Tanis, D. Tragoudaras, B. Frick and S. H. Anastasiadis, Structure and Dynamics of Hyperbranched Polymer/Layered Silicate Nanocomposites, *Macromolecules*, 46 (7), pp 2842–2855, 2013

- K. Chrissopoulou, K. S. Andrikopoulos, S. Fotiadou, S. Bollas, C. Karageorgaki, D. Christofilos, G. A. Voyiatzis and S. H. Anastasiadis, Crystallinity and Chain Conformation in PEO/Layered Silicate Nanocomposites, *Macromolecules*, 44 (24), pp 9710–9722, 2011

References

Prof. Dr. Karl-Heinz Ernst: Tel. Nr.: 058 765 4363, E-mail: Karl-Heinz.Ernst@empa.ch

Prof. Dr. Hans Hug: Tel. Nr.: 058 765 4125, E-mail: Hans-Josef.Hug@empa.ch

Dr. Roland Hauert: Tel. Nr.: 058 765 4558, E-mail: Roland.Hauert@empa.ch

References

[1] Lord Kelvin, Baltimore Lectures on Molecular Dynamics and Wave Theory of Light. The MIT Press, 1904

[2] C. J. Baddeley, Giving surfaces a hand, Nature Chemistry, 1: 345-346, 2009

[3] S. F. Mason, Origins of biomolecular handedness, NATURE, 311: 19-23, 1984

[4] A. Salam, The Role of Chirality in the Origin of Life, J. Mol. Evol., 33: 105-113, 1991

[5] L. Addadi, S. Weiner, Crystals, assymetry and life, NATURE, 411: 753-755, 2001

[6] L. Pasteur, Sur les relations qui peuvent exister entre la forme cristalline, la composition chimique et le sens de la polarisation rotatoire, Ann. Chim. Phys., 24: 442-459, 1848

[7] J. H. van 't Hoff, Bull. Soc. Chim., 1875

[8] J. A. Le Bel, Bull. Soc. Chim. 2, 1874

[9] H.Hao, G.Wang, J.Sun, Enantioselective pharmacokinetics of ibuprofen and involved mechanisms, Drug Metabolism Reviews, 1: 215–234, 2005

[10] J. H. Kim, A. R. Scialli, Thalidomide: The Tragedy of Birth Defects and the Effective, Toxicological Sciences 122 (1), 1–6, 2011

[11] http://nobelprize.org/nobel prizes/chemistry/laureates/2001/

[12] http://nobelprize.org/nobel prizes/chemistry/laureates/2007/

[13] G. Kyriakou, S. K. Beaumont, R. M. Lambert, Aspects of Heterogeneous Enantioselective Catalysis by Metals, Langmuir, 27, 9687-9695, 2011

[14] M. Lemaire, Heterogeneous asymmetric catalysis, Pure Appl. Chem., Vol. 76, No. 3, pp. 679-688, 2004

[15] N. Mizuno, M. Misono, Heterogeneous Catalysis, Chem. Rev., 98, 199-217, 1998

[16] M. E. Davis, Reflections on routes to enantioselective solid catalysts, Topics in Catalysis, Vol. 25, Nos. 1-4, 2003

[17] J. M. Thomas, T. Maschmeyer, B. F. G. Johnson, and D. S. Shephard, Constrained chiral catalysts. J. Mol. Catal. A, 141: 139-144, 1999

[18] Y. Izumi, Modified Raney Nickel (MRNi) Catalyst: Heterogeneous Enantio-Differentiating (Asymmetric) Catalyst**,** Adv. Catal. 32, 215, 1983

[19] Y. Orito, S. Imai, and S. Niwa, Asymmetric Hydrogenation of Methyl Pyruvate Using Pt-C Catalyst Modified with Cinchonidine, Nippon Kagaku Kaishi, 8: 1118-1120, 1979

[20] G. Webb and P. B. Wells, Asymmetric Hydrogenation, Catal. Today, 12: 319-337, 1992

[21] C. Baddeley, Fundamental investigations of enantioselective heterogeneous catalysis, Topics Catal., 25: 17-27, 2003

[22] A. Hoek and W. M. Sachtler, Enantioselectivity of Nickel Catalysts Modified with Tartaric Acid or Nickel Tartrate Complexes. J. Catal., 58: 276-286, 1979

[23] M. Studer, H.-U. Blaser, and C. Exner, Enantioselective Hydrogenation Using Heterogeneous Modified Catalysts: An Update, Adv. Synth. Catal., 345: 45-65, 2003

[24] M. Parschau, R. Fasel, K.-H. Ernst, O. Gröning, L. Brandenberger, R. Schillinger, T. Greber, A. Seitsonen, Y.-T. Wu, and J. S. Siegel, Buckybowls on Metal Surfaces: Symmetry Mismatch and Enantiomorphism of Corannulene on Cu(110), Angew. Chem., Int. Ed. 46, 8258, 2007

[25] L. Merz, M. Parschau, L. Zoppi, K. K. Baldridge, J. S. Siegel, K.-H. Ernst, Reversible Phase Transitions in a Buckybowl Monolayer. Angew. Chem. Int. Ed., 48: 1966–1969, 2009

[26] L. Zoppi, T. Bauert, J. S. Siegel, K. K. Baldridge, K.-H. Ernst, Pentagonal tiling with buckybowls: Pentamethylcorannulene on Cu(111), Phys. Chem. Chem. Phys. 14, 13365–13369, 2012

[27] R. Fasel, M. Parschau, K.-H. Ernst, Chirality transfer from single molecules into self-assembled monolayers, Angew. Chem. Int. Ed. 42, 5178-5181, 2003

[28] K.-H. Ernst, M. Parschau, R. Fasel, Differences in two-dimensional crystal structures: racemic and enantiopure heptahelicene on Cu(111), Surf. Sci. & Nanotech. 2, 136, 2004

[29] J. Seibel, O. Allemann, J. S. Siegel, K.-H. Ernst, Chiral conflict among different helicenes suppresses formation of one enantiomorph in 2D crystallization,J. Am. Chem. Soc. 135, 7434−7437, 2013

[30] O. Karis, J. Hasselström, N. Wasserdahl, M. Weinelt, The bonding of simple carboxylic acids on Cu(110), J. Chem. Phys., 112, 8146-8155, 2000

[31] D. I. Sayago, M. Polcik, G. Nisbet, C. L. A. Lamont, and D.P. Woodruff, Local structure determination of a chiral adsorbate: Alanine on Cu(110), Surf. Sci. 590, 76–87, 2005

[32] R. B. Rankin and D. S. Sholl, Structure of enantiopure and racemic alanine adlayers on Cu(110), Surf. Sci. 574, L1–L8, 2005

[33] S. M. Barlow, S. Louafi, D. Le Roux, J. Williams, C. Muryn, S. Haq, and R. Raval, Polymorphism in supramolecular chiral structures of R- and S-alanine on Cu(110), Surf. Sci. 590, 243–2263, 2005

[34] S. Haq, A. Massey, N. Moslemzadeh, A. Robin, S. M. Barlow and R. Raval, Racemic versus Enantiopure Alanine on Cu(110): An Experimental Study, Langmuir, 23, 10694-10700, 2007

[35] K.-H. Ernst and K. Christmann, The interaction of glycine with a platinum(111) surface, Surf. Sci. 224, 277, 1989

[36] R. B. Rankin and D. S. Sholl, Assessment of heterochiral and homochiral glycine adlayers on Cu(110) using density functional theory, Surf. Sci. 548, 301–308, 2004

[37] Y. Yun, A.J. Gellman, Enantioselective separation of DL-aspartic acid on naturally chiral $Cu(3,1,17)^{R\&S}$ surfaces, Angewandte Chemie International Edition 52, 3394-3397, 2013

[38] R. Raval, Creating chiral architectures at metal surfaces, J. Phys.: Condens. Matter, 14, 4119-4132, 2002

[39] R. Raval, Chiral expressions at metal surfaces, Chiral Opinion in Solid State and Materials Science 7, 67-74, 2003

[40] V. Humblot, S. M. Barlow, R. Raval, Two-dimensional organizational chirality through supramolecular assembly of molecules at metal surfaces, Progress in Surface Science, 76, 1-19, 2004

[41] K.-H. Ernst, Expression and amplification of chirality in two-dimensional molecular crystals, Chimia, 62(6): 471-475, 2008

[42] R. Raval, Chiral expression from molecular assemblies at metal surfaces: insights from surface science techniques, Chem. Soc. Rev., 38, 707-721, 2009

[43] K.-H. Ernst, Amplification of Chirality at Solid Surfaces, Orig. Life Evol. Biosph., 40: 41–50, 2010

[44] K.-H. Ernst, Molecular chirality at surfaces, Phys. Status Solidi B, 249, No. 11, 2057-2088, 2012

[45] K.-H. Ernst, Stereochemistry of 2D Molecular Crystallization, Chimia 68, 49–53, 2014

[46] E.A. Wood, Vocabulary of Surface Crystallography, J. Appl. Phys.,35, 1306, 1964

[47] R.L. Park, H.H. Madden Jr., Annealing changes on the (100) surface of palladium and their effect on CO adsorption, Surf. Sci., 11, 188, 1968

[48] L. Merz and K.-H. Ernst. Unification of the matrix notation in molecular surface science, Surf. Sci., 604 (15): 1049-1054, 2010

[49] V. H. Humblot, S. Haq, C. Muryn, W. A. Hofer, and R. Raval, From Local Adsorption Stresses to Chiral Surfaces: R,R-Tartaric Acid on Ni(110), J. Am. Chem. Soc., 124: 503-510, 2002

[50] V. H. Humblot, S. Haq, C. Muryn, R. Raval, (R,R)-Tartaric acid on Ni(110): the dynamic nature of chiral adsorption motifs, Journal of Catalysis, 228, 130-140, 2004

[51] W.A. Hofer, V. Humblot, R. Raval, Conveying chirality into the electronic structure of achiral metals: (*R*,*R*)-tartaric acid on nickel, Surface Science, 554, 141-149, 2004

[52] T.E. Jones, C.J. Baddeley, A RAIRS, STM and TPD study of the Ni(111)/*R*,*R*-tartaric acid system: Modelling the chiral modification of Ni nanoparticles, Surface Science, 513, 453–467, 2002

[53] T. Edmonds, R.C. Pitkethly, The adsorption of carbon monoxide and carbon dioxide at the (111) face of nickel observed by LEED, Surf. Sci. 15, 137, 1969

[54] M. Ortega Lorenzo, S. Haq, T. Bertrams, P. Murray, R. Raval, and C. J. Baddeley, Creating Chiral Surfaces for Enantioselective Heterogeneous Catalysis: R,R-Tartaric Acid on Cu(110), J. Phys. Chem. B, 103: 10661-10669, 1999

[55] M. Ortega Lorenzo, C. J. Baddeley, C. Muryn, and R. Raval, Extended surface chirality from supramolecular assemblies of adsorbed chiral molecules, Nature, 404: 376-379, 2000

[56] M. Ortega Lorenzo, V. Humblot, P. Murray, C. J. Baddeley, S. Haq, and R. Raval, Chemical Transformations, Molecular Transport, and Kinetic Barriers in Creating the Chiral Phase of (R,R)-Tartaric Acid on Cu(110), J. Catal., 205: 123-134, 2002

[57] L. A. M. M. Barbosa and P. Sautet, Stability of Chiral Domains Produced by Adsorption of Tartaric Acid Isomers on the Cu(110) Surface: A Periodic Density Functional Theory Study, J. Am. Chem. Soc., 123: 6639-6648, 2001

[58] C. G. M. Hermse, A. P. van Bavel, A. P. J. Jansen, L. A. M. M. Barbosa, P. Sautet, and R. A. van Santen, Formation of Chiral Domains for Tartaric Acid on Cu(110): A Combined DFT and Kinetic Monte Carlo Study, J. Phys. Chem. B, 108: 11035-11043, 2004

[59] P. Zeppenfeld, M. Krzyzowski, C. Romainczyk, G. Comsa, M. G. Lagally, Size Relation for Surface Systems with Long-Range Interactions, Phys. Rev. Lett. 72, 2737, 1994

[60] V. Humblot, M. Ortega Lorenzo, C. J. Baddeley, S. Haq, and R. Raval, Local and Global Chirality at Surfaces: Succinic Acid versus Tartaric Acid on Cu(110), J. Am. Chem. Soc., 126: 6460-6469, 2004

[61] R. Fasel, J. Wider, C. Quitmann, K.-H. Ernst, and T. Greber, Determination of the Absolute Chirality of Adsorbed Molecules, Angew. Chem. Int. Ed., 43: 2853-2856, 2004

[62] M. Parschau, T. Kampen, and K.-H. Ernst, Homochirality in monolayers of achiral meso tartaric acid, Chem. Phys. Lett., 407: 433-437, 2005

[63] M. Parschau, B. Behzadi, S. Romer, and K.-H. Ernst, Stereoisomeric influence on 2D lattice structure: achiral meso-tartaric acid versus chiral tartaric acid, Surf. Interface Anal., 38: 1607-1610, 2006

[64] T. J. Lawton, V. Pushkarev, D. Wei, F. R. Lucci, D. S. Sholl, A. J. Gellman and E. C. H. Sykes, Long Range Chiral Imprinting of Cu(110) by Tartaric Acid, J. Phys. Chem. C, 117, 22290−22297, 2013

[65] M. Bowker, S. Poulston, R. A. Bennett, P. Stone, Gross Rearrangement of Metal Atoms During Surface Reactions. J. Phys.: Condens. Matter, 10, 7713−7722, 1998

[66] D. B. Dougherty, P. Maksymovych, J. T. Jr. Yates, Direct STM Evidence for Cu−Benzoate Surface Complexes on Cu(110), Surf. Sci., 600, 4484−4491, 2006

[67] C. Roth, D. Passerone, L. Merz, M. Parschau, K.-H. Ernst, Two-Dimensional Self-Assembly of Chiral Malic Acid on Cu(110), J. Phys. Chem. C, 115, 1240-1247, 2011

[68] C. Roth, M. Parschau, K.-H. Ernst, Chiral Reconstruction of a Metal Surface by Adsorption of Racemic Malic Acid, Chem. Phys. Chem., 12, 1572-1577, 2011

[69] M. Parschau, S. Romer, and K.-H. Ernst, Induction of Homochirality in Achiral Enantiomorphous Monolayers, J. Am. Chem. Soc., 126: 15398-15399, 2004

[70] K.-H. Ernst, Amplification of chirality in two-dimensional molecular lattices, Current Opinion in Colloid & Interface Science, 13, 54–59, 2008

[71] N. Liu, S. Haq, G. R. Darling, and R. Raval, Direct Visualization of Enantiosepecific Substitution of Chiral Guest Molecules into Heterochiral Molecular Assemblies at Surfaces, Angew. Chem. Int. Ed., 46: 7613-7616, 2007

[72] B. Behzadi, S. Romer, R. Fasel, and K.-H. Ernst, Chiral Recognition in Surface Explosion, J. Am. Chem. Soc., 126: 9176-9177, 2004

[73] R. G. Sharpe and M. Bowker. Kinetic models of surface explosion. J. Phys.: Condens. Matter, 7: 6379-6392, 1995

[74] B. S. Mhatre, V. Pushkarev, B. Holsclaw, T. J. Lawton, E. C. H. Sykes and A. Gellman, A Window on Surface Explosions: Tartaric Acid on Cu(110), J. Phys. Chem. C, 117, 7577-7588, 2013

[75] C. Roth, K.-H. Ernst, Surface Explosion Chemistry of Malic Acid on Cu(110), Top. Catal., 54: 1378-1383, 2011

[76] S. Romer, B. Behzadi, R. Fasel and K.-H. Ernst, Homochiral Conglomerates And Racemic Crystals in Two Dimensions: Tartaric Acid on Cu(110), Chem. Eur. J., 11, 4149-4154, 2005

[77] http://www.nobelprize.org/nobel_prizes/physics/laureates/1981/

[78] S. Hüfner, Photoelectron Spectroscopy: Principles and Applications, Springer, ISBN 3-540-41802-4

[79] K. Christmann, Introduction to Surface Physical Chemistry, Steinkopff Verlag, 1991

[80] A. Zangwill, Physics at Surfaces, Cambridge University Press, 1988

[81] C. D. Wagner, W. M. Riggs, L. E. Davis, J. F. Moulder, and G. E. Muilenberg, Handbook of X-Ray Photoelectron Spectroscopy, Perkin-Elmer Corporation, 1979

[82] A. Klein, T. Mayer, A. Thissen, and W. Jaegermann, Photoelectron Spectroscopy in Materials Science and Physical Chemistry, BUNSEN-MAGAZIN, 4: 124-139, 2008

[83] http://www.nobelprize.org/nobel_prizes/physics/laureates/1921/

[84] C. Davisson and L. H. Germer, The Scattering of Electrons by a single Crystal of Nickel, NATURE, 119, 558, 1927

[85] C. Davisson and L. H. Germer, Diffraction of Electrons by a Crystal of Nickel, Phys. Rev., 30, 705, 1927

[86] K. A. R. Mitchell, Low-Energy Electron Diffraction, Contemporary Physics, 14: 3, 251-271, 1973

[87] F. Jona, J. A. Strozier Jr. and W. S. Yang, Low-Energy electron diffraction for surface structure analysis, Rep. Prog. Phys., Vol. 45, 1982

[88] G. M. Gavaza, Z. X. Yu, L. Tsang, C. H. Chan, S. Y. Tong and M. A. Van Hove, Theory of low-energy electron diffraction for detailed structural determination of nanomaterials: Ordered structures, Physical Review B, 75, 014114, 2007

[89] J. Henk, Handbook of Thin Film Materials, Volume 2: Characterization and Spectroscopy of Thin Films, 479-526, Academic Press, 2002

[90] R. G. Greenler, Infrared Study of Adsorbed Molecules on Metal Surfaces by Reflection Techniques, J. Chem. Phys., 44(1): 310-315, 1966

[91] R. G. Greenler, D. R. Snider, D. Witt, and R. S. Sorbello, The Metal-Surface Selection Rule For Infrared Spectra Of Molecules Adsorbed On Small Metal Particles, Surf. Sci., 118: 415-428, 1982

[92] F. M. Hoffmann, Infrared Reflection-Absorption Spectroscopy of Adsorbed Molecules, Surf. Sci. Rep., 3: 107-192, 1983

[93] H. Pearce and N. Sheppard, Possible Importance of A Metal-Surface Selection Rule in The Interpretation of The Infrared Spectra of Molecules Adsorbed on Particulate Metals, Surf. Sci., 59: 205-217, 1976

[94] http://www.nobelprize.org/nobel_prizes/physics/laureates/1986/

[95] G. Binnig, H. Rohrer, Ch. Gerber, and E. Weibel, Tunneling through a controllable vacuum gap., Appl. Phys. Lett., 40(2): 178-180, 1982

[96] G. Binnig, H. Rohrer, Ch. Gerber, and E. Weibel, Surface Studies by Scanning Tunneling Microscopy, Phys. Rev. Lett., 49(1) :57-61, 1982

[97] G. Binnig and H. Rohrer, Scanning tunneling microscopy – from birth to adolescence, Reviews of Modern Physics, 59, No. 3, Part I, 1987

[98] J. A. Golovchenko, The Tunneling Microscope: A New Look at the Atomic World, Science, 232, 4746, 48-53, 1986

[99] P. K. Hansma and J. Tersoff, Scanning tunneling microscopy, Journal of Applied Physics, 61, R1, 1987

[100] J. A. Stroscio and W. J. Kaiser, Scanning tunneling microscopy, Volume 27, Academic Press, Inc., 1993, ISBN: 0-12-475972-6

[101] P. A. Redhead, Thermal Desorption of Gases, Vacuum, 12: 2030211, 1962

[102] F. M. Lord and J. S. Kittelberger, On the Determination of Activation Energies in Thermal Desorption Experiments, Surf. Sci., 43: 173-182, 1974

[103] D. A. King, Thermal Desorption From Metal Surfaces: A Review, Surf. Sci., 47: 384-402, 1975

[104] D. L. Adams, Consequences of Adsorbate-Adsorbate Interactions For Thermal Desorption And LEED Measurements, Surf. Sci., 42: 12-36, 1974

[105] R. G. Sharpe and M. Bowker, Kinetic models of surface explosion, J. Phys.: Condens. Matter, 7: 6379-6392, 1995

[106] W. B. Jensen, The Origin of the Names Malic Acid, Maleic, and Malonic Acid, J. Chem. Ed., 84: 924, 2007

[107] R. M. Silverstein and F. X. Webster, Spectrometric Identification of Organic Compounds, Sixth Edition, John Wiley & Sons, Inc. ISBN: 0-471-13457-0

[108] L. J. Bellamy, Advances in Group Frequencies, 1968, Methuen & Co. LTD.

[109] K. Nakanishi, P. H. Solomon, Infrared Absorption Spectroscopy, Second Edition, Holden Day Inc., ISBN: 0-8162-6251-9

[110] G. Socrates, Infrared and Raman Characteristic Group Frequences, Third Edition, Wiley, 2001, ISBN: 0-471-85298-8

[111] C. Karageorgaki, D. Passerone and K.-H. Ernst, Chiral reconstruction of Cu(110) after adsorption of fumaric acid, Surface Science (2014), http://dx.doi.org/10.1016/j.susc.2014.01.010

[112] M. Parschau, D. Passerone, K.-H. Rieder, H.J. Hug, K.-H. Ernst, Switching the Chirality of Single Adsorbate Complexes, Angew. Chem. Int. Ed.48, 4065, 2009

[113] C. Karageorgaki, K.-H. Ernst, A metal surface with chiral memory, Chem. Commun., 50, 1814-1816, 2014

[114] M. Meier, Study of Acetylenedicarboxylic acid on Cu(110), University of Zürich, Master Thesis, 2013